Dynamic Analysis of Adaptive Modulation in Wireless Communications

Aijiwati Chandra Tjiam

Submitted in total fulfilment of the requirements of the degree of

Doctor of Philosophy

Faculty of Engineering and Industrial Sciences
Swinburne University of Technology
Melbourne, Australia

2013

Abstract

In the rapid development of wireless technology, adaptive modulation has become an important technique to increase the spectral efficiency of communication systems. Extensive study has been done to obtain an optimal solution for the adaptation problem. However, most solutions are based on complex optimization techniques which require numerical evaluation of the optimized parameters for a particular channel statistical characteristic.

In this thesis, adaptive modulation problem is investigated using a control theory approach, namely analysis of dynamical systems. The focus of this study is adaptive modulation technique for QAM transmission over frequency-flat Rayleigh fading channels. System dynamic equations of a discrete-time adaptive QAM scheme are established. Through the analysis of system stability, a feedback controller can be designed to achieve a stable closed-loop system that operates at the optimum operating point. The optimal rate adaptation is performed using an appropriate choice of feedback controller based on the channel condition and BER requirement. In addition to rate adaptation, transmit power can be further adjusted to increase the spectral efficiency without violating the BER requirement. The accuracy of the analytical model of the dynamical system is verified through simulations in MATLAB.

The assumption of perfect channel state information at the transmitter is relaxed by introducing channel prediction error. For Rayleigh channels, the actual channel gain is modeled as a Gaussian random variable with known statistical property. Kalman filtering algorithm is performed to obtain an optimal state

estimation of the stochastic dynamical system based on available measurement of the state and statistical knowledge of the noise. However, due to nonlinearity of the dynamical system that cannot be fully canceled in the presence of noise, Kalman filter gives less optimal performance of state estimation.

An alternative state-space representation of the adaptive QAM is proposed to characterize the nonlinearity in the system. Through stability analysis of the dynamical system, a feedback controller is developed to perform rate adaptation based on channel mean feedback. The effect of channel uncertainty on the system state is taken into account by estimating the system states using the expected value of BER based on the conditional mean of the channel gain.

Using the dynamic analysis approach does not only solve the adaptation problem without expensive computation of the optimal parameters but also results in more robust adaptation against various qualities of channel prediction and against different Doppler shift, compared to the conventional adaptation method that relies on finding the optimal SNR regions boundaries.

Acknowledgements

First, I would like to thank my coordinating supervisor, Prof. Zhihong Man, and my associate supervisor, Dr. Zhenwei Cao, for their thoughtful guidance and support in my whole course of Ph.D research over the past four years. Specifically, I would like to give the deepest gratitude to Prof. Zhihong Man for patiently guiding me with valuable discussions, teaching me to be a good researcher, and always encouraging me to strive for the best. I also want to thank my friends in the research group, Sui Sin, Fei Siang, Kevin, Edi, Manh Do, and Wang Hai for sharing their thoughts in our discussions and good companionship throughout the years.

I am grateful to Swinburne University, Faculty of Engineering and Industrial Science, for awarding me SUPRA scholarship and allowing me to conduct this research in a good working environment. I would like to thank Sophia, Victoria, Adriana, Melissa from research administration team who has always been helpful in responding to my inquiries regarding the paper works. Special thanks to ITS staff members who have helped me with technical difficulties with the software and hardware in the research office.

Lastly and most importantly, I would like to give the greatest praise and gratitude to God for blessing me with such lovely family, brothers and sisters in Christ, and friends who have made my study life so much more joyful. I also thank all my church friends who remember me in their prayers, cheer me up when I am frustrated, and stick together through thick and thin. Without their continuous support and encouragement, I would not have come this far. For all these blessings, I am forever grateful.

Declarations

This is to certify that:

1. This thesis contains no material which has been accepted for the award to the candidate of any other degree or diploma, except where due reference is made in the text of the examinable outcome.

2. To the best of the author's knowledge, this thesis contains no material previously published or written by another person except where due reference is made in the text of the examinable outcome.

3. The work is based on the joint research and publications; the relative contributions of the respective authors are disclosed.

_____

Aijiwati Chandra Tjiam, 2013

Contents

1 Introduction 1

1.1 Background 1

1.2 Motivation 2

1.4 Objectives and Major Contributions 3

1.2 Outline of Thesis 4

2 Literature Review 6

2.1 Overview of Wireless Communication Systems 6

2.2 Wireless Channel Characterization 9

2.2.1 Rayleigh Fading Channel 11

2.2.2 Channel Estimation and Prediction ..... 13~~14~~

2.3 Discrete Data Transmission over Wireless Channels ..... 17~~18~~

2.3.1 Quadrature Amplitude Modulation ..... 19~~20~~

2.3.2 Probability of Error for QAM ..... 21~~22~~

2.4 Adaptive Modulation 23

2.4.1 Adaptive Transmission System 24

2.4.2 Variable-rate Constant-power Adaptation for M-QAM 29

2.4.3 Variable-rate Variable-power Adaptation for M-QAM 33

2.5 Adaptive M-QAM for Predicted Wireless Channels 37

2.5.1 Discrete Rate Adaptation with Constant Power 40
2.5.2 Discrete Rate and Continuous Power Adaptation 41
2.6 Positioning of Contributions 45
3 Analytical Model and Analysis of Adaptive Modulation 46
3.1 Introduction 46
3.2 Background 47
3.2.1 State-space Representation of System Dynamics 47
3.2.2 State Observers 48
3.3 Adaptive M-QAM over a Wireless Link 50
3.3.1 System Modeling 51
3.3.2 Rate Adaptation via a State Feedback Controller 52
3.3.3 Singularity Avoidance 59
3.3.4 Implementation of a State Observer 61
3.3.5 Variable Power Adaptation 63
3.4 Performance Analysis 64
3.5 Conclusion 70
4 Adaptation Method with Imperfect Prediction of Channel Power Gain 72
4.1 Introduction 72
4.2 Overview of Discrete-time Kalman Filter 73
4.3 Adaptive Modulation based on Imperfect CSI 75
4.4 Simulation Results and Discussion 80
4.5 Conclusion 91
5 Non-linear Controller for Adaptation Method with Channel Mean Feedback 92
5.1 Introduction 92
5.2 Non-linear Adaptation System 93

5.2.1 State-space Representation 93
5.2.2 Stability Analysis 94
5.2.3 Rate Adaptation Based on Partial CSI 98
5.3 Performance Analysis 102
5.4 Conclusion 119
6 Conclusions and Future Work 121
6.1 Summary of Contributions 121
6.2 Future Research 123
List of Publications 125
Bibliography 126

List of Figures

2.1	A mathematical model of wireless signal transmission	10
2.2	Rayleigh probability density function	11
2.3	A flat Rayleigh fading envelope as a function of time	13
2.4	Power spectrum density of a flat Rayleigh channel	13
2.5	Signal constellation diagram of 4-PSK	19
2.6	(a) Circular 8-QAM signal constellation (b) Star 8-QAM signal constellation	20
2.7	(a) Square 16-QAM signal constellation (b) Cross 16-QAM signal constellation	21
2.8	BER performances of M-QAM over an AWGN channel	23
2.9	Adaptive modulation in wireless system	25
2.10	Spectral efficiency of exact water-filling and constant-power allocation	28
2.11	Maximum spectral efficiency vs. SNR per symbol for QAM with adaptive rate only	31
2.12	Average BER vs. SNR per symbol for QAM with adaptive rate only	32
2.13	Spectral efficiency of rate and power adaptation for QAM with $BER_{tg} = 10^{-3}$	35
2.14	Spectral efficiency vs SNR per symbol in Rayleigh fading channel for $BER_{tg} = 10^{-3}$	36
2.15	Adaptation of the transmit power $S(\hat{\gamma})/\bar{S}$	43
2.16	Spectral efficiency vs average received SNR for $BER_{tg} = 10^{-3}$ for adaptive M-QAM based on imperfect channel knowledge	44
3.1	Block diagram of a feedback control system with a state observer	49
3.2	Illustration of rate adaptive QAM based on outdated CSI	51

3.3	Block diagram of the adaptation system	54
3.4	A Cartesian plane of the control gain vector $\mathbf{K} = [k_1 \quad k_2]$	57
3.5	Closed-loop pole locations of the system	58
3.6	BER performance of the closed-loop system	58
3.7	Estimation errors of the state observer	62
3.8	Received BER of the adaptation system	63
3.9	Rate variations for adaptive modulation with 3 constellations	65
3.10	Power variations for adaptive modulation with 3 constellations	65
3.11	Resulted BER for adaptive modulation with 3 constellations	66
3.12	Rate variations for adaptive modulation with 6 constellations	67
3.13	Power variations for adaptive modulation with 6 constellations	67
3.14	Resulted BER for adaptive modulation with 6 constellations	68
3.15	Spectral efficiency vs. average SNR	69
3.16	Average transmit power vs. average SNR	69
3.17	Average received BER vs. average SNR	70
4.1	Block diagram of linear system, measurement model, and Kalman filter	75
4.2	Block diagram of the adaptation system with Kalman filter	79
4.3	Rate variations for adaptive modulation with $\sigma_{\epsilon p}^2 = 0.01$	81
4.4	Resulted BER for adaptive modulation with $\sigma_{\epsilon p}^2 = 0.01$	81
4.5	Rate variations for adaptive modulation with $\sigma_{\epsilon p}^2 = 0.1$	82
4.6	Resulted BER for adaptive modulation with $\sigma_{\epsilon p}^2 = 0.1$	83
4.7	Rate variations for adaptive modulation with $\sigma_{\epsilon p}^2 = 0.01$	83
4.8	Resulted BER for adaptive modulation with $\sigma_{\epsilon p}^2 = 0.01$	84
4.9	Rate variations for adaptive modulation with $\sigma_{\epsilon p}^2 = 0.1$	84
4.10	Resulted BER for adaptive modulation with $\sigma_{\epsilon p}^2 = 0.1$	85
4.11	Spectral efficiency vs SNR of for $BER_{tg} = 10^{-3}$	86
4.12	Rate variations for adaptive modulation with $\sigma_{\epsilon p}^2 = 0.02$	87
4.13	Transmit power variations for adaptive modulation with $\sigma_{\epsilon p}^2 = 0.02$	87
4.14	Resulted BER for adaptive modulation with $\sigma_{\epsilon p}^2 = 0.02$	88
4.15	Spectral efficiency vs SNR for $BER_{tg} = 10^{-3}$ and $\sigma_{\epsilon p}^2 = 0.02$	89
4.16	Average transmit power and average BER vs. SNR of for $BER_{tg} = 10^{-3}$ and $\sigma_{\epsilon p}^2 = 0.02$	90

5.1	System response for different values of control gain	98
5.2	Block diagram of the transmission system	101
5.3	Discrete rate adaptation based on partial CSI for $BER_{tg} = 10^{-3}$	102
5.4	Instantaneous BER for $BER_{tg} = 10^{-3}$	103
5.5	Discrete rate adaptation based on partial CSI for $BER_{tg} = 10^{-5}$	103
5.6	Instantaneous BER for $BER_{tg} = 10^{-5}$	104
5.7	Discrete rate adaptation based on partial CSI for $BER_{tg} = 10^{-7}$	104
5.8	Instantaneous BER for $BER_{tg} = 10^{-7}$	105
5.9	Spectral efficiency vs. SNR for discrete rate adaptation based on optimal boundaries solution	106
5.10	Spectral efficiency vs. SNR for discrete rate adaptation based on non-linear feedback controller	106
5.11	Rate adaptations with $\sigma_{\xi}^2 = 0.02$ for $BER_{tg} = 10^{-3}$	107
5.12	Power adaptations with $\sigma_{\xi}^2 = 0.02$ for $BER_{tg} = 10^{-3}$	108
5.13	Instantaneous BER of adaptive QAM with $\sigma_{\xi}^2 = 0.02$ for $BER_{tg} = 10^{-3}$	109
5.14	Rate adaptations with $\sigma_{\xi}^2 = 0.05$ for $BER_{tg} = 10^{-3}$	110
5.15	Power adaptations with $\sigma_{\xi}^2 = 0.05$ for $BER_{tg} = 10^{-3}$	110
5.16	Instantaneous BER of adaptive QAM with $\sigma_{\xi}^2 = 0.05$ for $BER_{tg} = 10^{-3}$	111
5.17	Rate adaptations with $\sigma_{\xi}^2 = 0.02$ for $BER_{tg} = 10^{-7}$	112
5.18	Power adaptations with $\sigma_{\xi}^2 = 0.02$ for $BER_{tg} = 10^{-7}$	113
5.19	Instantaneous BER of adaptive QAM with $\sigma_{\xi}^2 = 0.02$ for $BER_{tg} = 10^{-7}$	114
5.20	Rate adaptations with $\sigma_{\xi}^2 = 0.05$ for $BER_{tg} = 10^{-7}$	114
5.21	Power adaptations with $\sigma_{\xi}^2 = 0.05$ for $BER_{tg} = 10^{-7}$	115
5.22	Instantaneous BER of adaptive QAM with $\sigma_{\xi}^2 = 0.05$ for $BER_{tg} = 10^{-7}$	116
5.23	Spectral efficiencies vs. average SNR for $BER_{tg} = 10^{-3}$	117
5.24	Spectral efficiency vs. SNR for discrete rate and continuous power adaptation based on optimal region boundaries solution	118
5.25	Spectral efficiency vs. SNR for discrete rate and continuous power adaptation based on non-linear feedback controller	118

List of Acronyms

AR – Autoregressive model

AWGN – additive white Gaussian noise

BER – bit error rate

BPSK – binary phase shift keying

CSI – channel state information

CQLF – common quadratic Lyapunov function

FSMC – finite state Markov channel

GPS – global positioning system

GSM – global system for mobile communications

IMT-2000 – international mobile telecommunications-2000

ITU – international telecommunication union

LTE – long term evolution

M-QAM – multi-level quadrature amplitude modulation

MIMO – multiple input multiple output

MMSE – minimum mean square error

OFDM – orthogonal frequency division multiplexing

PAM – pulse amplitude modulation

PSAM – pilot symbol assisted modulation

QAM – quadrature amplitude modulation

QPSK – quadrature phase shift keying

RF – radio frequency

SNR – signal to noise ratio

VoIP – voice over internet protocol

WiMax – worldwide interoperability for microwave access

WLAN – wireless local area network

Chapter 1

Introduction

1.1 Background

One of the foremost goals of advancement in information technology is to be able to provide people with easy access to information worldwide. Wireless communication has captured the attention of media industry to serve this purpose. Its prominent ability of transmitting information over the air makes wireless technology a prominent solution for providing information to areas where it is geographically and economically challenging to build wired telecommunication infrastructure.

Advancement in communication technology in the last decade has enabled high bandwidth data transfer over the wireless channel, which in turn has increased the demand for high data speed and efficient allocation of the limited resources to the users. In answering this matter, adaptive transmission technique is developed to exploit the time variation of the wireless channel. The basic idea is to adjust the transmission parameters, such as transmit power and modulation rates, relative to the channel condition instead of fixing these parameters for the worst-case condition of the channel. Therefore, adaptive transmission can increase the average throughput of the channel and reduce the required transmit power while still maintaining the

prescribed quality of service. For communication systems, the quality of service is mainly evaluated in terms of the bit error rate (BER) for packet transmission, and time delay for data streaming. This study is concerned with reliable packet transmission between a transmitter and a receiver in particular. Therefore, the objective of adaptive modulation in this thesis is to achieve a high data rate while meeting the bit error rate requirement.

1.2 Motivation

The concept of adaptive transmission which requires accurate channel information feedback from the receiver was first investigated in the late 1960's when Hayes [1] adapted the signal amplitude according to channel condition through feedback channel between the transmitter and receiver that was assumed noiseless and free from latency. This idea did not receive attention at that point of time, perhaps because of the lack of good channel identification technique and hardware constraints. After a couple of decades, the demand for more bandwidth along with the advancement in communications technology motivated researchers to revisit adaptive modulation techniques. However, accurate channel estimation technique remains a stumbling block for optimal adaptation method in wireless system due to the random nature of the medium.

Even though various adaptive modulation techniques based on imperfect channel state information have been developed over the years, there is not one unique solution to this problem due to the complexity of the system. To the best of the author's knowledge, adaptive modulation proposed in literature requires complex numerical computation to obtain the optimal solution, and this solution is different for different channel statistical characteristics and prediction. The lack of a general solution to the adaptation problem for different channel statistical characteristics has motivated this research to investigate the problem from a different approach by the modeling and analysis of the behavior of adaptive modulation system.

1.3 Objectives and Major Contributions

This thesis aims to develop a simple and flexible adaptive modulation technique that is applicable for different channel statistical characteristics by means of analytical modeling and analysis of the system dynamic.

The following list outlines the major contributions of this thesis.

1. Introduce a new approach from the perspective of control theory to solve the constraint optimization problem in the framework of adaptive modulation scheme.
2. Address the general problem of adaptation in quadrature amplitude modulation (QAM) systems in the presence of transmission and feedback delay as described by the discrete-time relationship of transmit power, constellation size, channel power gain, and bit error rate.
3. Establish mathematical models of the system dynamic in the form of state-space equations.
4. Develop a novel rate adaptation method by an appropriate feedback controller that drives the closed-loop system state to a stable equilibrium point. This results in optimal performance of the adaptive system.
5. Develop a non-linear feedback control of modulation rate by using state estimations based on the partial channel state information, namely channel mean feedback.
6. Investigate the effect of various Doppler shifts and different qualities of channel prediction to the performance of adaptation systems.

In summary, the work of this thesis has the potential to significantly improve the performance of adaptive modulation systems by the initial mathematical modeling and analysis of the system dynamic. By using system dynamic analysis approach, it is

possible to design a robust controller to serve the purpose of optimal rate and power adaptation against the uncertainty of the channel state.

1.4 Outline of Thesis

This thesis is concerned with the dynamic analysis of adaptive modulation in wireless communications, particularly for quadrature amplitude modulation schemes in digital transmission over a frequency-flat Rayleigh fading channel. The rest of the thesis is organized as follows.

Chapter 2 presents a brief overview of the literature in the area of wireless communications and adaptive modulation. Hence it serves to give the context for this study and its contributions to this field.

Chapter 3 proposes a mathematical model of system dynamics in the form of state-space representation. Assuming perfect channel information at the transmitter, the adaptation of constellation size is performed by an appropriate state feedback controller that results in a stable closed-loop system. The dynamical model of the adaptation problem is verified and it builds the foundation for further design of controller feedback in the presence of noise.

Chapter 4 addresses the practical noisy estimation of channel gain at the transmitter in contrast to the assumption of perfect channel state information feedback. Rate adaptation is performed based on predicted channel power gain and Kalman filtering algorithm is applied to mitigate the effect of channel prediction error. The effect of different qualities of channel prediction on the system performance is also investigated.

Chapter 5 develops a novel non-linear feedback control scheme to adjust the constellation size of the modulation relative to the partial knowledge of the channel gain. The new rate adaptation method is developed based on the stability analysis of

system dynamic. The performance of the adaptation method over various Doppler effects on the channel variation is investigated as well.

Chapter 6 summarises the main contributions of this thesis and presents some open problems associated with the work in this thesis for future research direction.

Chapter 2

Literature Review

This chapter presents a brief overview of the literature in the area of wireless communications and adaptive modulation. Hence it serves to give the context for this study and its contributions to this field.

2.1 Overview of Wireless Communication Systems

The first wireless communication was performed in the form of telegraphy in 1890s before Gugliemo Marconi successfully demonstrated the first long-distance radio transmission [2] . Following the invention of radio for wireless communication in 18^{th} century, digital signal processing and radio frequency (RF) technology rapidly advanced, thereby enabling reliable transmissions over large distances with cheaper devices. As the result, most radio systems today transmit digital signals composed of binary bits, where the bits are mapped onto a data signal by performing digital modulation.

The most successful application of wireless networking has been the cellular telephone system, which has greatly evolved since its inception. The first commercial cellular network was deployed in Japan by Nippon Telegraph and Telephone Corporation in 1979. It was purely analog signal transmission over the air, and nowadays it is known as the first generation (1G) cellular system. The cellular system quickly attracted the public, leading to the explosive growth of cellular industry and demand for higher speed and power efficiency of devices. As the answer to these matters, digital transmission system emerged in early 1990s which is referred to as the second generation (2G) cellular system. The most popular 2G technology that is

used worldwide is called Global System for Mobile Communications (GSM) standard, which supports data transfer speeds of up to 14.4 kpbs [3] and allocate eight time slotted users for each 200 kHz radio channel. Data transmission based on GSM standard is utilizing different frequency bands in different countries. The frequency bands generally used for GSM are the 850 MHz and 1900 MHz in United States and other countries in America and 900 MHz and 1800 MHz in Europe, Australia, Asia, and Africa.

Since the introduction of 2G technology, various enhancements have been made in order to provide mobile data services and applications such as text messaging, still-image transmission, and internet browsing. People started to use mobile phones on daily basis and clearly the radio spectrum became highly populated. In 1992, International Telecommunication Union (ITU), the international body that regulates the use of radio spectrum, identified 230 MHz of new radio spectrum [4] for mobile industry to apply International Mobile Telecommunications-2000 (IMT-2000) standard, which is associated with the third generation (3G) mobile system technology. This standard was introduced as result of more than a decade of research on development and evolution of the GSM standard. The new bands of frequency, 1885-2025 MHz and 2110-2200 MHz, certainly contribute to greater user capacity. The advanced technology in 3G standard allows higher data transmission rates of at least 144 kbps for devices used in moving vehicles to 2 Mbps for indoor devices [5]. As the result of the greater channel bandwidth and faster data transfer, high-bandwidth data services as mobile television, voice over Internet Protocol (VoIP), video conferencing, and global positioning system (GPS) became possible for cellular devices. These applications have become almost indispensable to today's lifestyle. To meet the growing demands in network capacity and high speed data transfer of the multimedia applications, 3G standard is evolving with more advanced and efficient technologies, leading towards the next generation, 4G technology [6], [7]. Long Term Evolution (LTE) and Worldwide Interoperability for Microwave Access (WiMax) are the two most advanced mobile communication technologies to date that are considered as the part of pre-4G [8] - [10] and mobile industries worldwide keep competing to improve these technologies to meet the 4G standard.

In parallel with cellular mobile networks, wireless local area networks (WLANs), with Wi-Fi technology in particular, are widely used to connect two or more devices via the radio channels. In addition to the peer-to-peer networking, these networks also provide connection to the internet through an access point, which is the most common purpose of Wi-fi connection nowadays. Wireless LAN technology is established based on IEEE 802.11 family standard to support a high data transmission rate on a wideband channel. In 2003, wireless LAN based on IEEE 802.11g standard was developed to support up to 54 Mbps on 2.4 GHz frequency band with orthogonal frequency division multiplexing (OFDM) based multi-carrier transmission scheme [11]. Wireless LAN is mostly installed in shared accommodations, schools, companies, and commercial complexes to provide a shared access of internet to both fixed and mobile devices that support Wi-fi technology. As is the case in the cellular networks, the ever increasing use of Wi-fi devices compels the wireless service providers to keep improving on efficient utilization of the limited radio channels. In addition, higher frequency bands of 3.6 GHz and 5 GHz have also been allocated to accommodate the heavy wireless traffic over WLANs. To the best of the author's knowledge, the communications industries are currently working on a new WLAN standard that will allow wireless transmission at 60 GHz frequency band which will offer a theoretical maximum data rate of 7 Gbps.

Aside from cellular network and WLAN, various applications of wireless technology including cordless phones, wireless sensors, satellite televisions, and GPS are actively in use these days. These systems need to share the limited wireless spectrum in a similar way to the preceding systems and the wireless service providers share the same question of how to dynamically allocate the radio spectrum to different users to achieve the most efficient resource utilization while still maintaining the quality of service requirement. This challenge has motivated extensive research in the area of wireless channel characterization and adaptive modulation to adjust the transmission parameters such as transmit power and data rate in accordance with the variation of the channel gain.

2.2 Wireless Channel Characterization

In wireless communications, the transmitted signal will experience some time-varying distortion during propagation due to the ever changing nature of wireless channels, and this problem has been one of the significant areas for exploratory study for efficient wireless data transmission [12] - [20]. The rapid change of the wireless channels over time is called fading and it occurs due to the propagation of signal through different paths and the motion of either transmitter or receiver which causes a shift in frequency of the transmitted signal along each path. Signals traveling along different paths can have different frequency shifts and the maximum frequency shift is known as the Doppler spread, given by

$$f_{dm} = \frac{v}{\lambda} \tag{2.1}$$

where v is the maximum speed of the mobile user and λ is the wavelength of the signal. Doppler shift is inversely related to coherence time which is as the time duration over which the channel is relatively invariant [11]. In digital transmission over wireless channels, if the coherence time of the channel is longer than the transmit symbol period of the signal, the channel is classified as slow fading channel. On the contrary, if the coherence time of the channel is shorter than the transmit symbol period of the signal, the channel is said to be fast fading channel [11], [21], [22].

Multipath propagation also contributes to different versions of signal arriving at receiver at different times. The time difference between the earliest and the latest arrival of the signal is called delay spread and it is used as a measure of the multipath fading in wireless channels in time domain. Coherence bandwidth is the counterpart of delay spread to characterize fading in frequency domain and it can be interpreted as the range of frequencies over which the channel appears constant [11]. If the bandwidth of the transmitted signal is smaller than the coherence bandwidth of the channel, the received signal undergoes frequency-flat fading. Contrarily, the channel is classified as frequency selective fading channel. Frequency-flat fading channel,

also known as flat fading channel, is a befitting model for a narrowband wireless channel and it is used to model a subchannel in multicarrier wireless systems [23]. Moreover, frequency selective fading channels can be described by time-varying tap coefficient [24], [25], where each tap coefficient represents a flat fading channel.

In addition to fading, as in any other communication system, the transmitted signal is also susceptible to noise, which is commonly modeled as additive white Gaussian noise (AWGN). The wireless propagation is illustrated in Figure 2.1 in which $h(t)$ represents the multiplicative distortion imposed by the fading channel and $w(t)$ denotes the AWGN with a particular signal to noise ratio (SNR) [16], [26].

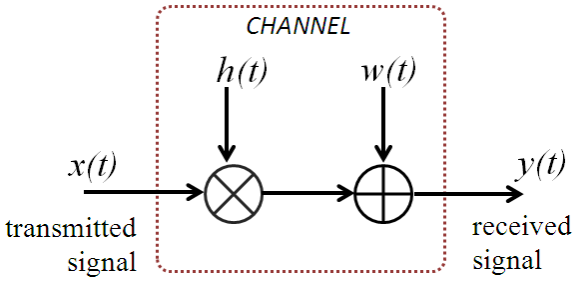

Figure 2.1 A mathematical model of wireless signal transmission

The multiplicative channel gain $h(t)$ which describes the time-varying nature of the fading channel can be modeled by a complex random variable with a certain distribution. In the absence of line of sight path, the channel is said to experience Rayleigh fading and the distribution of the random variable has zero mean. Rayleigh fading is a reasonable model for environments with many objects that reflect and scatter the signal, typically in the city with heavily built-up buildings. On the other hand, in the presence of line of sight path, the distribution will have non-zero mean and the channel is described as a Rician fading channel which is typical in maritime [27], [28], [29] and land satellite mobile communications [30], [13], [31]. In the following section, Rayleigh model is further discussed as the appropriate model of wireless channel that is used for the rest of this study.

2.2.1 Rayleigh Fading Channel

For Rayleigh fading channels, $h(t)$ is modeled as a zero mean circularly symmetric complex Gaussian process $h(t) = h_r(t) + jh_i(t)$ where h_r and h_i are independent and identically distributed (i.i.d) Gaussian random variables with a zero mean and variance of σ^2 [22]. The amplitude of the fading, $|h(t)| = \sqrt{h_r(t) + h_i(t)}$ is Rayleigh distibuted with following probability density function, as depicted in Figure 2.2:

$$f_{|h|}(|h(t)|) = \frac{2|h(t)|}{\sigma_h^2} exp\left(-\frac{|h(t)|^2}{\sigma_h^2}\right) \tag{2.2}$$

where $\sigma_h^2 = E\{|h|^2\} = 2\sigma^2$ is the average channel power gain.

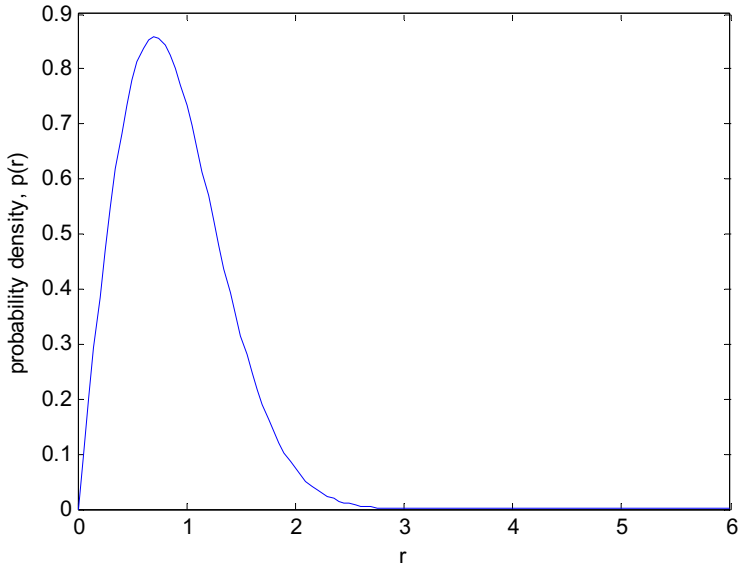

Figure 2.2 Rayleigh probability density function

As mentioned above, a Rayleigh fading channel itself can be constructed by generating the real and imaginary parts of a complex number according to independent normal Gaussian variables. However, in most cases, the magnitude fluctuations are of greater interest which is described by the power spectrum density

function, and its inverse Fourier transform, the autocorrelation function of the fading channel [22]. Jakes model [12] is a widely known statistical fading model along with autoregressive (AR) model [19], [32] which is also associated with finite state Markov channel (FSMC) model [33] - [35] for generating a Rayleigh channel with a specific autocorrelation function, given by:

$$\rho(\tau) = J_0(2\pi\tau f_{dm}) \tag{2.3}$$

where τ is the time delay and $J_0(.)$ is a zero-th order Bessel function of the first kind. Another important property of the time-varying channel is the Doppler spectrum or power spectral density which can be obtained as the Fourier transform of the autocorrelation function. Doppler spectrum of a flat Rayleigh fading channel [21] with a uniform angle of arrival from 0 to 2π is given by:

$$S(f) = \frac{1.5}{\pi f_{dm}\sqrt{1-\left(\frac{f-f_c}{f_{dm}}\right)^2}} \tag{2.4}$$

A typical flat Rayleigh fading amplitude and its normalized power spectrum density for maximum Doppler frequency of 400 Hz are shown in Figure 2.3 and Figure 2.4 respectively.

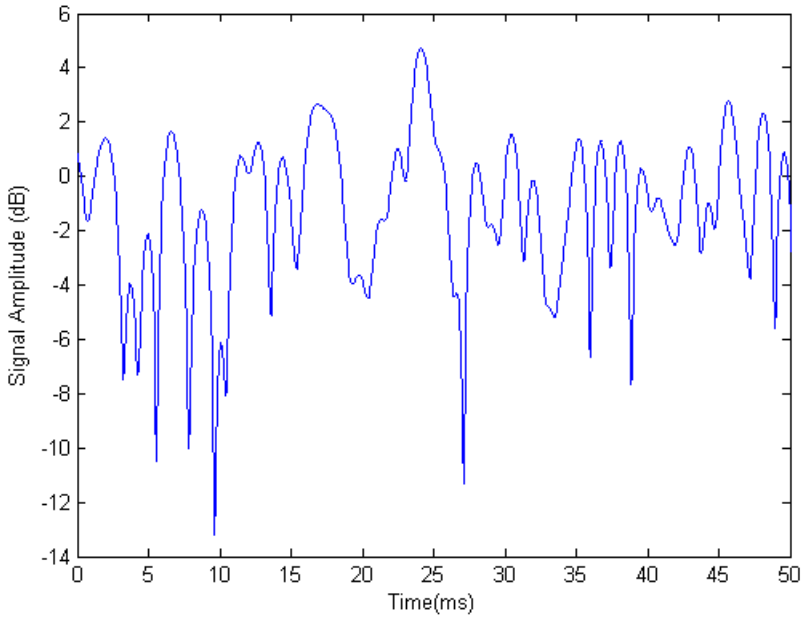

Figure 2.3 A flat Rayleigh fading envelope as a function of time

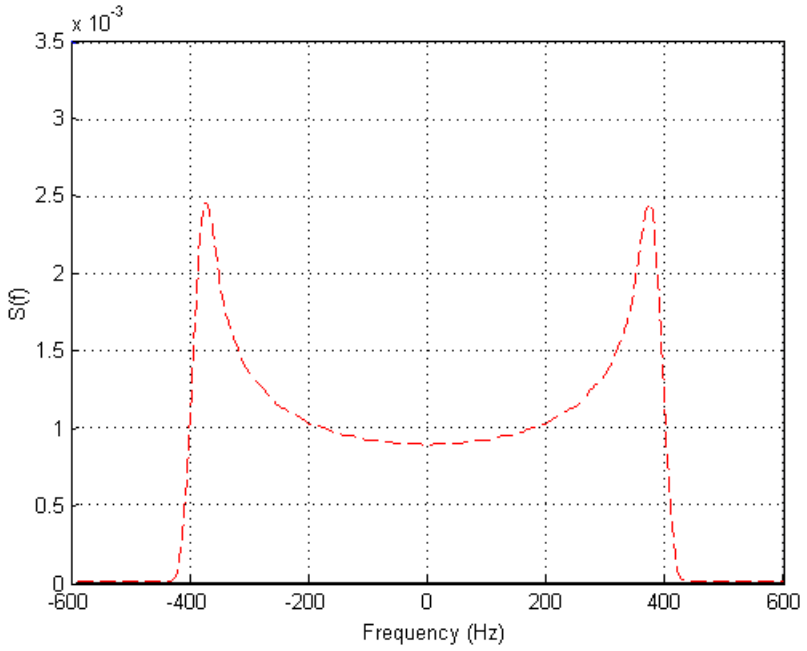

Figure 2.4 Power spectrum density of a flat Rayleigh channel

The knowledge on statistical properties of the channel allows periodical channel gain estimation at symbol rate and channel gain prediction to support adaptive transmission techniques, as discussed in the next section.

2.2.2 Channel Estimation and Prediction

Since the channel varies over time, the instantaneous channel state information (CSI) needs to be observed regularly at the receiver for reliable communication [21]. One of the popular methods to obtain the channel gain at the receiver is by facilitating pilot symbols transmission, which is the underlying concept of the pilot symbol assisted modulation (PSAM). In PSAM systems, transmitter periodically inserts known symbols or pilots into the data stream, from which the receiver may obtain some

measurements of the fading channel gain and learn the amplitude and phase reference for coherent demodulation of the data symbols [36]-[39].

Consider a point-to-point channel with single antenna transmitter and receiver. As discussed in the earlier section, the fading channel can be represented by a circularly symmetric complex Gaussian random variable, $h(t)$, based on Rayleigh fading model. Figure 2.1 depicts the point-to-point transmission of signal $x(t)$ through the wireless channel, and received signal can be represented as:

$$y(t) = h(t)x(t) + w(t) \tag{2.5}$$

where $w(t)$ denotes the zero mean AWGN with variance σ_w^2. Upon reception of the distorted signal $y(t)$, the receiver measures the instantaneous channel gain based on pilot symbols sent from the transmitter. Furthermore, channel estimation at symbol rate is performed through filtering and interpolation based on the periodical pilot symbols and the statistical knowledge of the channel [26], [40]-[46]. Least square estimator is the most basic form of channel identification using pilot symbols [47]-[50]. The estimation error is highly dependent on the noise that is present in the wireless environment. While pilot symbols are vital for reliable data detection and channel identification, they can be considered as overhead information that reduces the spectral efficiency. In several research articles [51]-[54] adaptive PSAM schemes have been discussed, where the spacing and the power allocation between pilot symbols can be arranged in such a way that minimizes the overhead information while still producing reliable channel tracking.

In addition to reliable detection and demodulation at the receiver, the instantaneous knowledge of channel is also crucial in the concept of adaptive transmission. In this case, the channel state information that is acquired at receiver is sent back to the transmitter to be used for adaptation of transmission parameters relative to the time-varying channel condition. Several literatures [55]-[58] have presented adaptive modulation techniques with perfect knowledge of channel gain at transmitter, but in practice, the CSI has become outdated due to the inevitable feedback delay. Channel prediction has become a popular topic in wireless

communications due to this reason. For Rayleigh fading channel modeled as a complex circular Gaussian random variable with zero mean and variance σ_h^2, minimum mean square error (MMSE) optimal linear prediction [49], [59], [60]-[65], has been widely used to predict the channel gain in wireless communications due to the ease of implementation.

Consider a flat Rayleigh fading channel, the single tap channel gain can be predicted based on the statistical characteristics and imperfect past observations of the channel gain with equal delay spacing ΔT, given by [49]:

$$\tilde{h}(t+L|t) = \boldsymbol{\varphi}^H(t)\boldsymbol{\theta}, \tag{2.6}$$

$$\boldsymbol{\varphi}(t) = [\,\hat{h}(t) \quad \hat{h}(t-\Delta T) \quad \ldots \quad \hat{h}(t-(M-1)\Delta T)\,]^H \tag{2.7}$$

where $\boldsymbol{\varphi}(t)$ is the vector of the past M noisy observations and $\boldsymbol{\theta}$ is the optimal complex coefficients of the linear FIR predictor, and L is the range of prediction as an integer multiply of delay spacing ΔT.

The complex coefficients of the linear FIR predictor that is optimal in MMSE sense is expressed as:

$$\boldsymbol{\theta} = \boldsymbol{R}_{\varphi}^{-1}\,\boldsymbol{r}_{h\varphi} \tag{2.8}$$

where $\boldsymbol{R}_{\varphi}$ is the covariance matrix of the regressors and $\boldsymbol{r}_{h\varphi}$ is the cross-covariance between the channel and the regressor $\boldsymbol{\varphi}(t)$, subsequently given by:

$$\boldsymbol{R}_{\varphi} = \boldsymbol{R}_h + \boldsymbol{R}_e \tag{2.9}$$

$$\boldsymbol{R}_h = \begin{bmatrix} \sigma_h^2 & \rho_h{}^*(\Delta t) & \ldots & \rho_h{}^*((M-1)\Delta t) \\ \rho_h(\Delta t) & \sigma_h^2 & & \vdots \\ \vdots & & \ddots & \rho_h{}^*(\Delta t) \\ \rho_h((M-1)\Delta t) & & & \sigma_h^2 \end{bmatrix} \tag{2.10}$$

$$\boldsymbol{r}_{h\varphi} = [\rho_h(L) \quad \rho_h(L+\Delta t) \quad \ldots \quad \rho_h(L+(M-1)\Delta t)]^T \tag{2.11}$$

where $\rho_h(\Delta t) = E\{h(t)h^*(t-\Delta t)\}$ is the autocorrelation function of the complex channel gain, according to Jakes' model, given by (2.3) and $\boldsymbol{R}_e$ is the covariance of the channel estimation error at the receiver. For least square estimation of fading channel with AWGN, the covariance of estimation error has a simple form:

$$\boldsymbol{R}_e = \sigma_w^2 \boldsymbol{I} \tag{2.12}$$

where σ_w^2 is the variance of the noise.

The complex valued prediction error is given by:

$$\varepsilon_c(t) = h(t) - \tilde{h}(t|t-L) \tag{2.13}$$

The actual channel gain and the estimation error are both modeled by zero mean circularly complex Gaussian random variables. The mean square error is equal to the variance of the prediction error, given by:

$$\sigma_{\epsilon c}^2 = \sigma_h^2 - \boldsymbol{r}_{h\varphi}^H \boldsymbol{R}_\varphi^{-1} \boldsymbol{r}_{h\varphi} \tag{2.14}$$

In addition to channel gain, $h(t)$, the channel power is of equally important information in the adaptive modulation, which is given by the absolute value of the complex channel gain:

$$p_c(t) = |h(t)|^2 \tag{2.15}$$

With the linear prediction in (2.8), the absolute square of the predicted channel gain is given by:

$$\tilde{p}_c(t) = \left|\tilde{h}(t+L|t)\right|^2 = \boldsymbol{\theta}^H \boldsymbol{\varphi}(t) \boldsymbol{\varphi}^H(t) \boldsymbol{\theta} \tag{2.16}$$

which is a quadratic function of the regressors and thus is a non-linear predictor, of which prediction error can be written by:

$$\varepsilon_p(t) = |h(t)|^2 - \left|\tilde{h}(t|t-L)\right|^2 \tag{2.17}$$

The variance of this power prediction error is given by:

$$\begin{aligned} E\{\varepsilon_p(t)\} &= E\left\{|h(t)|^2 - \left|\tilde{h}(t|t-L)\right|^2\right\} \\ &= \sigma_h^2 - \boldsymbol{\theta}^{\boldsymbol{H}} \boldsymbol{R}_\varphi^{-1} \boldsymbol{\theta} \end{aligned} \tag{2.18}$$

which is equal to the channel prediction error for the optimal linear FIR with coefficients given by (2.8). The absolute square of the complex prediction thus results in a power prediction with non-zero mean. Based on this analysis, an unbiased power predictor [49], [62] is proposed:

$$\widetilde{p_c}(t+L|t) = \boldsymbol{\theta^H \varphi}[k]\boldsymbol{\varphi}^H[k]\boldsymbol{\theta} + \sigma_h^2 - \boldsymbol{\theta^H R_\varphi \theta} \tag{2.19}$$

such that the power prediction error will have zero mean, and the minimum mean square of the optimal unbiased predictor is given by:

$$\sigma_{\varepsilon_p}^2 = (\sigma_h^2)^2 - \left|\boldsymbol{r}_{h\varphi}^H \boldsymbol{R}_\varphi^{-1} \boldsymbol{r}_{h\varphi}\right|^2 \tag{2.20}$$

This mean square error is equal to the variance of the power prediction [49] and is bounded by $0 < \sigma_{\varepsilon_p}^2 < (\sigma_h^2)^2$.

The predicted complex channel gain and power obtained in this section will be used in the later sections for the purpose of adapting transmission parameters based on the partial knowledge of CSI.

2.3 Discrete Data Transmission over Wireless Channels

In the transmission of digital information, digital modulation refers to the mapping of a sequence of binary digits into a set of corresponding signal waveforms that are suitable for transmission over the communication medium. In general, the mapping is done per blocks of $k = log_2 M$ bits at a time from the discrete data sequence to be associated with one of M deterministic, finite energy waveforms in a set:

$$\mathcal{S} = \{s_1(t), s_2(t), \dots, s_M(t)\} \tag{2.21}$$

where $s_i(t) \in \mathcal{S}$ is a unique waveform defined on the time interval $[0, T)$ and the energy of the signal is defined by:

$$E_{s_i} = \int_0^T {s_i}^2(t)dt, \tag{2.22}$$

These waveforms may differ in amplitude, in phase, or in frequency, or any combination of two or more of these signal parameters in representing the unique information bits.

In accordance with Gram-Schmidt orthogonalization procedure [66], a set of M real signals defined on with finite energy can be represented as linear combinations of $N \leq M$ real orthonormal basis functions $\{\phi_1(t), \ldots, \phi_N(t)\}$. It is said that these orthonormal basis functions span the set $\mathcal{S} = \{s_1(t), s_2(t), \ldots, s_M(t)\}$, and the modulation scheme that utilizes this set of waveforms is said to be a linear modulation [67], which is popular in wireless communications as a result of their good bit error rate performance and bandwidth efficiency.

In general linear passband modulation techniques, the set of *M* possible waveforms can be represented by a set of two orthonormal basis functions with 90 degree phase shift between them, such as:

$$\phi_1(t) = \sqrt{\frac{2}{T}}\, cos(2\pi f_c t) \tag{2.23}$$

$$\phi_2(t) = \sqrt{\frac{2}{T}} sin(2\pi f_c t) \tag{2.24}$$

where $\sqrt{2/T}$ is needed to meet the orthonoramality condition [5] and T is the time duration of a symbol. Thus, the set of *M* signals can be represented by signal vectors in two dimensional signal space or constellation as shown in Figure 2.5 for 4-PSK scheme. The in-phase (I) axis is associated with a sine basis function and the quadrature (Q) axis is associated with the cosine basis function. The projection of the signal vector onto the I-axis and Q-axis are called the in-phase component and quadrature component respectively. The angle of the signal vector represents the phase of the signal and the amplitude is given by the distance from the origin.

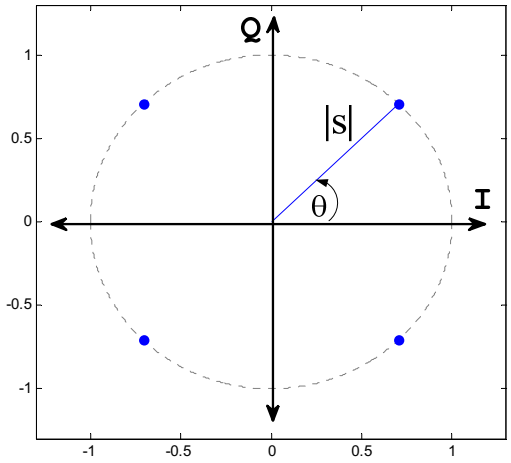

Figure 2.5 Signal constellation diagram of 4-PSK

In the simplest form, linear modulation can be performed by using only one basis function and all information is encoded in the amplitude of the signal. This is called pulse amplitude modulation (PAM), of which modulated signals over a symbol period T is given by:

$$s_i(t) = A_i \cos(\theta_i)\, g(t) \cos(2\pi f_c t)\,, \qquad 0 \le t < T \tag{2.25}$$

where $g(t)$ is the signal pulse that is chosen to maintain the orthonormal property of the basis functions. Although PAM is not a highly efficient modulation scheme, the signals set can be used to generate QAM signals which is discussed in the following section.

2.3.1 Quadrature Amplitude Modulation

One of the most common forms of linear modulation used in digital system is multi-level quadrature amplitude modulation (M-QAM) which encodes information bits in both amplitude and phase of the modulated signals. It is more spectrally efficient relative to only amplitude or phase modulation techniques as it can encode the most number of bits per symbol for a given average energy. For this reason, M-QAM techniques appeal to be the more suitable in the limited bandwidth of wireless systems [68] and it is extensively implemented in modern cellular services, wireless broadband networks, video broadcasting, and satellite systems.

The transmitted signal is given by:

$$s_i(t) = A_i \cos(\theta_i)\, g(t) \cos(2\pi f_c t) - A_i \sin(\theta_i)\, g(t)\, sin(2\pi f_c t),$$

$$0 \leq t < T \qquad (2.26)$$

The energy of the signal over one symbol period is given by:

$$E_{s_i} = \int_0^T {s_i}^2(t)dt = {A_i}^2 \qquad (2.27)$$

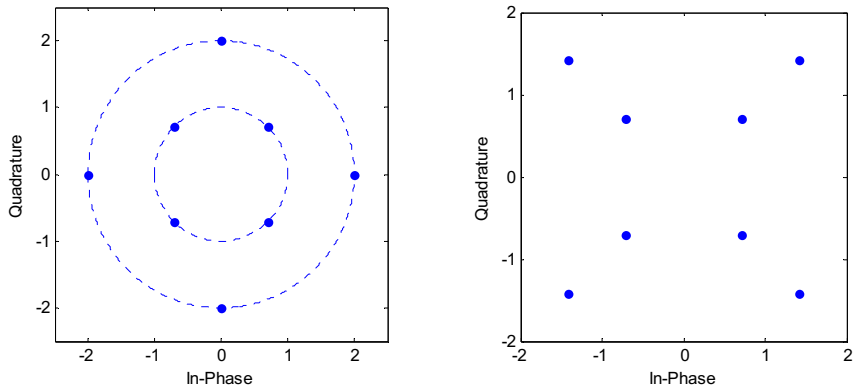

(a) (b)

Figure 2.6 8-QAM signal constellations: (a) circular constellation (b) a star constellation

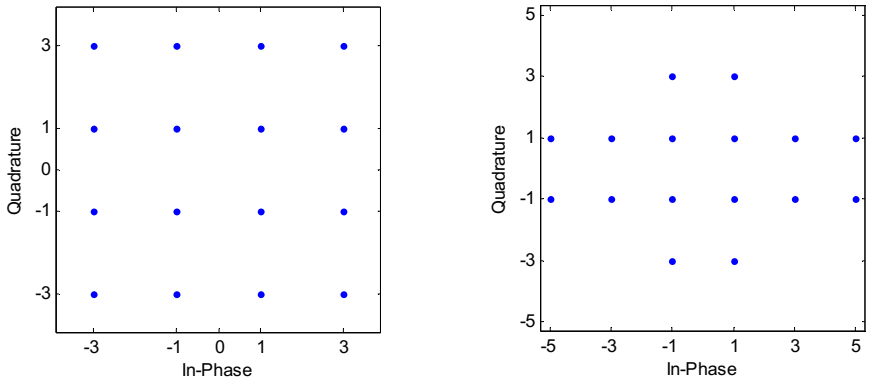

(a) (b)

Figure 2.7 16-QAM signal constellations: (a) square constellation (b) cross constellation

The lowest constellation size for QAM encountered in practice is 8-QAM, because 2-QAM and 4-QAM are essentially binary phase shift keying (BPSK) and

quadrature phase shift keying (QPSK), where information bits are conveyed in the variation of phase alone. It is clear that the more bits per symbol, the more possible arrangements of signal points there are in the M levels of QAM. Some of the common constellations sets are rectangular, circular, cross, and star constellations, as shown in Figure 2.6 and 2.7. Fundamentally, the best constellation set is the one that results in the least average transmit power for a given minimum Euclidean distance. In practice however, the choice of constellation depends on many other factors, including the hardware complexity and the probability of bit error that is dominated by the minimum distance between pairs of constellation points.

Even though rectangular M-QAM constellations are not the best choice of constellation as they do not maximally space the constellation points for a given average power, they are most frequently used in practice. This is because rectangular M-QAM constellations can be readily generated as two PAM signals impressed on phase quadrature carriers, and their demodulation process are relatively easier compared to non-rectangular M-QAM constellations.

2.3.2 Probability of Error for QAM

As digital modulation is performed at the transmitter to transform the information bits into analog signals, demodulation and detection need to be performed at the receiver to recover the information bits from the received signal. Furthermore, the signal received at the receiver is also slightly distorted by the noise from the channel, and it might result in some error of the demodulated information bits. The probability of detection error is dependent on the noise and signal power, which is represented by the SNR of the channel, and also by the spacing of signal points in the signal space [66], [69]. For this reason the exact calculation of the error probability is quite unique

for a particular constellation set and it usually results in a nonclosed-form solution that requires numerical evaluation.

Much work has been done [69]-[72] to evaluate the probability of error for digital modulation schemes over a transmission channel as it is one of the major performance parameters that define the quality of the transmission system. In [66], the probability of a symbol error for square M-QAM with Gray bit mapping over an AWGN channel is given by:

$$P_e = 2\left(1 - \frac{1}{\sqrt{M}}\right) erfc\left(\frac{1.5}{M-1}\frac{\mathcal{E}_s}{N_0}\right) - \left(1 - \frac{2}{\sqrt{M}} + M\right) erfc^2\left(\frac{1.5}{M-1}\frac{\mathcal{E}_s}{N_0}\right) \quad (2.28)$$

where $\mathcal{E}_s/N_0$ is the average SNR per symbol and $erfc(.)$ is the well-known complementary error function. However, the exact closed form of bit error probability or bit error rate (BER) of QAM with arbitrary constellation size has not been established. In [73], the exact analysis of bit error probability is approached using signal-space diagram to find the coherent detection statistic of each Gray-coded bit to obtain the BER. Some general expressions have been established [69], [74] for BER of square M-QAM assuming perfect carrier recovery and symbol synchronization. In [75], an approximation of this BER over AWGN channel is established as a function of received SNR per symbol:

$$BER\left(\frac{\mathcal{E}_s}{N_0}\right) \approx 0.2\, exp\left(\frac{-1.6}{M-1}\frac{\mathcal{E}_s}{N_0}\right) \quad (2.29)$$

This expression of BER is used as it is easily invertible for mathematical analysis of adaptive modulation systems as will be discussed in the later section, and it is claimed to be tight within 1 dB for $M \geq 4$ and BER $\leq 10^{-3}$. The comparison between these approximations and the exact expression (2.29) is presented in Figure 2.8

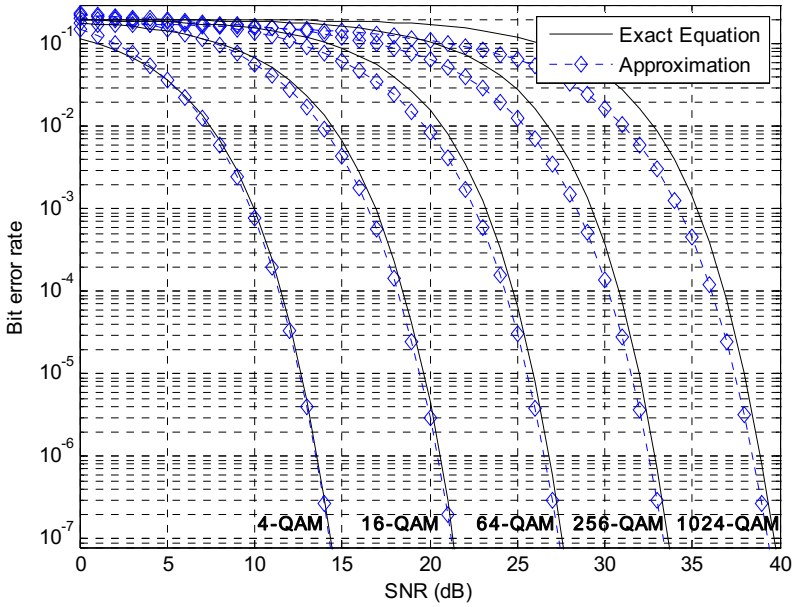

Figure 2.8 BER performances of M-QAM over an AWGN channel

2.4 Adaptive Modulation

Wireless communications systems offer the solution to providing ubiquitous access to communication for the ability of sending data using the air as the medium. At the same time, these wireless links are limited and they have become more and more congested as the wireless services have increased in the last decades. With the advanced technology that enables high bandwidth data transfer over the wireless channel, the wireless service providers are faced with the challenge to utilize the limited radio spectrum in the most efficient way while maintaining a good standard of service. One way of solving this problem is by performing adaptive signaling relative to the channel condition. Instead of fixing the transmission parameters for the worst-case condition of the channel, the parameters can be optimally adjusted to take advantage of the fading characteristic of the wireless channel.

Adaptive transmission was first investigated in the late sixties [1], [76] but the hardware constraint did not allow the realization of this concept. As technology advanced efficient transmission gained priority in wireless systems, adaptive modulation method received more attention from the experts. Several research articles [77]- [79], have demonstrated that uncoded adaptive modulation produces a significant gain in system performance over Rayleigh fading channels given that perfect channel state information is available the transmitter.

The initial idea of adaptive transmission is to maintain a constant signal to noise ratio per bit by varying the transmitted power level [1], [80], [77], constellation size [81]- [84], symbol transmission rate [76], coding [85], [86], or any other combination of transmission parameters [56], [57], [75], [87]- [89]. In terms of choosing the parameters to be adapted, it is shown in [75] that even adjusting only either power or data rate yields close to the maximum possible spectral efficiency obtained by optimal power and rate adaptation. For this reason, rate adaptation with and without power adjustment are both considered in this dissertation.

Adaptive modulation has been widely adopted into 3G cellular systems [90]-[92], WLANs [93]-[95], personal communications [96], wireless sensor networks [97], [98], satellite links [99], [100], and many other wireless systems.

2.4.1 Adaptive Transmission System

A typical discrete-time model of wireless system containing a transmitter, slowly time-varying channel, and a receiver [56] is shown in Figure 2.9. The initial model assumes instantaneous transmission between the transmitter and receiver. The input data $s_T[k]$ is modulated into signal $x_T[k]$ to be sent over a wireless channel. Upon reception of the distorted signal $y_R[k]$, channel identification is performed at the receiver based on some statistical knowledge of the channel and pilot symbols as discussed in the previous section.

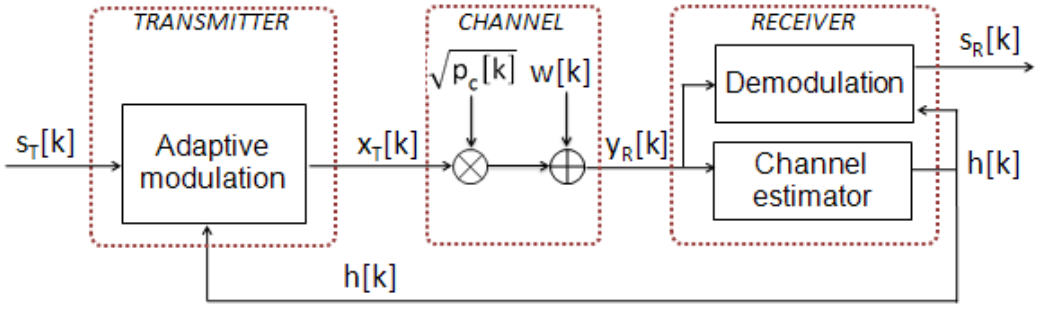

Figure 2.9 Adaptive modulation in wireless system

The channel gain obtained is then used in the demodulation and detection process to retrieve the information bits $s_R[k]$, and it is also sent back to the receiver to be used for decision making. In this section, it is assumed that the channel gain is perfectly obtained at the receiver and instantaneously fed back to the transmitter.

For transmissions with a constant transmit power S, the instantaneous received SNR per symbol is given by $\gamma[k] = \frac{Sp_c[k]}{N_0 B}$, where B denotes the received signal bandwidth . Hence, with the adaptation of transmit power, $S(\gamma[k])$, the received SNR can be written as $\frac{\gamma[k]S(\gamma[k])}{\bar{S}}$, where $\gamma[k]$ is the SNR resulting from transmission with constant transmit power $\bar{S}$. In power adaptation scheme in general, this constant parameter $\bar{S}$ further denotes the average transmit power. Furthermore, with an appropriate scaling of $\bar{S}$, the average channel gain, denoted by σ_h^2, can be normalized to one and the average received SNR becomes $\bar{\gamma} = \frac{\bar{S}}{N_0 B}$.

It is well known that a time-invariant AWGN channel with received SNR γ has capacity of $C_\gamma = Blog_2(1+\gamma)$. For a fading channel with a particular probability distribution of received SNR, $p(\gamma)$, and given that the channel power gain, $p_c[k] = = |h[k]|^2$, is known to both the transmitter and receiver at time k, the average capacity of the time-varying channel can be written as:

$$C = \int_0^\infty Blog_2(1+\gamma)p(\gamma)d\gamma \qquad (2.30)$$

Consider a transmit power adaptation that is subject to an average power constraint $\bar{S}$:

$$\int_0^\infty S(\gamma)p(\gamma)d\gamma \leq \bar{S} \tag{2.31}$$

Adaptation of transmit power with this average power constraint will result in the average capacity of the channel given by (2.30) with the power optimally distributed over time, which leads to a standard definition for the fading channel capacity derived in [101]:

$$C = \int_0^\infty Blog_2\left(1 + \frac{S(\gamma)\gamma}{\bar{S}}\right)p(\gamma)d\gamma \tag{2.32}$$

And the power adaptation which maximizes this capacity follows a water-filling algorithm [102], [103] that depends on $p(\gamma)$ only through an optimal cut-off value of the SNR, denoted by γ_0. The optimal power adaptation strategy is derived as:

$$S(\gamma) = \begin{cases} \frac{1}{\gamma_0} - \frac{1}{\gamma}, & \gamma \geq \gamma_0 \\ 0\,, & \gamma < \gamma_0 \end{cases} \tag{2.33}$$

This adaptation strategy outlines a general rule that more power is allocated for transmission with more favorable channel. Conversely, less power is allocated for transmission when the channel quality degrades and if the channel power gain drops below a limit, the channel will not be used for transmission.

Substituting the power adaptation strategy (2.33) into the average power constraint (2.31) gives:

$$\int_{\gamma_0}^\infty \left(\frac{1}{\gamma_0} - \frac{1}{\gamma}\right)p(\gamma)d\gamma = 1 \tag{2.34}$$

Hence, the cut-off value γ_0 that satisfies this equation leads to an optimal power allocation scheme for a particular time-varying channel with known statistical property $p(\gamma)$.

In [103], Chow proposes a constant-power allocation strategy where transmitter allocates zero power when the channel condition is below a cut-off value and allocates constant power otherwise, mathematically written:

$$S(\gamma) = \begin{cases} S, & \gamma \geq \gamma_0 \\ 0, & \gamma < \gamma_0 \end{cases} \tag{2.35}$$

It is further shown in [77], [104] that this constant-power water-filling strategy is very close to the optimal water-filling algorithm. In particular, the constant-power adaptation algorithm is at most 0.266 bits/s/Hz away from the capacity on Rayleigh channels with perfect channel information at transmitter and receiver [104]. Furthermore, the constant-power adaptation method has low complexity as it is free from logarithm operations.

The performance of this low-complexity power adaptation algorithm is simulated on Rayleigh channel for average channel gain of -10dB and spectral efficiency of this allocation algorithm together with that of the exact water-filling algorithm are plotted against the average power constraint in Figure 2.10. It is seen that the low-complexity algorithm and the exact water-filling [104] give indistinguishable results. Therefore, the constant-power allocation is more favorable to be implemented due to the inexpensive computational cost in achieving almost optimal spectral efficiency.

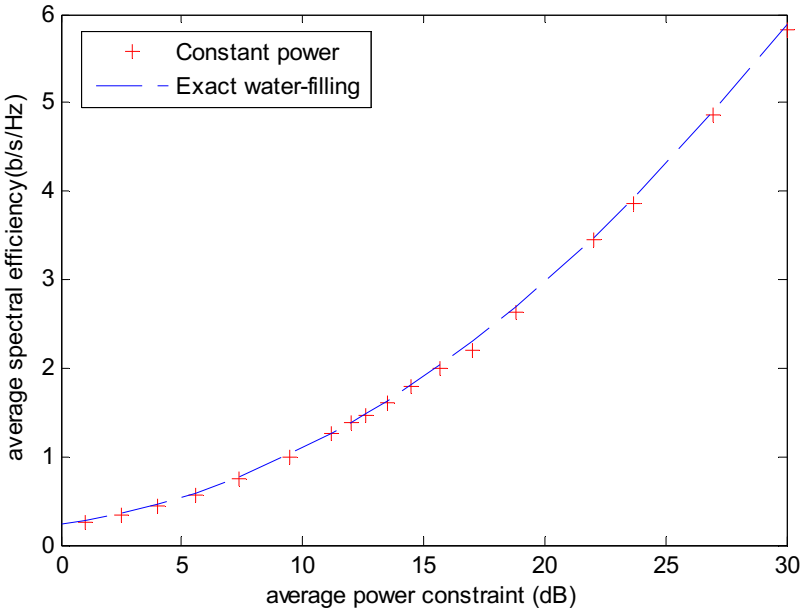

Figure 2.10 Spectral efficiency of exact water-filling and constant-power allocation

In this dissertation, the adaptive modulation scheme is focused on M-QAM over Rayleigh fading channel with a known probability distribution of instantaneous SNR per symbol [105]:

$$p(\gamma) = \frac{1}{\Gamma} exp\left(-\frac{\gamma}{\Gamma}\right) \tag{2.36}$$

where Γ is the average SNR per symbol. Rayleigh fading model is chosen as it has been long established as an acceptable model for a wide range of wireless systems. For interested readers, adaptive modulation schemes over Nakagami fading channels have been discussed in a number of literatures [106], [107], [108], [109], [110]. For M-QAM based transmission via AWGN channel, the approximation of BER can be formulated as a direct function of transmit power, data rate, and SNR [75], as given in chapter 2, and it is used as the design requirement in the adaptation schemes as suggested in the literature.

2.4.2 Variable-rate Constant-power Adaptation for M-QAM

In its simplest form, rate adaptive modulation is performed by switching the modulation mode according to the anticipated SNR, γ, which is proportional to the channel power gain. For a set of N different modulations modes $\boldsymbol{M} = \{M_i, i = 0, \dots, N-1\}$, each with k_i bits per symbol, the i^{th} constellation is applied when the SNR falls with the region $\gamma_i \leq \gamma < \gamma_{i+1}$, where $\gamma_N = \infty$ and γ is the received SNR when the transmit power is constant.

The lowest level of the SNR region boundaries, γ_0, is also known as the threshold SNR, below which transmitter stops transmitting signal. In other words, if the channel condition passed the threshold value, γ_0, then the transmitter sends signal with a constant transmit power S as given by:

$$S(\gamma) = \begin{cases} S, & \gamma \geq \gamma_0 \\ 0, & \gamma < \gamma_0 \end{cases} \tag{2.37}$$

so that it meets the average power constraint:

$$\overline{S} = E[S(\gamma)] = S \int_{\gamma_0}^{\infty} p(\gamma)\, d\gamma \tag{2.38}$$

where $p(\gamma)$ is the probability density function of γ that describes the statistics of a wireless channel model.

This means that the transmit power can be increased above the average value when transmission occur, resulting in a higher received SNR for a given channel power gain compared with the case when the transmit power equals the average value. For channels with a unity channel power gain, the instantaneous received SNR can be given by $\gamma_s = \frac{\gamma S}{\overline{S}}$. Thus, wireless channels with lower power gains, to a certain level, can be used without violating the BER requirement and this in turn increases the spectral efficiency of the link.

The BER requirement refers to the maximum BER that can be tolerated in the transmission system, denoted by BER_{tg}. In [75], the received BER over additive

white Gaussian noise (AWGN) channel for an M-QAM systems with Gray coding and ideal coherent phase detection can be written as:

$$BER(\gamma_s) = 0.2\ exp\left(\frac{-1.6\gamma_s}{M-1}\right) \tag{2.39}$$

where γ_s is the resulted SNR for transmission with transmit power S and constellation size M. When the transmitter applies M-QAM with $k = log_2(M)$ bits per symbol, the instantaneous data rate is equal to $r = k/T_s$, where T_s is the symbol period. Therefore, the rate adaptation problem is equivalent to obtaining the optimal constellation size that fulfills the BER and average power constraints, provided that the same symbol period is used for every modulation mode. In literatures, this adaptation problem can be solved by finding the optimal transmit power gain, $\frac{S}{\overline{S}}$, and the optimal SNR threshold level, γ_0, so that $\text{BER}(\gamma_s) \leq BER_{tg}$ for all $\gamma \geq \gamma_0$. This method of variable-rate constant-power modulation for a Rayleigh channel with known average SNR by solving the average power constraint:

$$S\int_{\gamma_0}^{\infty} p(\gamma)\, d\gamma = \overline{S} \tag{2.40}$$

where the threshold value is founded by solving the equations:

$$0.2\ exp\left(\frac{-1.6}{M_0 - 1}\frac{\gamma_0 S}{\overline{S}}\right) = BER_{tg} \tag{2.41}$$

The performance of this adaptation scheme over a flat Rayleigh fading with a known probability distribution of fading (2.36) is illustrated in [111]. The M-QAM constellation size is restricted to square constellations due to their inherent spectral efficiency and ease of implementation [66]. Two sets of modulation modes are available, the first set contains 3 constellation sizes, $\boldsymbol{M} = \{4, 16, 64\}$ and the second set contains 6 available modulation modes, where the constellation size is chosen from $\boldsymbol{M} = \{4, 16, 64, 512, 1024, 4096\}$. The rate adaptation scheme is designed for maximum $BER_{tg} = 10^{-3}$ and $BER_{tg} = 10^{-7}$, resulting in four designs of rate adaptive modulation. Spectral efficiency and the average BER are the two most important parameters to the measure the performance of adaptive modulation

schemes. These parameters are evaluated for a given value of N, a given value of $\bar{S}$ and a given average SNR, Γ. The spectral efficiency is defined as the average data rate per unit bandwidth, denoted by R/B. Assuming ideal Nyquist data pulses with bandwidth $B = 1/T_s$, the spectral efficiency of a rate adaptive modulation system is equal to the expected number of bits per symbol sent over the wireless channel. For a system applying discrete rate adaptation scheme, it is given by:

$$\frac{R}{B} = \sum_{i=0}^{N-1} k_i \int_{\gamma_i}^{\gamma_{i+1}} p(\gamma) d\gamma \tag{2.42}$$

The average BER for discrete rate adaptation scheme is given by:

$$\overline{BER} = \frac{\sum_{i=0}^{N-1} k_i \int_{\gamma_i}^{\gamma_{i+1}} BER(\gamma) p(\gamma) d\gamma}{\sum_{i=0}^{N-1} k_i \int_{\gamma_i}^{\gamma_{i+1}} p(\gamma) d\gamma} \tag{2.43}$$

The actual average BER is lower than the targeted value by a factor of 10 and it keeps decreasing with an increasing value of average SNR.

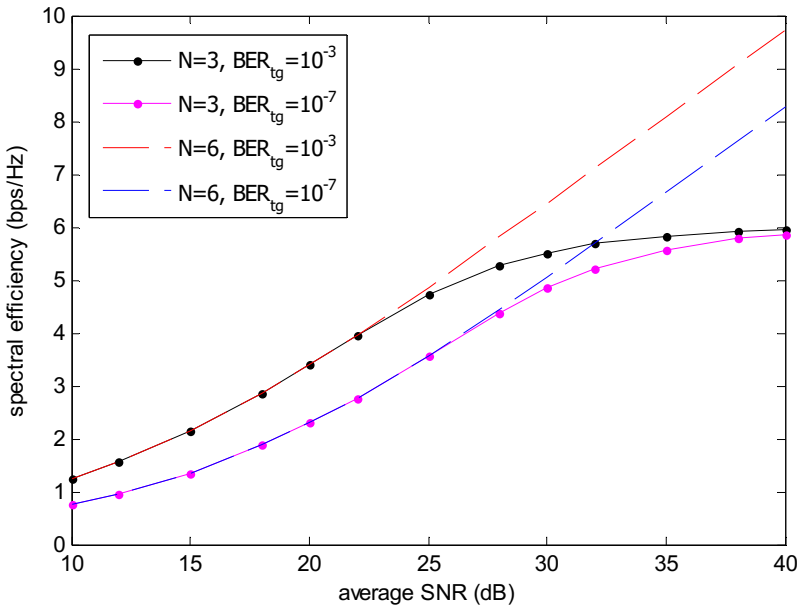

Figure 2.11 Maximum spectral efficiency vs. SNR per symbol for QAM with adaptive rate only

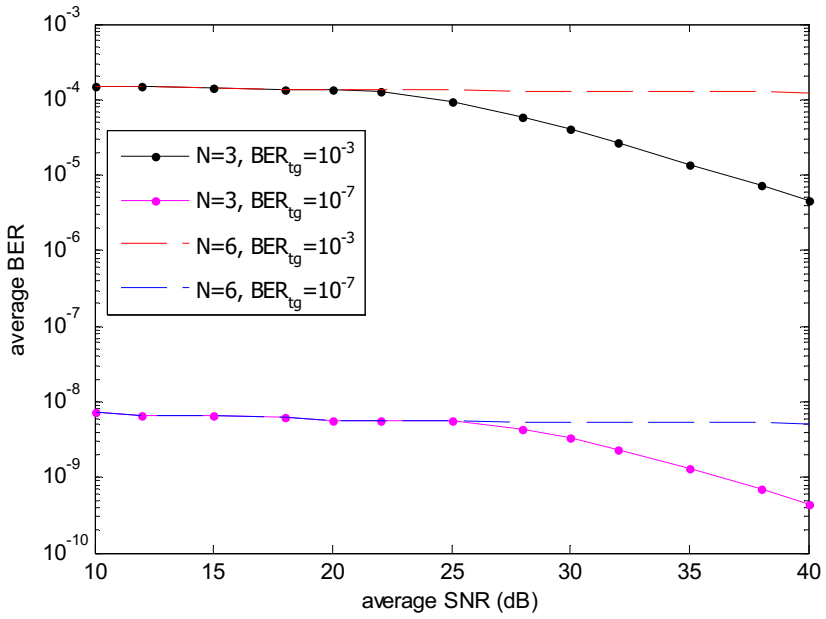

Figure 2.12 Average BER vs. SNR per symbol for QAM with adaptive rate only

It is seen in Figure 2.11 that for average SNR of 10 dB, the spectral efficiency of 2 bps/Hz can be obtained, which implies that mostly BPSK is used, and this is not surprising since this modulation is the most robust to the noise. As the SNR increases, higher level of modulations are used more often, which results in higher the spectral efficiency. With three modulations, however, the spectral efficiency eventually converges to the maximum value of 6 bps/Hz as there is no modulation with more than 6 bits/symbol available, and the BER will be much lower than the prescribed value as seen in Figure 2.12. One way of reducing this gap between the actual and the targeted value of BER is by applying a lower transmit power, which also results in a lower average transmit power. On the other hand, the transmit power can also be increased so that more bits can be sent without violating the BER requirement, as long as the it meets the average transmit power constraint. This leads us to the case of variable rate and variable power modulation scheme.

2.4.3 Variable-rate Variable-power Adaptation for M-QAM

Consider a restricted constellations size $\{M_i, i = 0, \dots, N\}$ where M_0 corresponds to the case of no data transmission. The choice of constellation depends on the instantaneous SNR of the channel γ which is assumed constant during a symbol period for a flat-fading channel. We determine the constellation size corresponding to each γ by discretizing the possible range of SNR into $N + 1$ fading regions, and associate the constellation size M_i with the i^{th} region. In other words, the data rate corresponding to γ falling in the i^{th} region is given by $log_2 M_i$ bits/symbol.

First of all, the case of continuous rate $M(\gamma)$ and continuous power adaptation $S(\gamma)$, subject to a BER requirement and an average power constraint (2.40) is considered. The received SNR becomes $\frac{\gamma S(\gamma)}{\bar{S}}$, and the BER for each value of γ becomes:

$$BER(\gamma) = 0.2\, exp\left(\frac{-1.6\gamma}{M(\gamma) - 1}\frac{S(\gamma)}{\bar{S}}\right) \tag{2.44}$$

For a targeted value of BER, the maximum constellation size that meets the BER requirement can be written as:

$$M(\gamma) = 1 - \frac{1.6\gamma}{ln(5BER_{tg})}\frac{S(\gamma)}{\bar{S}} \tag{2.45}$$

And the power adaptation that maximizes the spectral efficiency for this continuous rate adaptation [56] is similar to the water-filling formula (2.34) outlined in the previous section:

$$\frac{S(\gamma)}{\bar{S}} = \begin{cases} \frac{1}{\gamma_0} - \frac{1}{\gamma K}, & \gamma \geq \frac{\gamma_0}{K} \\ 0\,, & \gamma < \frac{\gamma_0}{K} \end{cases} \tag{2.46}$$

where $\frac{\gamma_0}{K}$ is the optimised cut-off SNR and $K = \frac{-1.6}{ln(5BER_{tg})}$.

Substituting this power allocation into (2.44) gives the relationship between constellation size $M(\gamma)$ and the instantaneous SNR γ :

$$M(\gamma) = \frac{K\gamma}{\gamma_0} \tag{2.47}$$

However, due to the restriction of the constellation size, the largest value of M_i that is smaller than $M(\gamma)$ for the fading level γ is chosen. In other words, M_i is chosen when $\gamma_i^* \leq \gamma < \gamma_{i+1}^*$, with $\gamma_{N+1}^* = \infty$. Thus the SNR region boundaries are located at $\gamma_i^* = M_i \frac{K}{\gamma_0},\ i = 1, \dots, N+1$. Thus, the optimal boundaries can be determined easily for a set of discrete constellation M_i once the optimal γ_0 is obtained.

Once the SNR region boundaries and the associated constellation size are fixed, the transmit power needs to be adjusted to satisfy the average power constraint and the BER requirement. By (2.44), the resulted BER will be fixed for the constellation $M_i > 0$ if the transmit power is adjusted accordingly. This power adaptation can be written as:

$$\frac{S_i(\gamma)}{\bar{S}} = \begin{cases} \dfrac{(M_i - 1)}{K\gamma}, & \gamma_i^* \leq \gamma < \gamma_{i+1}^* \\ 0, & \gamma < \gamma_i^* \end{cases} \tag{2.48}$$

The solution of boundaries can be found by solving for γ_0 that satisfies the average power constraint equation:

$$\sum_{i=1}^{N} \int_{\frac{K}{\gamma_0}M_i}^{\frac{K}{\gamma_0}M_{i+1}} \frac{S_i(\gamma)}{\bar{S}} p(\gamma) d\gamma = 1 \tag{2.49}$$

The maximum spectral efficiency for the discrete-rate continuous power adaptation can be given as the sum of the data rates associated with each of the regions multiplied by the probability that falls in that region:

$$\frac{R}{B} = \sum_{i=1}^{N} log_2(M_i) p(\gamma_i^* \leq \gamma < \gamma_{i+1}^*) \tag{2.50}$$

For Rayleigh fading channel with a known probability distribution of fading (2.36), the maximum spectral efficiency is plotted in Figure 2.13 against the average SNR for different number of constellations *N*.

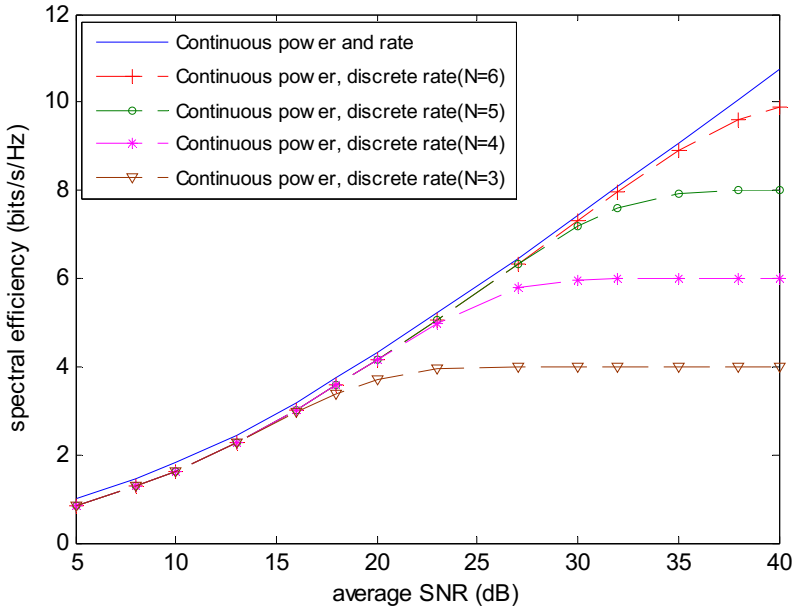

Figure 2.13 Spectral efficiency of rate and power adaptation for QAM with $BER_{tg} = 10^{-3}$

As shown in Figure 2.13, increasing the number of discrete signal constellation N yields a better approximation to the continuous adaptation (2.45), resulting in a higher spectral efficiency. However the choice of number of modulation modes is dictated by how many regions to use and it depends on how fast the channel is changing. For constellation adaptation on a per-symbol basis, the number of regions must be chosen such that the channel gain remains within a region over a symbol time. The trade-off between the number of regions and the rate of power and constellation adaptation is further discussed in [56]. It is seen that restricting the adaptation policy to just six different signal constellation results in a spectral efficiency that is within 1dB of that of continuous rate, yet this restriction is less costly to implement, particularly in a fast fading environments. The average BER for each cases are not shown since it will become equal to the value used for the design, in this case it will be 10^{-3} regardless of the channel conditions, as the power and rate are adapted to maintain the fixed value of BER.

The spectral efficiency of the discrete rate adaptation with and without power adaptation are plotted together in Figure 2.14 for $BER_{tg} = 10^{-3}$. The solid lines and the dashed lines represent the spectral efficiency of variable rate and constant power

adaptive QAM and of variable rate and constant power adaptive QAM respectively. In the case of 3 constellation the choice of modulations are BPSK, QPSK,16-QAM. Therefore the maximum spectral efficiency that can be obtained is 4 bps/Hz, as shown in Figure 2.14. For 6 constellation, the choice of modulations are BPSK, QPSK,16-QAM, 64-QAM, 256-QAM, and 1024-QAM, resulting in maximum spectral efficiency of 10 bps/Hz that is achieved for average SNR of 40 dB with variable rate and power adaptation. More importantly, the diagram pictures the increase in spectral efficiency for a particular channel that is obtained by adjusting transmit power along with the modulation mode.

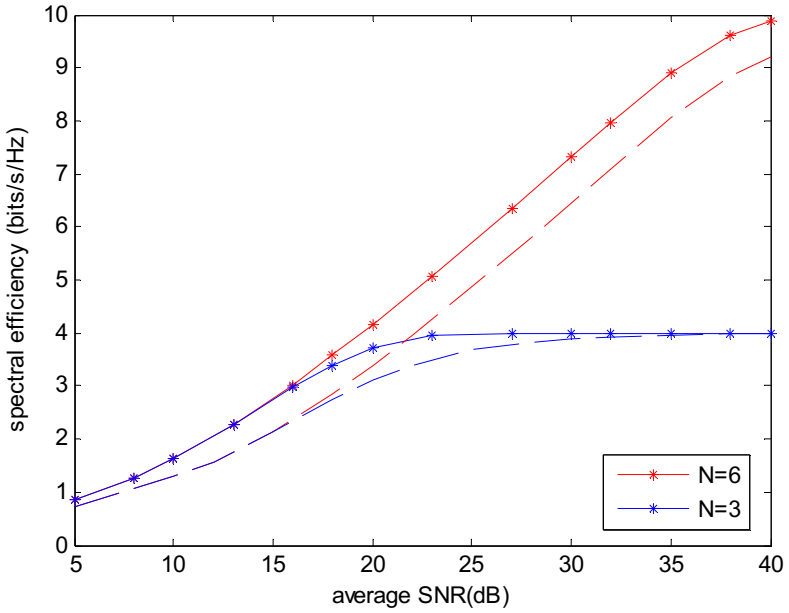

Figure 2.14 Spectral efficiency vs. SNR per symbol in Rayleigh fading channel for $BER_{tg} = 10^{-3}$

2.5 Adaptive M-QAM for Predicted Wireless Channels

In the previous section the channel power gain is assumed perfectly known by the transmitter when the modulation schemes were to be chosen. Nonetheless, obtaining a perfect up-to-date channel state at the transmitter remains a challenge to resolve in wireless communication. In practical systems, there is a delay between the time for which a channel power gain is estimated until this estimated gain is available at the transmitter. Several factors contribute to this delay but the most dominant term is the time it takes to transmit the estimate from receiver to the transmitter through a feedback channel. In systems where the time delay for making the channel power gain available at the transmitter is in the order of the channel coherence time or larger, the estimate will be outdated by the time it reaches the transmitter. This is common to many wireless systems where either the transmitter or the receiver, or both are moving.

The impact of the error of channel estimates on the system performance has been addressed in the literature [109], [112], [113]. In these systems, the error of the estimated value will be simply too large to make it usable for selecting the appropriate modulation scheme. Therefore, a predictor that predicts the channel power gain into future is necessary. Several channel prediction methods have been generally accepted [59], [62], [63], [114], for wireless channels experiencing Rayleigh fading.

An adaptive modulation scheme assisted by an MMSE optimal power predictor is presented in [115], where the optimal rate and transmit power adaptation scheme is derived based on the predicted channel power gain and prediction error variance. It is assumed that the second order channel statistics are known and channel gain is perfectly obtained at receiver for the coherent demodulation. Consider the unbiased quadratic power prediction for Rayleigh fading channels (2.19), the discrete-time channel power gain can be predicted ahead of L multiples of sampling period, as given by:

$$\widehat{p_c}[k+L|k] = \left|\hat{h}[k+L|k]\right|^2 + \sigma_{\varepsilon c}^2 \tag{2.51}$$

where the regressor $\boldsymbol{\varphi}[k]$ is obtained as in (2.7) and the variance for the complex channel prediction error, $\sigma_{\varepsilon c}^2$ is given by (2.14).

The channel gain predictor used for power prediction above is composed by linear filtering of the observed channel gain $h[k]$ which is modeled by a complex circular Gaussian random variable, $h \sim CN(0, \sigma_h^2)$. The predicted channel gain thus has the same distribution trend as it is only a proportional sum of these random variables. Hence, the distribution of the predicted power can also be expressed by an exponential distribution, shifted by $\sigma_{\varepsilon c}^2$:

$$f_{\widehat{p_c}}(\widehat{p_c}) = \frac{1}{\sigma_h^2 - \sigma_{\varepsilon c}^2} exp\left(\frac{\left|\hat{h}\right|^2}{\sigma_h^2 - \sigma_{\varepsilon c}^2}\right) H(\left|\hat{h}\right|^2) \tag{2.52}$$

For transmission with constant power $\bar{S}$, the received SNR can be expressed as a proportional function of the channel power gain:

$$\gamma\{k\} = \bar{\gamma}\frac{p_c[k]}{\sigma_h^2}, \tag{2.53}$$

and the predicted instantaneous received SNR is proportional to the predicted channel power gain, $\widehat{p_c}[k+L|k]$, by:

$$\hat{\gamma}[k+L|k] = \Gamma\frac{\widehat{p_c}[k+L|k]}{\sigma_h^2} \tag{2.54}$$

The Jacobian for the transformation from predicted power to predicted SNR is:

$$\frac{d\hat{\gamma}[k+L|k]}{\widehat{dp_c}[k+L|k]} = \frac{\Gamma}{\sigma_h^2} \tag{2.55}$$

The pdf for the predicted power can thus be obtained as:

$$f_{\hat{\gamma}}(\hat{\gamma}) = \frac{f_{\widehat{p_c}}\left(\widehat{p_c} = \frac{\Gamma}{\sigma_h^2}\hat{\gamma}\right)}{\left|\frac{d\hat{\gamma}}{\widehat{dp_c}}\right|}$$

$$= \frac{H(\hat{\gamma} - \delta)}{\Gamma - \delta} exp\left(-\frac{\hat{\gamma} - \delta}{\Gamma - \delta}\right) \tag{2.56}$$

where $\delta = \Gamma \frac{\sigma_{\varepsilon c}^2}{\sigma_h^2}$, and the conditional probability function of SNR given the predicted value [49] is given by:

$$f_\gamma(\gamma|\hat{\gamma}) = \frac{H(\gamma)H(\hat{\gamma} - \delta)}{\delta} exp\left(-\frac{\gamma + \hat{\gamma} - \delta}{\delta}\right) I_o\left(\frac{2}{\delta}\sqrt{\gamma(\hat{\gamma} - \delta)}\right) \tag{2.57}$$

where $H(.)$ is a Heaviside step function and $I_o(.)$ is the zeroth order modified Bessel function.

Because the constellation size and power are adapted based on the predicted SNR, $\hat{\gamma}$, the instantaneous BER is also in an indirect function of $\hat{\gamma}$, and it is written as:

$$BER(\gamma, \hat{\gamma}) = 0.2\ exp\left(\frac{-1.6\gamma}{M(\hat{\gamma}) - 1}\frac{S(\hat{\gamma})}{\bar{S}}\right) \tag{2.58}$$

The problem of adaptation based on predicted channel gain is solved in [115] to fulfill an expected value of BER over the distribution of γ conditioned on the predicted value $\hat{\gamma}$, for one specific modulation scheme, as given by:

$$BER(\hat{\gamma}) = \int_0^\infty BER(\gamma, \hat{\gamma}) f_\gamma(\gamma|\hat{\gamma}) d\gamma \tag{2.59}$$

where $f_\gamma(\gamma|\hat{\gamma})$ is the pdf of the instantaneous SNR conditioned on the predicted value.

The expected BER for the particular pdf (2.57) is approximately given by:

$$BER(\hat{\gamma}) \approx 0.2\ z(\hat{\gamma})\ exp\left[\left(1 - \frac{\hat{\gamma}}{\delta}\right)\left(1 - z(\hat{\gamma})\right)\right] \tag{2.60}$$

$$z(\hat{\gamma}) = \frac{1}{1 + \mathrm{A}(\hat{\gamma})S(\hat{\gamma})},$$

$$\mathrm{A}(\hat{\gamma}) = \frac{1.6\ \delta}{\bar{S}(M(\hat{\gamma}) - 1)} \tag{2.61}$$

2.5.1 Discrete Rate Adaptation with Constant Power

In this section, the case of variable rate M-QAM with a constant transmit power $S(\hat{\gamma}) = S$ is considered. The fixed transmit power must satisfy the average power constraint:

$$\int_0^\infty S(\hat{\gamma}) f_{\hat{\gamma}}(\hat{\gamma}) d\hat{\gamma} = \bar{S} \tag{2.62}$$

First of all, the choice of constellation size is restricted to a set of values, $\{M_i, i = 0, \dots, N-1\}$. The optimal constellation M_i will be chosen according to the predicted SNR, $\hat{\gamma}$ in a similar manner to the optimal choice of constellation size with a perfect knowledge of SNR in section 2.4.2. The possible range of SNR, $\hat{\gamma}$, is divided into $N+1$ fading regions, and a unique constellation size M_i is associated with the i^{th} region. There will be no transmission if the predicted SNR falls below a cut-off value, $\widehat{\gamma_0}$, otherwise, M_i is chosen when $\hat{\gamma}_i \leq \hat{\gamma} < \hat{\gamma}_{i+1}$.

The expression of BER (2.60) for a constant transmit power, S, and a discrete constellation size M_i can be simplified to:

$$BER(\hat{\gamma}) = \frac{0.2}{1 + A_i S} exp\left[\frac{A_i S}{1 + A_i S}\left(1 - \frac{\hat{\gamma}}{\delta}\right)\right] \tag{2.63}$$

$$A_i = \frac{1.6\,\delta}{\bar{S}(M_i - 1)} \tag{2.64}$$

The average power constraint (2.62) implies that the cut-off SNR $\widehat{\gamma_0}$ should satisfy

$$\frac{S}{\bar{S}} = \frac{1}{\int_0^\infty f_{\hat{\gamma}}(\hat{\gamma}) d\hat{\gamma}} \tag{2.65}$$

which implies that the transmit power used when transmission does occur will be higher than the average value, and the ratio of the constant transmit power and the average power is given by:

$$S_n = \frac{S}{\bar{S}} = exp\left(\frac{\widehat{\gamma_o} - \delta}{\Gamma - \delta}\right) \tag{2.66}$$

In addition to fulfilling the average power constraint, the constellation size needs to be chosen such that the resulting BER meets the requirement, such that:

$$BER(\hat{\gamma}) \leq BER(\hat{\gamma}_i) = BER_{tg}\,, \quad \hat{\gamma} \in [\hat{\gamma}_i, \hat{\gamma}_{i+1}),\ 0 \leq i \leq N-1 \tag{2.67}$$

Substituting (2.63) into (2.67) results in:

$$\hat{\gamma}_i = \delta\left(1 - \frac{1 + A_i S}{A_i S} ln\big(5BER_{tg}(1 + A_i S)\big)\right) \tag{2.68}$$

which is the optimal region boundaries $\{\hat{\gamma}_i\}_0^{N-1}$ that maximizes the spectral efficiency of the variable rate and constant power M-QAM system implementing FIR channel prediction as given in [115].

2.5.2 Discrete Rate and Continuous Power Adaptation

In addition to adapting the modulation scheme, a variable transmit power is implemented to further increase the spectral efficiency of the system. In this case, the transmit power is adjusted for each constellation size M_i such that the BER constraint (2.63) and the average power constraint (2.62) are not violated. This power adjustment within an SNR region associated with constellation size M_i is obtained [115] as:

$$S_i(\hat{\gamma}) = \frac{1}{A_i}\left(\frac{-\delta\ ln(5BER_{tg})}{\hat{\gamma} + \delta\ ln(5BER_{tg})}\right) H\left(\hat{\gamma} + \delta\ ln\big(5BER_{tg}\big)\right),\ \ \hat{\gamma} \in [\hat{\gamma}_i, \hat{\gamma}_{i+1}) \tag{2.69}$$

This adaptation problem is classified as a constraint optimization problem which tries to maximize the spectral efficiency subject to the average constraint and the method of Lagrange multipliers can used to solve this problem. A new variable, λ, called Lagrange multiplier, is introduced and Lagrangian equation is defined by:

$$J(\hat{\gamma}_0, \cdots, \hat{\gamma}_{N-1}, \lambda) = \sum_{i=0}^{N-1} k_i \int_{\hat{\gamma}_i}^{\hat{\gamma}_{i+1}} f_{\hat{\gamma}}(\hat{\gamma}) d\hat{\gamma} + \lambda \left[\sum_{i=0}^{N-1} \int_{\hat{\gamma}_i}^{\hat{\gamma}_{i+1}} S_i(\hat{\gamma}) f_{\hat{\gamma}}(\hat{\gamma}) d\hat{\gamma} - \bar{S}\right] \tag{2.70}$$

Solving for zero partial derivatives:

$$\frac{\partial J}{\partial \lambda} = 0$$

$$\frac{\partial J}{\partial \hat{\gamma}_i} = 0 \quad , \qquad 0 \le i \le N-1$$

results in:

$$S_{i-1}(\hat{\gamma}_i) - S_i(\hat{\gamma}_i) = \frac{k_i - k_{i-1}}{\lambda} \, , \qquad 0 \le i \le N-1 \tag{2.71}$$

where $k_{-1} = 0$ and $S_{-1}(\hat{\gamma}_0) = 0$.

Substituting (2.69) into (2.71) gives:

$$\hat{\gamma}_i = ln(5BER_{tg})\left(\frac{\bar{S}}{1.6}\lambda\Delta_i - \delta\right) \tag{2.72}$$

where

$$\Delta_i = \frac{M_i - M_{i-1}}{k_i - k_{i-1}} \, , \qquad 0 \le i \le N-1 \tag{2.73}$$

The average power constraint for adaptive modulation with a set of discrete constellation size $\{M_i \, \epsilon \, \mathbb{N}, i = 0, 1, \dots, N-1\}$ given the power adaptation (2.71) is given by:

$$\sum_{i=0}^{N-1} \int_{\hat{\gamma}_i}^{\hat{\gamma}_{i+1}} S_i(\hat{\gamma}) f_{\hat{\gamma}}(\hat{\gamma}) d\hat{\gamma}$$

$$= \rho \, exp\left(\frac{\delta\big(1 + ln(5BER_{tg})\big)}{\Gamma - \delta}\right) \times \sum_{i=0}^{N-2} (M_i - 1)\big(Ei(\rho\lambda\Delta_i) - Ei(\rho\lambda\Delta_{i+1})\big)$$

$$+ (M_{N-1} - 1)Ei(\rho\lambda\Delta_{N-1}) \le \bar{S} \tag{2.74}$$

where $Ei(.)$ is the exponential integral and ρ is given by:

$$\rho = \frac{ln(5BER_{tg})\bar{S}}{1.6(\Gamma - \delta)} \, , \tag{2.75}$$

The Lagrange multiplier,λ, can be numerically evaluated for this power constraint and the corresponding optimal SNR region boundaries can be obtained by substituting the computed λ into (2.72).

The variation of normalized transmit power over SNR for the adaptive modulation based on predicted channel with two difference error variances are given in Figure 2.15. The dotted line corresponds to power adaptation in the case of the perfect knowledge of channel.

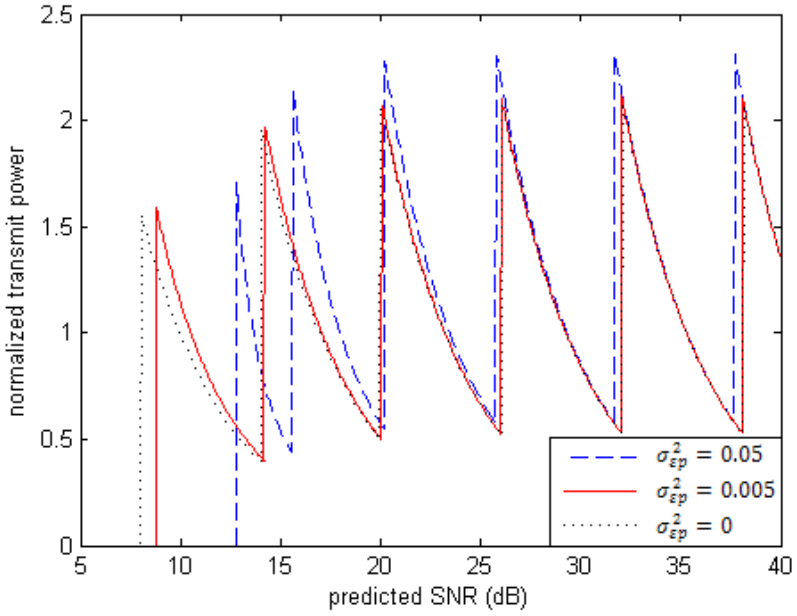

Figure 2.15 Adaptation of the transmit power $S(\hat{\gamma})/\bar{S}$

The discontinuities in the curve correspond to the boundaries of the SNR regions. It is seen that the SNR region boundaries of the upper increases significantly when the variance of the power prediction error is high.

The spectral efficiency of the modulation scheme based on predicted SNR is given by:

$$\frac{R}{B} = \sum_{i=0}^{N-1} k_i \int_{\hat{\gamma}_i}^{\hat{\gamma}_{i+1}} f_{\hat{\gamma}}(\hat{\gamma}) d\hat{\gamma} \tag{2.76}$$

The theoretical value of spectral efficiency can be computed for a given channel with known statistics.

The spectral efficiency for adaptive QAM applying discrete rate and continuous power adaptation and rate adaptation with constant power discussed in in section 2.5.1 are illustrated in Figure 2.16 for two different channel prediction qualities.

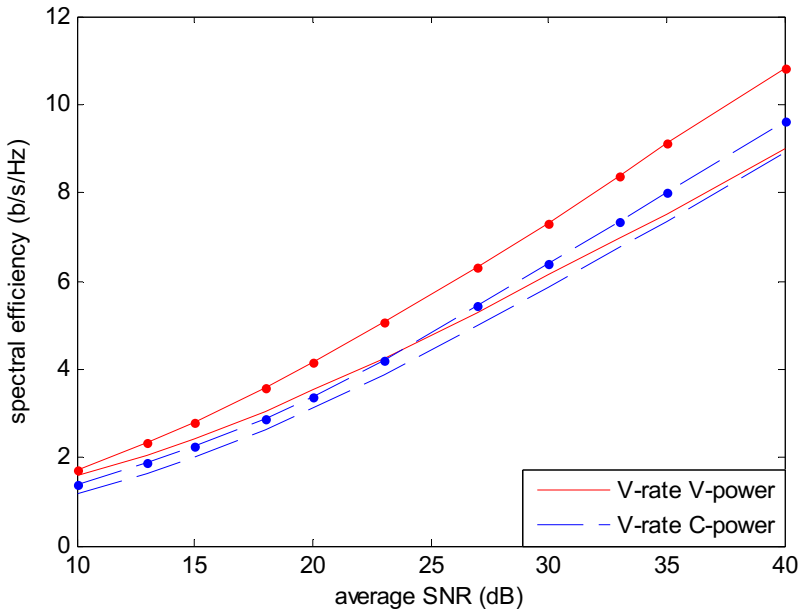

Figure 2.16 Spectral efficiency vs. average received SNR for $BER_{tg} = 10^{-3}$ for adaptive M-QAM based on imperfect channel knowledge. Lines with and without dots correspond to $\sigma_{\varepsilon p}^2 = 0.005$ and $\sigma_{\varepsilon p}^2 = 0.05$ respectively

It is shown that the gain in spectral efficiency when using good predictors is considerable, as compared with the poor predictors. Furthermore, it is seen that when poor predictor is used, the spectral efficiencies of both cases come closer together as the average SNR increases, hence adjusting transmit power alongside constellation side loses its advantage if the channel prediction error is high.

2.6 Positioning of Contributions

It has been demonstrated in the literature that adaptation of rate and transmit power relative to channel condition is essential to maximize the capacity of the wireless channels. Extensive study has been done to obtain an optimal solution of this adaptation problem. A conventional adaptation method has been discussed in the previous section, where adaptation problem for QAM is solved by the optimal SNR region boundaries for switching of modulation modes. For adaptive modulation schemes based on imperfect channel prediction at the transmitter, the optimal solution is based on complex optimization technique which requires complex numerical evaluation of the optimized parameter based on the particular channel statistical characterization.

In this thesis, the problem of adaptive QAM is approached from a new perspective, where the system dynamic equations are established and through the analysis of system stability, a feedback controller is developed to achieve a stable closed-loop system that operates at the optimum operating point. The optimal adaptation is performed using this feedback controller based on the channel condition and BER requirement. The proposed mathematical modeling of the system dynamic also provides the platform for further design of robust adaptation against the channel prediction error.

The same system dynamics equation applies to QAM systems for a particular channel statistical characteristic and average signal-to-noise ratio. Therefore, the same method can be used for any channel in general without expensive computation of the optimal SNR region boundaries for the constraint optimization problem.

Chapter 3

Analytical Model and Analysis of Adaptive Modulation

3.1 Introduction

With the rapid development of wireless technology to deliver high bandwidth data, the demand for greater network capacity keeps increasing and efficient allocation of wireless channels becomes highly significant in the industry. Literature has established that adaptive modulation and coding is one of the key features in achieving highly efficient wireless networks as it allows the data rate to be dynamically adjusted in accordance with the varying quality of the wireless links. In particular, it is demonstrated in [77]- [79] that uncoded adaptive M-QAM significantly increases the capacity of wireless channels experiencing flat Rayleigh fading. However, as it is widely known, adaptive modulation method requires accurate information of the channel gain at the transmitter and different qualities of channel estimation leads to different optimal solutions.

In this chapter, a new perspective to adaptive modulation problem is introduced. The system dynamic equations are established to describe the nature of the adaptation problem for M-QAM systems based on the BER criterion. There are a

number of methods for modeling and analysis of dynamic behavior of a system. One of the prominent models of dynamic systems is transfer function. However, state-space method is chosen in this study for its advantage of fully representing the behavior of a system over time, and it can be easily expanded to accommodate multiple inputs and multiple outputs.

Having established the state-space representation of the system, a feedback controller can be designed to adjust the modulation parameter to meet the adaptation criteria. Through the analysis of system stability, an optimal adaptation technique is proposed that operates at the optimum operating point. Therefore, the adaptation problem can be solved without expensive computation of the optimal SNR region boundaries. The proposed adaptation method based on the system dynamics analysis is verified in MATLAB simulations and the results show that, in the presence of perfect CSI, it behaves similarly to the conventional adaptation method in literature [56], [111], [115],. The imperfection of the channel state information can then be integrated easily into the model for a more suitable design of feedback controller as will be discussed in chapter 4.

3.2 Background

This section presents some concepts in control theory that will be used in the later sections.

3.2.1 State-space Representation of System Dynamics

The use of state-space representation greatly simplifies the mathematical model of system dynamics. In addition, system analysis based on state-space concept enables engineers to design control systems with respect to given performance indexes for specific initial conditions [116]. The state variables of a dynamic system [117] is the smallest set of variables such that the knowledge of these variables at some fixed time

t_0 and the system inputs at all $t \geq t_0$ completely determines the behavior of the system for any instant of time $t \geq t_0$. Given the state of the systems at time t_0 and the input between times t_0 and t_1, one can predict the output at time t_1 for all $t_1 \geq t_0$. A typical discrete-time state-space representation is given by:

$$\boldsymbol{x}[k+1] = \boldsymbol{f}(\boldsymbol{x}[k], \boldsymbol{u}[k], k)$$

$$\boldsymbol{y}[k] = \boldsymbol{g}(\boldsymbol{x}[k], \boldsymbol{u}[k], k) \tag{3.1}$$

$\boldsymbol{x}[k] \in \mathcal{R}^n$ is the state vector, with n representing the number of state variables of the dynamic system, $\boldsymbol{u}[k] \in \mathcal{R}^m$ is the input vector, with m number of inputs to the system, $\boldsymbol{y}[k] \in \mathcal{R}^r$ is the output vector, and $\boldsymbol{f}(.)$ and $\boldsymbol{g}(.)$ each represents a vector of algebraic functions of $\boldsymbol{x}[k]$ and $\boldsymbol{u}[k]$.

Depending on the choice of state variables, which is not unique for a dynamic system, the can be represented by different state-space representations. The state equations, however, are related to each other by some transformation functions.

3.2.2 State Observers

State-space representations describe the dynamics of a system and are commonly used in designing a state feedback controller to achieve a stable closed-loop system. In practice however, not all state variables are available for direct measurement. Hence it is necessary to have a subsystem that can estimate the state variables from the measurable output and control variables, which is also known as a state observer. Nonetheless, state observers can be designed if and only if the observability condition is satisfied [116]. In other words, given that a system is observable, the measurable outputs $\boldsymbol{y}[k]$, can be used to estimate the internal states of the system and additional terms may be included in order to ensure that the estimated states converge to the actual states of the system.

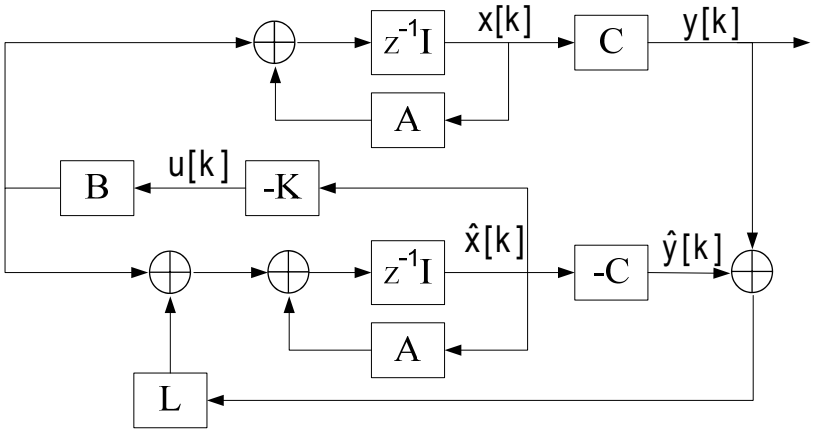

Figure 3.1 Block diagram of a feedback control system with a state observer

Consider a time-invariant linear system represented by the following state-space equations:

$$\boldsymbol{x}[k+1] = \mathbf{A}\boldsymbol{x}[k] + \mathbf{B}\boldsymbol{u}[k]$$

$$\boldsymbol{y}[k] = \mathbf{C}\boldsymbol{x}[k] \tag{3.2}$$

where **A** is an $n \times n$ non-singular matrix**,** **B** is an $n \times r$ matrix**,** and **C** is an $m \times n$ matrix. The system is said to be completely observable if the following condition is met:

$$rank \begin{bmatrix} \mathbf{C}\mathbf{A}^{n-1} \\ \mathbf{C}\mathbf{A}^{n-2} \\ \vdots \\ \mathbf{C} \end{bmatrix} = n \tag{3.3}$$

The states of the system $\boldsymbol{x}[k]$ can then be approximated using a state observer whose states $\hat{\boldsymbol{x}}[k]$ are updated based on a dynamical model:

$$\hat{\boldsymbol{x}}[k+1] = \mathbf{A}\hat{\boldsymbol{x}}[k] + \mathbf{B}\boldsymbol{u}[k] + \mathbf{L}(\boldsymbol{y}[k] - \hat{\boldsymbol{y}}[k])$$

$$\hat{\boldsymbol{y}}[k] = \mathbf{C}\hat{\boldsymbol{x}}[k] \tag{3.4}$$

where **L** is an observer feedback gain matrix of size $n \times m$. Assuming that the system is also completely controllable, a linear combination of the estimated states can be used to control the system, $\boldsymbol{u}[k] = -\mathbf{K}\hat{\boldsymbol{x}}[k]$. The observer gain matrix **L** shall

be chosen such the states estimation errors converge to zero. This condition is further described by the error dynamics of the state observer. The observation error is given by $\boldsymbol{e}[k] = \hat{\boldsymbol{x}}[k] - \boldsymbol{x}[k]$, and the error dynamics can be obtained by subtracting $\boldsymbol{x}[k+1]$ in (3.3) from $\hat{\boldsymbol{x}}[k+1]$ in (3.1):

$$\hat{\boldsymbol{x}}[k+1] - \boldsymbol{x}[k+1] = \mathbf{A}\hat{\boldsymbol{x}}[k] - \mathbf{A}\boldsymbol{x}[k] + \mathbf{L}(\boldsymbol{y}[k] - \hat{\boldsymbol{y}}[k])$$

$$\boldsymbol{e}[k+1] = \mathbf{A}(\hat{\boldsymbol{x}}[k] - \boldsymbol{x}[k]) + \mathbf{LC}(\boldsymbol{x}[k] - \hat{\boldsymbol{x}}[k])$$

$$\boldsymbol{e}[k+1] = \mathbf{A}(\boldsymbol{e}[k]) - \mathbf{LC}(\boldsymbol{e}[k])$$

Hence, the resulting error dynamics are also linear and it is fully described by:

$$\boldsymbol{e}[k+1] = (\mathbf{A} - \mathbf{LC})\boldsymbol{e}[k] \tag{3.5}$$

and the stability of the state observer is determined by the eigenvalues of matrix $\mathbf{A} - \mathbf{LC}$. In control theory, it has been long established that a linear dynamics system in the form of (3.5) is stable if eigenvalues of the transition matrix $\mathbf{A} - \mathbf{LC}$ are located inside the unit circle. Hence, for a given linear system in (3.2), the observer gain matrix $\mathbf{L}$ should be chosen such this condition is fulfilled.

3.3 Adaptive M-QAM over a Wireless Link

Consider the adaptive modulation system model in Section 2.4, it is assumed that the transmission delay and feedback delay are equal and the value is taken as one sampling period, T_s, to introduce a fundamental analytical model. The block diagram of the discrete-time system is shown in Figure 3.2.

Due to the transmission delay, the received signal at receiver is actually the signal transmitted one sampling period earlier. Therefore, in the presence of transmission delay the expression of BER for M-QAM systems with Gray coding and ideal coherent phase detection is written as:

$$BER[k] = 0.2exp\left(\frac{-1.6\Gamma S[k-1]p_c[k-1]}{M[k-1]-1}\right) \tag{3.6}$$

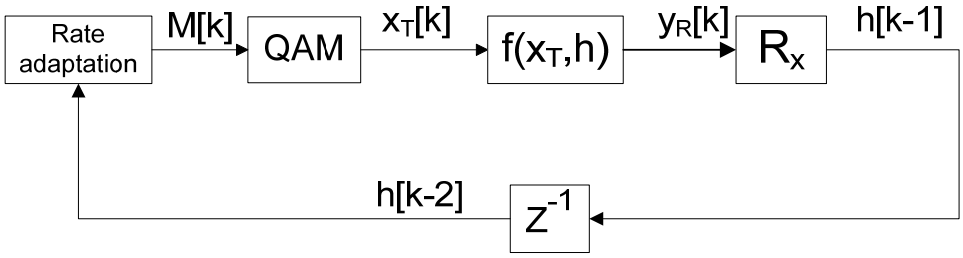

Figure 3.2 Illustration of rate adaptive QAM based on outdated CSI

where Γ is the average received SNR per symbol, S_n is the transmit power normalized by the average value, $p_c[k-1] = |h[k-1]|^2$ is the channel power gain during the last transmission, $S[k-1]$ and $M[k-1]$ subsequently denote the corresponding transmit power and constellation size applied.

3.3.1 System Modeling

The state-space representation of the system is proposed based on the relationship between transmit power, constellation size, and the resulting BER in (3.6) to describe the internal dynamics of the system. The system state variables should be defined to describe the behavior of the system with respect to time. For adaptive modulation systems, with the BER as one of the important system performance parameters, it is essential to observe this parameter. Moreover, in standard communication systems, it is desirable that the BER is equal or lower than an acceptable value, denoted as BER_{tg}. Hence, a state variable can be defined to represents the difference between the BER and the required criterion, which should converge to zero to achieve an optimal performance. Another feature that would be beneficial to observe is the rate of change of BER over time, to provide more information on the trend of the BER. Due to the feedback delay, the BER received at transmitter is the delayed version. Therefore, the output of the adaptation system is defined as a function of the delayed BER. Thus, the state-space variables and output of the system are defined as:

$$x_1[k] = ln(5BER[k-1]) - ln(5BER_{tg})$$

$$x_2[k] = ln(5BER[k]) - ln(5BER[k-1])$$

$$y[k] = x_1[k] \tag{3.7}$$

In the case of transmission ($M[k] > 1$), the dynamics of the adaptation system can be fully described by the state-space equations:

$$x_1[k+1] = \mathrm{x}_1[\mathrm{k}] + \mathrm{x}_2[\mathrm{k}]$$

$$x_2[k+1] = \frac{-1.6\Gamma S_n[\mathrm{k}]\, p_c[k]}{M[k]-1} - \mathrm{x}_1[\mathrm{k}] - \mathrm{x}_2[\mathrm{k}] - ln(5BER_{tg}) \tag{3.8}$$

where $S_n[k] = S[k]/\bar{S}$ denotes the normalized transmit power against the average power. Assuming a perfect knowledge of the channel power at the transmitter, the transmit power and the constellation size can then be adjusted as control inputs to regulate the system output BER such that the system state variables converge to zero and the system remains at this state.

In the next section, a novel approach to the adaptation problem based on system dynamics analysis is proposed in which the constellation size and transmit power are adjusted independently in the attempt of achieving the maximum spectral efficiency for the given BER criterion. In other words, the proposed optimal solution is divided into two stages. First, a variable-rate constant-power adaptation is designed to establish a closed-loop system and the control gain is chosen to ensure the stability of system dynamics. In the second stage, the restriction of available modulation levels in standard digital systems is considered and an independent transmit power allocation scheme is proposed to compensate for the quantization of the data rate.

3.3.2 Rate Adaptation via a State Feedback Controller

For a constant transmit power $\overline{S_n}$, a simple continuous-rate adaptation can be performed by a feedback controller to adjust $M[k]$ such that the system states converge to the equilibrium. First of all, a new input $u[k]$ is introduced such that the

system is input-to-state linearized. The constellation size is therefore chosen as a function of $p_c[k]$ and $u[k]$, mathematically written as:

$$M[k] = \frac{-1.6\Gamma S_n \, p_c[k]}{u[k] + ln(5BER_{tg})} + 1 \tag{3.9}$$

where $u[k]$ is a new control input of the linearized system.

Substituting (3.9) into (3.8) transforms the system dynamics to be:

$$x_1[k+1] = \mathrm{x}_1[\mathrm{k}] + x_2[k]$$

$$x_2[k+1] = \frac{-1.6\Gamma S_n \, p_c[k]}{\left(\frac{-1.6\Gamma S_n \, p_c[k]}{u[k] + ln(5BER_{tg})} + 1\right) - 1} - \mathrm{x}_1[\mathrm{k}] - \mathrm{x}_2[\mathrm{k}] - ln(5BER_{tg})$$

$$= u[k] - \mathrm{x}_1[\mathrm{k}] - \mathrm{x}_2[\mathrm{k}] \tag{3.10}$$

Hence the system is linear and the dynamics of the system can be fully described by a linear matrix equation:

$$\boldsymbol{x}[k+1] = \mathbf{A}\boldsymbol{x}[k] + \mathbf{B}u[k]$$

where

$$\mathbf{A} = \begin{bmatrix} 1 & 1 \\ -1 & -1 \end{bmatrix}, \quad \mathbf{B} = \begin{bmatrix} 0 \\ 1 \end{bmatrix} \tag{3.11}$$

Thus the linear control law $u[k] = -\mathbf{K}\boldsymbol{x}[k]$with an appropriate choice of control gain vector, $\mathbf{K} = [k_1 \quad k_2]$, is sufficient to stabilize the closed-loop system.

The block diagram of the proposed rate adaptive system is shown in Figure 3.3, where block M(.) represents equation (3.9) and the block X(.) represents $\frac{-1.6\Gamma S_n[\mathrm{k}] \, p_c[k]}{M[k]-1} - ln(5BER_{tg})$ in equation (3.8).

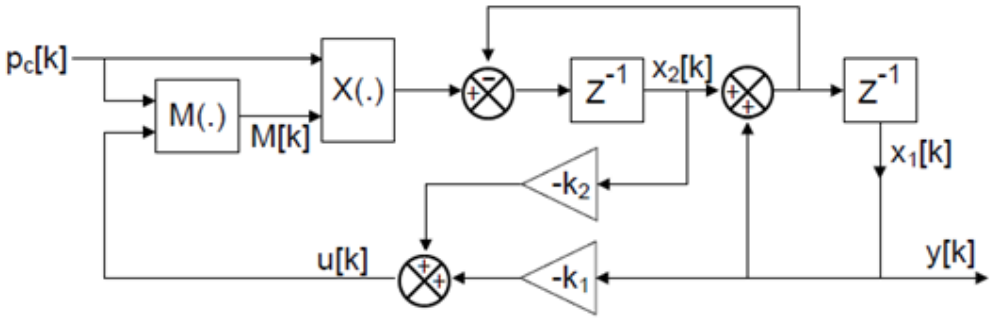

Figure 3.3 Block diagram of the adaptation system

The resulting closed-loop dynamics are as follows:

$$\boldsymbol{x}[k+1] = (\mathbf{A} - \mathbf{BK})\boldsymbol{x}[k] \tag{3.12}$$

The above system is stable if the eigenvalues of matrix $(\mathbf{A} - \mathbf{BK})$ are inside the unit circle. The characteristic equation is given by$|\mathbf{A} - \mathbf{BK} - \lambda\mathbf{I}| = 0$.

$$\begin{aligned} |\mathbf{A} - \mathbf{BK} - \lambda\mathbf{I}| &= \left| \begin{bmatrix} 1 & 1 \\ -1-k_1 & -1-k_2 \end{bmatrix} - \begin{bmatrix} \lambda & 0 \\ 0 & \lambda \end{bmatrix} \right| \\ &= \begin{vmatrix} 1-\lambda & 1 \\ -1-k_1 & -1-k_2-\lambda \end{vmatrix}, \end{aligned} \tag{3.13}$$

and the characteristic equation is given by:

$$\lambda^2 + k_2\lambda + +k_1 - k_2 = 0 \tag{3.14}$$

Hence $\boldsymbol{K}$ must be chosen such that:

$$|\lambda_{12}| = \left| -k_2 \pm \sqrt{{k_2}^2 - 4(k_1 - k_2)} \right| < 2 \tag{3.15}$$

The solution is divided into two cases: real numbered and complex numbered eigenvalues. First, the eigenvalues are real numbers if ${k_2}^2 > 4(k_1 - k_2)$. In order to simplify the equations in the analysis, a new notation is introduced:

$$c = \sqrt{{k_2}^2 - 4(k_1 - k_2)} > 0 \tag{3.16}$$

Equation (3.15) becomes:

$$\left|\lambda_{1,2}\right| = |-k_2 \pm c| < 2 \tag{3.17}$$

which is satisfied only if $|k_2| < 2$.

For the case $|\lambda_1| = |-k_2 + c| < 2$, this inequality leads to:

$$-2 < -k_2 + c < 2$$

$$-2+k_2 < \quad c \quad < 2+k_2 \tag{3.18}$$

By definition, $-2+k_2 \leq -2 + |k_2|$ and it is noted that $|k_2| \leq 2$. Consequently, $-2+k_2 \leq 0$ and therefore the inequality above becomes:

$$0 < \quad c \quad < -2+k_2 \tag{3.19}$$

Substituting (3.16) into the inequality leads to:

$$0 < {k_2}^2 - 4k_1 + 4k_2 < (2+k_2)^2$$

$$-{k_2}^2 < -4k_1 + 4k_2 < 4 + 4k_2$$

$$-4 - 4k_2 < 4k_1 - 4k_2 < {k_2}^2 \tag{3.20}$$

Note that right hand side inequality is also the condition for the real numbered eigenvalues. Furthermore, the left hand side inequality can be simplified as:

$$-1 < k_1 \tag{3.21}$$

In a similar manner, for the case $|\lambda_2| = |-k_2 - c| < 2$, the inequality leads to:

$$-2 < k_2 + c < 2$$

$$-2-k_2 < \quad c \quad < 2-k_2 \tag{3.22}$$

Fundamentally, $-2-k_2 \leq -2 + |k_2|$ and it is noted that $|k_2| \leq 2$. Consequently, $-2-k_2 \leq 0$ and the inequality above becomes:

$$0 < \quad c \quad < 2+k_2 \tag{3.23}$$

Substituting (3.16) into the inequality leads to:

$$0 < {k_2}^2 - 4k_1 + 4k_2 < (2-k_2)^2$$

$$-{k_2}^2 < -4k_1 + 4k_2 < 4 - 4k_2$$

$$-4 + 4k_2 < 4k_1 - 4k_2 < {k_2}^2 \tag{3.24}$$

Once again, the right hand side inequality is also the condition for the real numbered eigenvalues and the left hand side inequality is simplified as:

$$-1 < k_1 - 2k_2 \tag{3.25}$$

Hence, for real numbered eigenvalues, condition (3.15) is satisfied when $4k_1 - 4k_2 < {k_2}^2, k_1 > -1$ and $2k_2 < k_1 + 1$. The domain of k_1 and k_2 that satisfies all three inequalities is marked by shaded region (i) depicted in Figure 3.4.

The next analysis is performed for the case of complex numbered eigenvalues, which is the case if ${k_2}^2 < 4(k_1 - k_2)$. The eigenvalues and their magnitudes are respectively written as:

$$\lambda_{12} = -k_2 \pm \sqrt{-1(-{k_2}^2 + 4(k_1 - k_2))}$$

$$= -k_2 \pm j\sqrt{-{k_2}^2 + 4k_1 - 4k_2} \tag{3.26}$$

$$|\lambda_{12}| = \sqrt{{k_2}^2 + (-{k_2}^2 + 4k_1 - 4k_2)} = \sqrt{4k_1 - 4k_2} \tag{3.27}$$

Hence, the condition (3.13) is satisfied when $k_1 - k_2 < 1$and ${k_2}^2 < 4(k_1 - k_2)$, and the solution to these constraints is showed by shaded region (ii) in Figure 3.4.

Combining the cases of real and complex numbered eigenvalues for the system (3.12), the closed loop system is stable if **K** is chosen within the shaded regions shown in Figure 3.4.

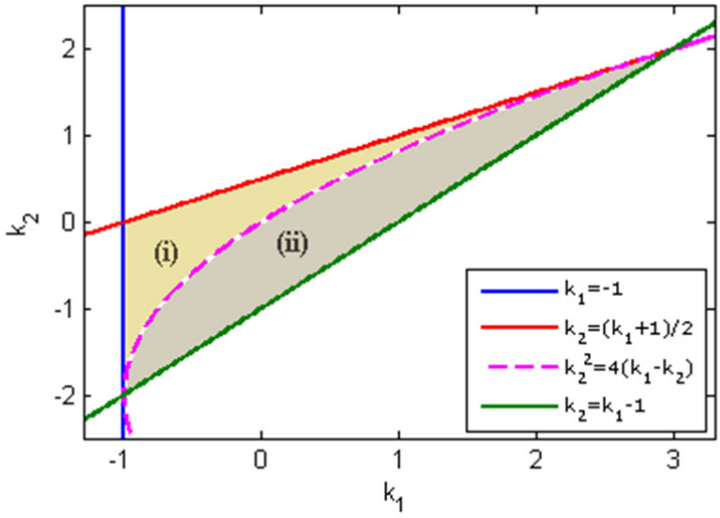

Figure 3.4 A Cartesian plane of the control gain vector $\mathbf{K} = [k_1 \quad k_2]$. The shaded area shows the region in which **K** results in a stable closed loop system. If **K** is located on the left of dashed curve, the eigenvalues are real numbers. Otherwise, the eigenvalues are complex conjugates.

The impact of different locations of closed-loop poles on the z-plane towards the system response is further discussed in the following. The feedback control **K** can be chosen by pole placement method as the closed-loop poles of a system greatly affect the overall system response. For discrete-time systems, the angle of the pole vector with respect to the positive real axis on the z-plane is proportional to the damped frequency, and is related to the natural frequency, ω_n, of the system response. Hence, poles with bigger angle will result in more chattering of the system response. The location of the poles on the z-plane also determines the damping ratio of the system, denoted as ζ. For underdamped systems ($\zeta < 1$), higher damping ratio decreases the maximum percent overshoot of the system response. Furthermore, for second order underdamped systems, the higher ω_n and ζ are, the faster a stable system reaches the steady state. Therefore a moderate value of ω_n and damping ratio within 0.7 and 1 promise a reasonably smooth transient response.

The closed-loop system (3.12) is simulated in MATLAB with different values of control gain **K**, to support the analysis. The closed-loop poles are plotted on the z-

plane with constant ζ and ω_n grids in Figure 3.5 and the corresponding system outputs (3.7) are plotted in Figure 3.6.

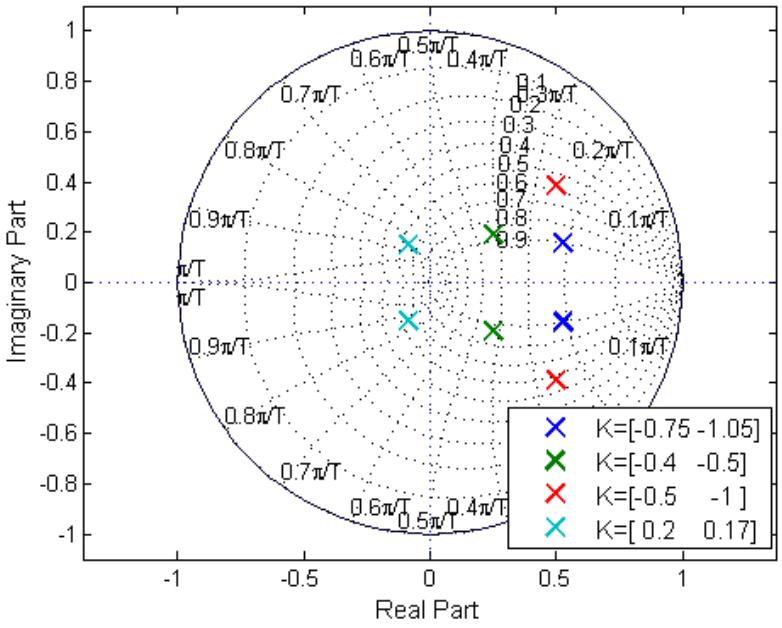

Figure 3.5 Closed-loop pole locations of the system

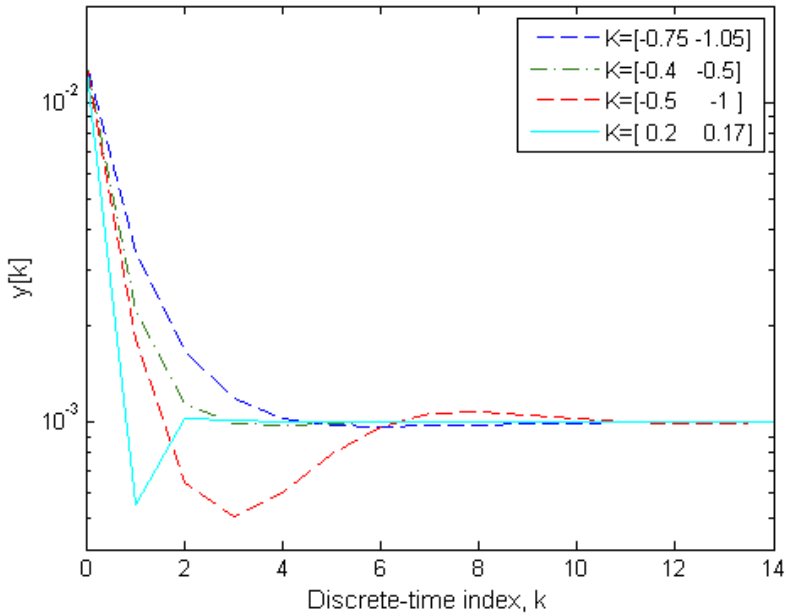

Figure 3.6 BER performance of the closed-loop system

These results show that the systems with closed-loop poles associated with higher ω_n converge faster to the equilibrium. Moreover, the maximum overshoot decreased as ζ increased. It is also seen that, having closed-loop poles associated with $\omega_n = 0.4\pi/T_s$ and $\zeta = 0.9$, control gain $\boldsymbol{K} = [-0.4 \ -0.5]$ results in a damped system with reasonably small settling time, as predicted from the analysis.

3.3.3 Singularity Avoidance

The control input, $M[k]$, however, is not defined when $u[k] = -ln(5BER_{tg})$, hence with $u[k] = -\mathbf{K}\boldsymbol{x}[k]$, the above system in (3.8) has a singularity at:

$$\mathbf{K}\boldsymbol{x}[k] = ln\big(5BER_{tg}\big) \tag{3.28}$$

Switching control input can be designed by adding a small constant to proportional gain such that the system skips this singularity point as the system approaches equilibrium point:

$$M[k] = \begin{cases} \dfrac{-1.6\Gamma S_n \, p_c[k]}{-\mathbf{K}\boldsymbol{x}[k] + ln(5BER_{tg})} + 1, & \mathbf{K}\boldsymbol{x}[k] \neq ln\big(5BER_{tg}\big) \\ \dfrac{-1.6\Gamma S_n \, p_c[k]}{-(1+\delta)\mathbf{K}\boldsymbol{x}[k] + ln(5BER_{tg})} + 1, & \mathbf{K}\boldsymbol{x}[k] = ln\big(5BER_{tg}\big) \end{cases} \tag{3.29}$$

where δ is a small constant to shift the control input such that it is driving the system away from singular point towards the origin. The stability of the system with the switching of input at singularity is analyzed based on Lyapunov stability analysis.

Due to the switching control law in (3.29), the closed-loop system consists of two subsystems, and resulting matrices are derived as:

$$\boldsymbol{x}[k+1] = \begin{cases} \boldsymbol{G_1}\boldsymbol{x}[k], & \boldsymbol{K}\boldsymbol{x}[k] \neq ln\big(5BER_{tg}\big) \\ \boldsymbol{G_2}\boldsymbol{x}[k], & \boldsymbol{K}\boldsymbol{x}[k] = ln\big(5BER_{tg}\big) \end{cases} \tag{3.30}$$

$$\boldsymbol{G_1} = \begin{bmatrix} 1 & 1 \\ -1-k_1 & -1-k_2 \end{bmatrix}, \qquad \boldsymbol{G_2} = \begin{bmatrix} 0 & 1 \\ -1-k_1-\delta k_1 & -1-k_2-\delta k_2 \end{bmatrix}$$

If $\boldsymbol{G_1}, \boldsymbol{G_2}, \dots, \boldsymbol{G_N}$ satisfy simultaneously the linear matrix inequalities

$$\mathbf{G}_i{}^T\mathbf{P}\mathbf{G}_i - \mathbf{P} < 0 \tag{3.31}$$

where **P** is a symmetric positive definite matrix, then a common quadratic Lyapunov function (CQLF) $V(\boldsymbol{x}) = \boldsymbol{x}^T\mathbf{P}\boldsymbol{x}$ exists for the switched system in (3.30). Hence, the overall system is stable under arbitrary switching signal [118], [119].

Let us consider the closed-loop system with control gain $\mathbf{K} = [-0.4 \ -0.5]$ as discussed in the previous section and shifting constant $\delta = 0.01$ such that the matrices of the closed loop system in (3.30) are given by:

$$\boldsymbol{G}_1 = \begin{bmatrix} 1 & 1 \\ -0.6 & -0.5 \end{bmatrix}, \quad \boldsymbol{G}_2 = \begin{bmatrix} 1 & 1 \\ -0.596 & -0.495 \end{bmatrix} \tag{3.32}$$

The switched system is stable if there is a common **P** which simultaneously satisfies the Lyapunov equations:

$$\mathbf{G}_1{}^T\mathbf{P}\mathbf{G}_1 - \mathbf{P} = -\mathbf{Q}_1, \tag{3.33}$$

$$\mathbf{G}_2{}^T\mathbf{P}\mathbf{G}_2 - \mathbf{P} = -\mathbf{Q}_2, \tag{3.34}$$

for some symmetric positive definite matrices $\mathbf{Q}_1$ and $\mathbf{Q}_2$.

Let us choose a symmetrical positive definite matrix $\mathbf{P} = \begin{bmatrix} 0.55 & 0.48 \\ 0.48 & 1.5 \end{bmatrix}$

For $\mathbf{G}_1 = \begin{bmatrix} 1 & 1 \\ -0.6 & -0.5 \end{bmatrix}$,

$$\mathbf{Q}_1 = -(\mathbf{G}_1{}^T\mathbf{P}\mathbf{G}_1 - \mathbf{P}) = \begin{bmatrix} 0.036 & 0.008 \\ 0.008 & 1.055 \end{bmatrix} \tag{3.35}$$

For $\mathbf{G}_2 = \begin{bmatrix} 1 & 1 \\ -0.6 + 0.4\delta & -0.5 + 0.5\delta \end{bmatrix} = \begin{bmatrix} 1 & 1 \\ -0.596 & -0.495 \end{bmatrix}$,

$$\mathbf{Q}_2 = -(\mathbf{G}_2{}^T\mathbf{P}\mathbf{G}_2 - \mathbf{P}) = \begin{bmatrix} 0.039 & 0.011 \\ 0.011 & 1.058 \end{bmatrix} \tag{3.36}$$

It is shown that there exists at least one common Lyapunov function for the proposed system such that the switched linear system is asymptotically stable.

3.3.4 Implementation of a State Observer

As mentioned in the earlier section, in the design of feedback controller, a state observer is implemented to estimate the states from the measurable output, provided that the system meets the observability condition. For the system above, the states are observable as the row rank of the observability matrix $\boldsymbol{O}$ equals to the number of state variables:

$$\boldsymbol{O} = \begin{bmatrix} \boldsymbol{C} \\ \boldsymbol{CA} \end{bmatrix} = \begin{bmatrix} 1 & 0 \\ 1 & 1 \end{bmatrix} \tag{3.37}$$

With state observer, the input of the non-linear system becomes:

$$M[k] = \begin{cases} \dfrac{-1.6\Gamma S_n\, p_c[k]}{-\mathbf{K}\hat{\boldsymbol{x}}[k] + ln(5BER_{tg})} + 1, & \mathbf{K}\hat{\boldsymbol{x}}[k] \neq ln\left(5BER_{tg}\right) \\ \dfrac{-1.6\Gamma S_n\, p_c[k]}{-(1+\delta)\mathbf{K}\hat{\boldsymbol{x}}[k] + ln(5BER_{tg})} + 1, & \mathbf{K}\hat{\boldsymbol{x}}[k] = ln\left(5BER_{tg}\right) \end{cases} \tag{3.38}$$

The closed loop system becomes:

$$\boldsymbol{x}[k+1] = \begin{cases} \boldsymbol{A}\boldsymbol{x}[k] - \boldsymbol{B_1}(\boldsymbol{K}\hat{\boldsymbol{x}}[k]), & \boldsymbol{K}\hat{\boldsymbol{x}}[k] \neq ln\left(5BER_{tg}\right) \\ \boldsymbol{A}\boldsymbol{x}[k] - \boldsymbol{B_2}(\boldsymbol{K}\hat{\boldsymbol{x}}[k]), & \boldsymbol{K}\hat{\boldsymbol{x}}[k] = ln\left(5BER_{tg}\right) \end{cases}$$

$$y[k] = \mathbf{C}\boldsymbol{x}[k],$$

$$\mathbf{A} = \begin{bmatrix} 1 & 1 \\ -1 & -1 \end{bmatrix}, \quad \boldsymbol{B}_1 = \begin{bmatrix} 0 \\ 1 \end{bmatrix}, \quad \boldsymbol{B}_2 = \begin{bmatrix} 0 \\ 1+\delta \end{bmatrix}, \quad \mathbf{C} = [1 \quad 0] \tag{3.39}$$

The state observer dynamics are given by:

$$\hat{\boldsymbol{x}}[k+1] = \begin{cases} \boldsymbol{A}\hat{\boldsymbol{x}}[k] + \boldsymbol{L}(y[k] - \hat{y}[k]) - \boldsymbol{B_1}(\boldsymbol{K}\hat{\boldsymbol{x}}[k]), & \boldsymbol{K}\hat{\boldsymbol{x}}[k] \neq ln\left(5BER_{tg}\right) \\ \boldsymbol{A}\hat{\boldsymbol{x}}[k] + \boldsymbol{L}(y[k] - \hat{y}[k]) - \boldsymbol{B_2}(\boldsymbol{K}\hat{\boldsymbol{x}}[k]), & \boldsymbol{K}\hat{\boldsymbol{x}}[k] = ln\left(5BER_{tg}\right) \end{cases}$$

$$\hat{y}[k] = \boldsymbol{C}\hat{\boldsymbol{x}}[k] \tag{3.40}$$

Let us consider the stable subsystem individually for the analysis of the observer error dynamics. First of all, the error dynamics for the first subsystem can be derived as:

$$\boldsymbol{e}[k+1] = \boldsymbol{A}\hat{\boldsymbol{x}}[k] + \boldsymbol{L}(y[k] - \hat{y}[k]) - \boldsymbol{B_1}\boldsymbol{K}\hat{\boldsymbol{x}}[k] - (\boldsymbol{A}\boldsymbol{x}[k] - \boldsymbol{B_1}\boldsymbol{K}\hat{\boldsymbol{x}}[k])$$

$$= \boldsymbol{A}(\hat{\boldsymbol{x}}[k] - \boldsymbol{x}[k]) + \boldsymbol{L}(\boldsymbol{C}\boldsymbol{x}[k] - \boldsymbol{C}\hat{\boldsymbol{x}}[k])$$

$$= \boldsymbol{A}(\hat{\boldsymbol{x}}[k] - \boldsymbol{x}[k]) - \boldsymbol{LC}(\hat{\boldsymbol{x}}[k] - \boldsymbol{x}[k])$$

$$= (\boldsymbol{A} - \boldsymbol{LC})\boldsymbol{e}[k] \tag{3.41}$$

For the second subsystem, it is expected that the error dynamics will be governed by the same closed-loop matrix $\boldsymbol{A} - \boldsymbol{LC}$, since the control input does not affect the error dynamic equation due to the cancelation as shown in the equations above. Therefore the error dynamics of the state observer are asymptotically stable if the eigenvalues of matrix $\boldsymbol{A} - \boldsymbol{LC}$ are located inside the unit circle. As stated by separation principle in control theory, **K** and **L** can be designed independently without harm to the overall stability of the systems.

The observer errors for the system with $\mathbf{K} = [-0.4 \quad -0.5\,]$ and $\mathbf{L} = \begin{bmatrix} 0.3 \\ -0.4 \end{bmatrix}$ is shown in Figure 3.7 and the BER performance is shown in Figure 3.8, where the dashed line represents the resulting BER in the perfect scenario where the true states are available.

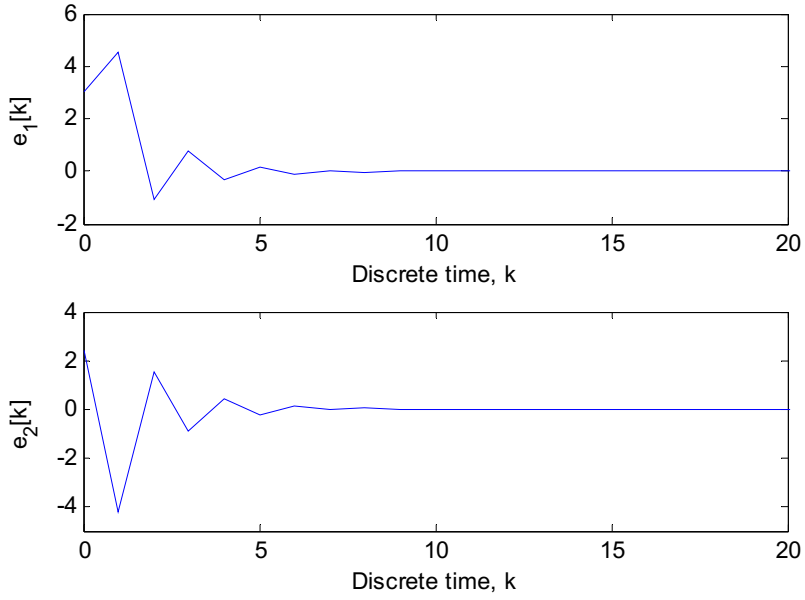

Figure 3.7 Estimation errors of the state observer

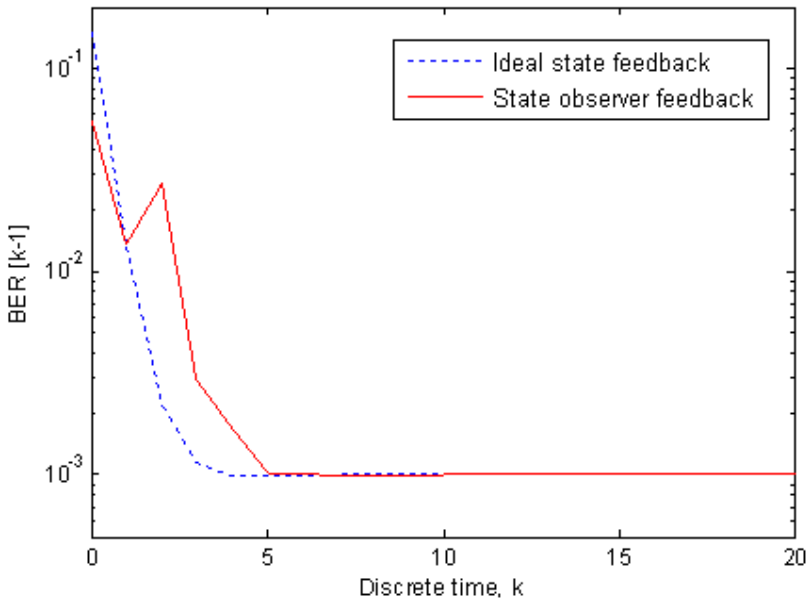

Figure 3.8 Received BER of the adaptation system

3.3.5 Variable Power Adaptation

Although transmission with non-integral rate is possible [120], it requires much higher complexity than the standard integer modulation. Therefore it is better to restrict the modulation modes to a group of *N* square M-QAMs. Clearly, changing the control input will affect the system states based on the dynamics equations. Hence, the transmit power is further adjusted to compensate for this change such that the system states remain unchanged. For a constant targeted BER value and a particular received SNR γ, equation (3.6) can be rearranged to show the proportional relationship between transmit power and constellation size:

$$-1.6\gamma S_n[k] = ln\left(5BER_{tg}\right)\left(M[k]-1\right) \tag{3.42}$$

Therefore, upon the computation of decimal constellation size, the transmit power can be adjusted accordingly to allow transmission with the next higher modulation size within the available sets without changing the overall system dynamics. However, if the resulted transmit power is higher than its upper bound,

S_{max}, the immediate lower constellation size is chosen instead. The instantaneous transmit power adaptation is mathematically written as:

$$S_q[k] = \frac{M_q[k]-1}{M[k]-1}\overline{S_n}, \qquad S_q[k] \le S_{max} \tag{3.43}$$

where $\overline{S_n}$ is the initial constant transmit power, $M[k]$ is the continuous constellation size computed from feedback control input, $M_q[k]$ is the quantized constellation size, and $S_q[k]$ is the corresponding transmit power subject to S_{max}.

Unlike the conventional method, the discrete-rate continuous-power adaptation is performed without the need to determine the optimum SNR region boundaries, and hence reduces the computational complexity of the adaptation scheme. The resulting average power however, is highly depending on the maximum power set for the system. Hence, S_{max} should be chosen so that the average power would be close to the desired value. Furthermore, the system dynamics model allows further development of adaptation to achieve robustness against imperfect channel information.

3.4 Performance Analysis

In this section, the accuracy of the proposed model is examined through comparisons of the several parameters of the adaptive modulation system with the existing optimal adaptation methods presented in literatures. Both the proposed and the conventional discrete-rate continuous-power adaptation schemes are simulated over the same Rayleigh channel for comparison purposes. First of all, a random flat Rayleigh fading channel object based on Jake's model is generated in MATLAB with sampling rate of 20 kHz and the maximum Doppler shift is set to 200 Hz. The additive white Gaussian noise with SNR of 23 dB is used and the required BER is set to 10^{-3}. As discussed in an earlier section, for the proposed feedback based adaptation method, control gain vector of $\mathbf{K} = [-0.4 \;\; -0.5]$ is chosen for a smooth transient response. Two independent sets of simulations are performed for two different modulation sets $\boldsymbol{M} =$

{2, 4, 16} and $\boldsymbol{M} = \{2, 4, 16, 64, 256, 1024\}$ to analyze the behavior of the adaptation schemes with different number of modulation modes over a period of time. The first set of simulation is performed for adaptive modulation systems with three constellations, $\boldsymbol{M} = \{2, 4, 16\}$. The resulted variations of the rate and power over time for boundaries based adaptation method [56] and the proposed feedback based adaptation method are plotted in Figures 3.9 and Figure 3.10 respectively.

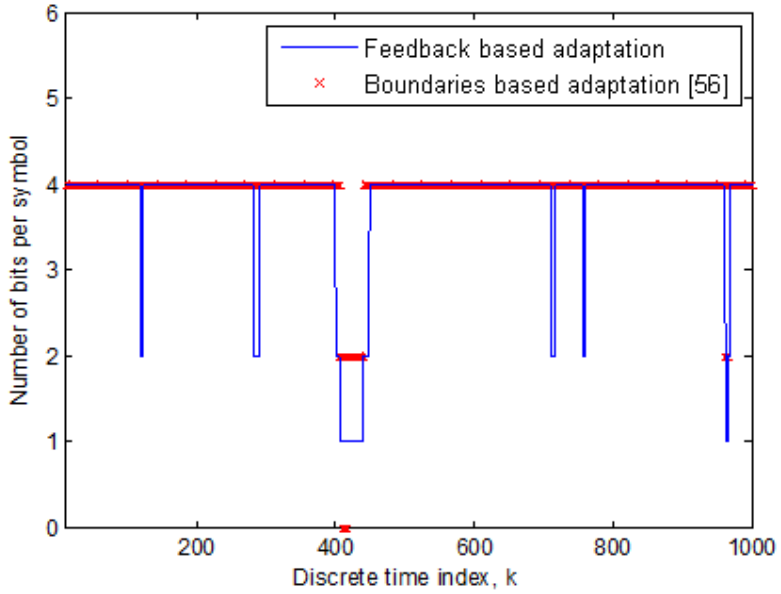

Figure 3.9 Rate variations for adaptive modulation with 3 constellations

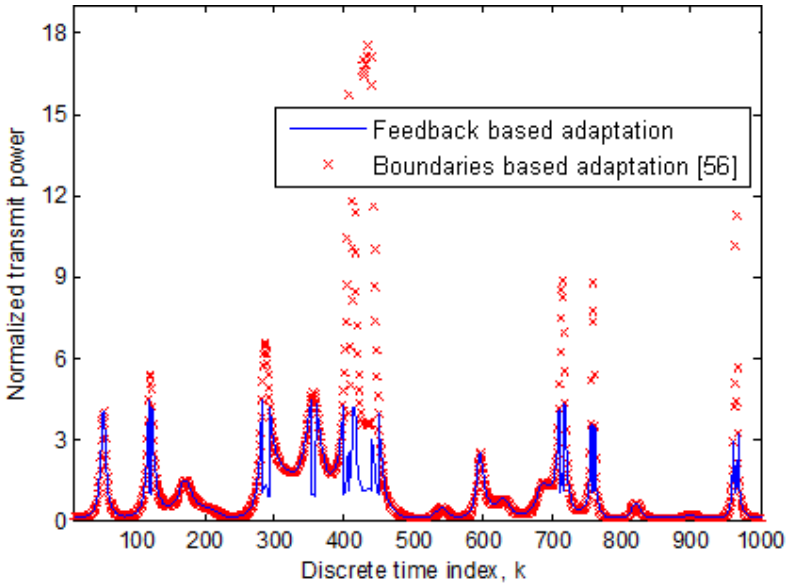

Figure 3.10 Power variations for adaptive modulation with 3 constellations

The results show that the proposed rate adaptation behaves in a similar way to the conventional adaptation method, but with a clear distinction in the power allocation. As seen in Figure 3.10, with the conventional discrete-rate continuous-power in [56], the normalized transmit power, $S[k]/\bar{S}$, occasionally boosts to 18 as the adaptation scheme attempts to fulfill the BER and average power requirements. This extreme power burst in the proposed adaptation method since the power adjustment is performed within an upper bound. The resulted BER for both adaptation schemes is presented in Figure 3.11, which clearly shows that both adaptation methods meet the BER requirement. For this reason, the proposed adaptation method is more feasible for adaptive modulation with few modulation modes.

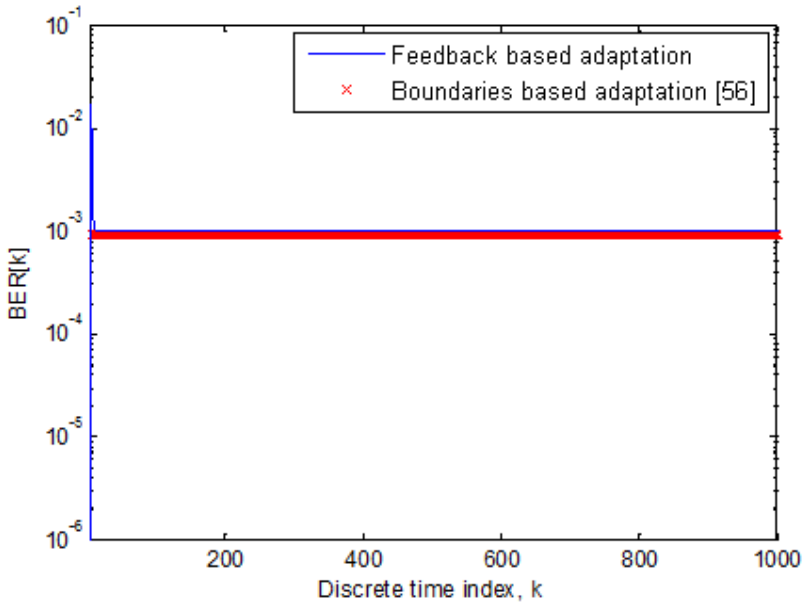

Figure 3.11 Resulted BER for adaptive modulation with 3 constellations

The same simulation is performed for a set of six constellations, $\boldsymbol{M} = \{2, 4, 16, 64, 256, 1024\}$. Both the proposed and the conventional discrete-rate continuous-power adaptation schemes are again simulated over the same Rayleigh channel model and the BER requirement is set to 10^{-3}. The rate and power variations are plotted in Figures 3.12 and Figure 3.13, and the resulted BER is presented in Figures 3.14. The results clearly show that the proposed rate adaptation scheme along with the power adjustment behaves similarly with the conventional adaptation method.

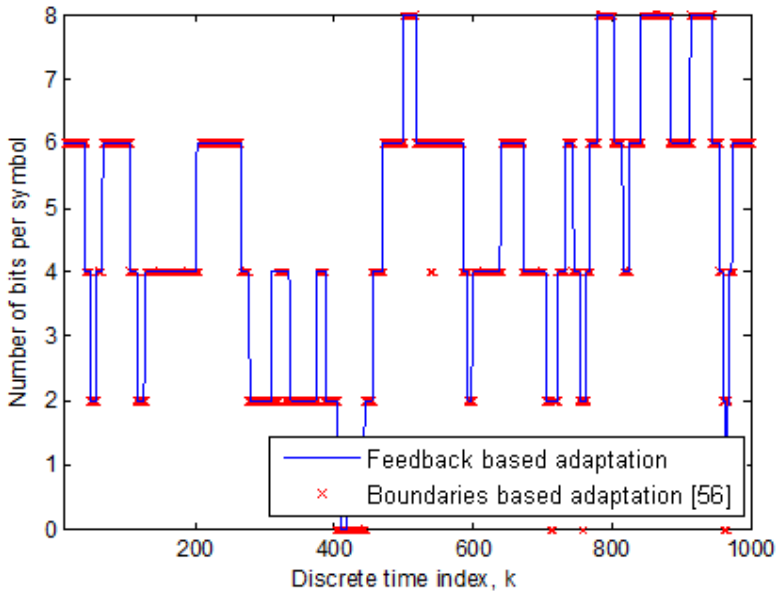

Figure 3.12 Rate variations for adaptive modulation with 6 constellations

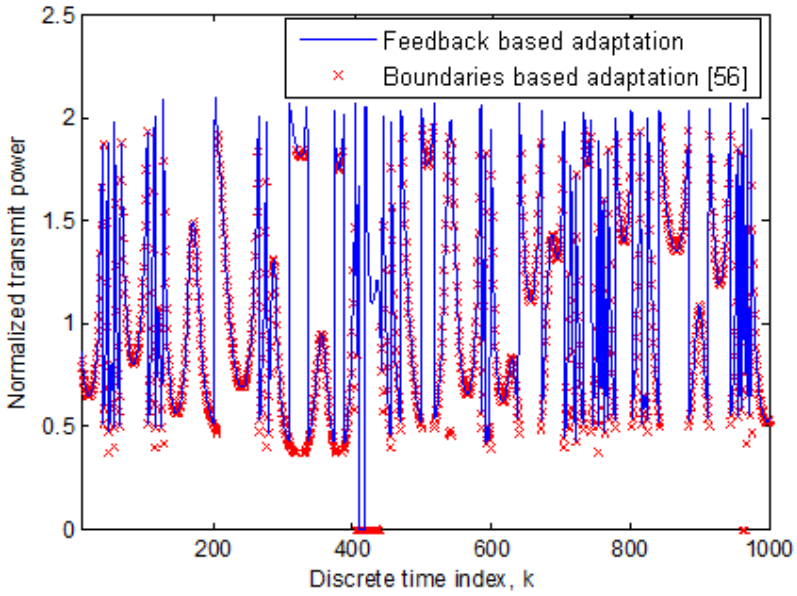

Figure 3.13 Power variations for adaptive modulation with 6 constellations

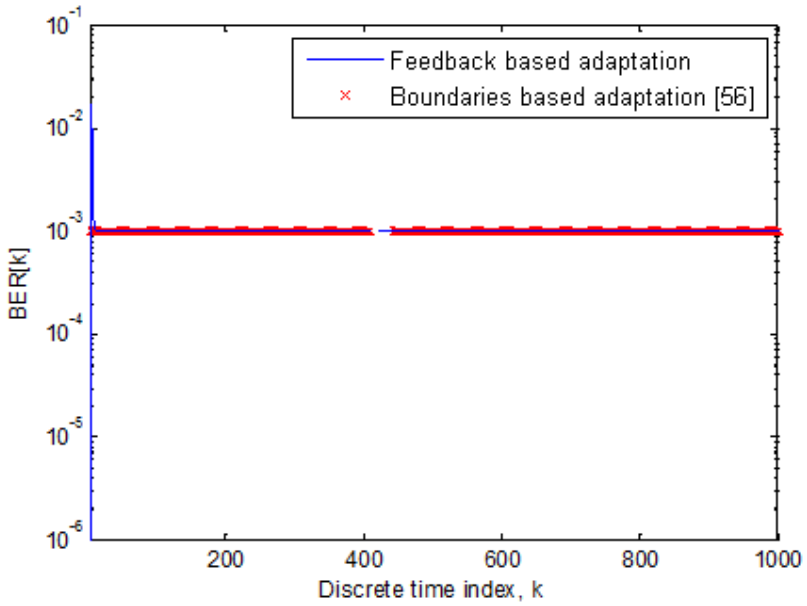

Figure 3.14 Resulted BER for adaptive modulation with 6 constellations

Another set of simulations is performed to evaluate the performance of the M-QAM adaptive system in terms of the spectral efficiency, average transmit power and average received BER. Both the proposed discrete-rate continuous-power adaptation method and the conventional method are performed on the same M-QAM system, under the same fading environment and BER requirements. The same set of constellations, $\boldsymbol{M} = \{2, 4, 16, 64, 256, 1024\}$, is used for a fair comparison of the system performance. Assuming ideal Nyquist data pulses with bandwidth $B = 1/T_s$, the spectral efficiency of a channel in a fixed M-QAM system is equal to the number of bits per symbol. Hence, for a variable M-QAM system, the spectral efficiency can be computed as the expected number of bits per transmitted symbol. In the simulations, the spectral efficiency is numerically computed as the average number of bits sent over a total number of samples, given by:

$$\frac{R}{B} = \frac{1}{L}\sum_{k=1}^{L} log_2\big(M_q[k]\big), k = 1, \dots, L \tag{3.44}$$

Similarly, the transmit power is averaged over L sampling points for each Rayleigh fading channel with a particular average SNR. In this simulation, the

average values are computed over 2 million points and the results are plotted over a range of average SNR values, Γ, for several BER_{tg} of 10^{-3}, 10^{-5}, and 10^{-7}.

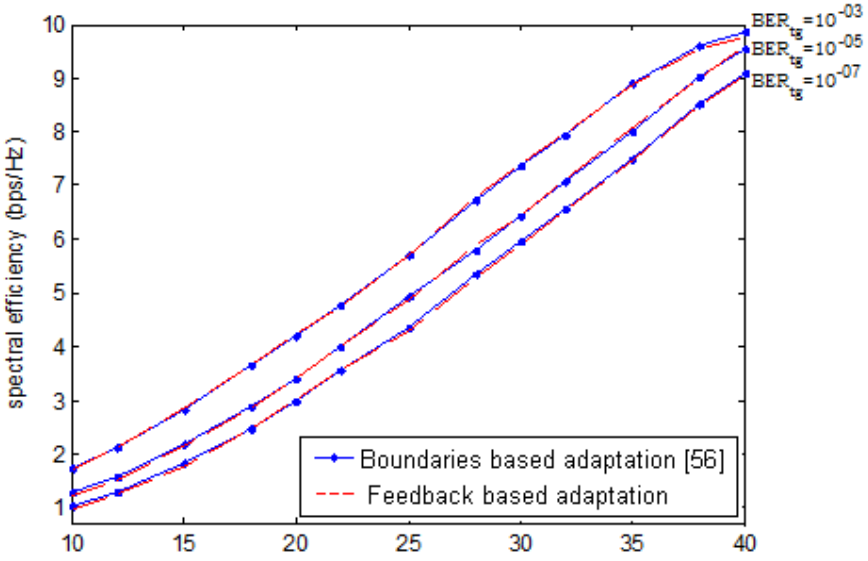

Figure 3.15 Spectral efficiency vs. average SNR

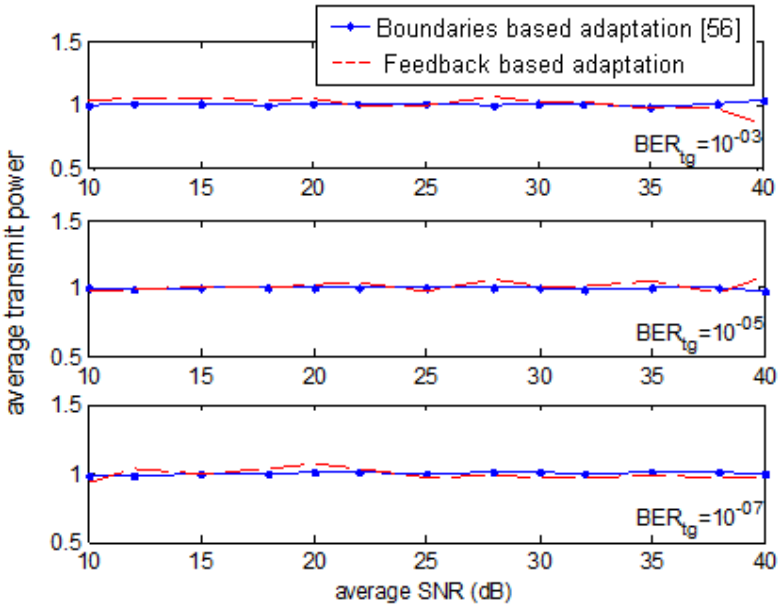

Figure 3.16 Average transmit power vs. average SNR

Figure 3.15 and Figure 3.16 show that the spectral efficiency and the average transmit power of the M-QAM system based on the system dynamics analysis agree with that of the existing method presented in literature and the BER requirements are well observed as shown in Figure 3.17.

Hence, the accuracy of the system dynamics model is verified. Moreover, the analytical model of the M-QAM adaptive system developed in this paper has its potential to be used in the further design of an optimal controller that is robust to channel interference and other disturbances from the environment.

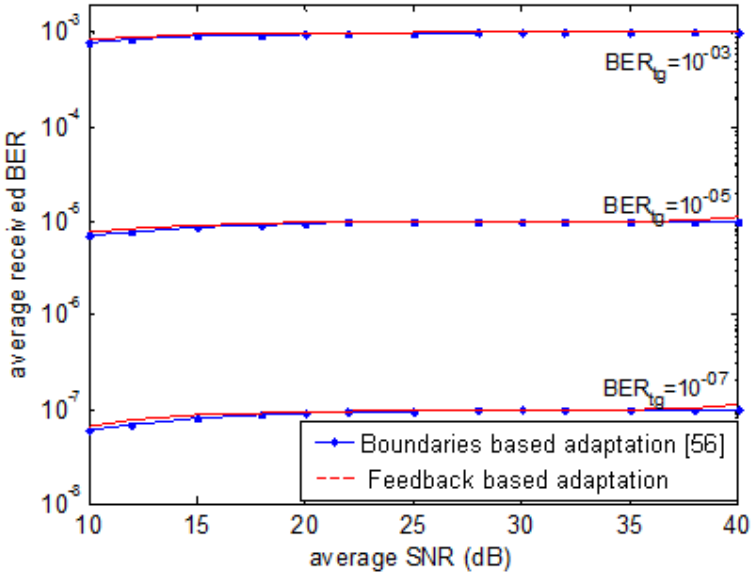

Figure 3.17 Average received BER vs. average SNR

3.5 Conclusion

In this chapter, discrete-rate continuous-power adaptation problem is approached from a different perspective by means of system dynamics analysis. A state-space representation of the M-QAM system is introduced where the state variables are defined as the discrepancies between the recent received BER and the targeted BER in logarithmic form. A continuous-rate constant-power adaptation scheme is first

realized via an appropriate state feedback controller to drive the states asymptotically to zero. The transmit power is further adjusted to accommodate for the limited choices of discrete square constellation size. Moreover, some extreme power bursts could be prevented by constraining the permissible transmits power.

Simulations are carried out in MATLAB to compare the performance of system with the proposed method and with the conventional optimal SNR boundaries based adaptation method. The results uncovered that the spectral efficiency and average transmit power of both methods were very close, while the BER constraints are not violated. However, the proposed adaptation scheme does not involve any complex optimization problem and hence reduces the computational complexity of the system. In the next chapter, the system dynamics established in this paper is used as the basic mathematical model for designing a robust controller to handle the inaccuracy of channel state information in the wireless environment.

Chapter 4

Adaptation Method with Imperfect Prediction of Channel Power Gain

4.1 Introduction

It has long been known that the performance of adaptive modulation techniques is highly dependent on the accurate information of the current channel state. However, in wireless communications, this up-to-date channel condition is not feasible at the transmitter due to the rapid variation of the wireless channel. Even though advances in technology these days have made it possible to model and predict the channel state to a certain extent, a consistently accurate estimation still remains a challenge. Therefore, it is more practical to take into account the prediction error in the design of adaptation system, which is the focus of this chapter. In Chapter 3, the fundamental system dynamics equations with assumption of perfect CSI are established and verified through simulations. In this chapter, the actual channel power gain is represented by the predicted value and its prediction error, which can be modeled as a Gaussian random variable with zero mean and a known variance. The resulted system dynamics therefore are described by stochastic difference equations. In stochastic systems analysis, Kalman filtering is a well known recursive algorithm for

performing statistically optimal estimation of unknown states of a system based on a series of noisy measurement [121]. For this reason, the author chooses to implement Kalman filter as a state observer in the proposed adaptation system to optimally estimate the system states in the presence of channel prediction error.

4.2 Overview of Discrete-time Kalman Filter

Kalman filter is a minimum error variance estimator of the unknown states of a dynamic system that involves random perturbations. It is shown in [122] that Kalman filter is the optimal estimator for a well-modeled, one-dimensional linear system with measurement errors drawn from a Gaussian distribution with zero-mean.

Consider a linear stochastic system with state-space representation:

$$\boldsymbol{x}[k+1] = \mathbf{A}\boldsymbol{x}[k] + \mathbf{B}\boldsymbol{u}[k] + \mathbf{G}\boldsymbol{w}[k] \tag{4.1}$$

with a measurement vector:

$$\boldsymbol{z}[k] = \mathbf{C}\boldsymbol{x}[k] + \boldsymbol{v}[k] \tag{4.2}$$

where $[k] \in \mathcal{R}^n$, $\boldsymbol{u}[k] \in \mathcal{R}^m$, $\boldsymbol{w}[k] \in \mathcal{R}^n$, $\boldsymbol{z}[k] \in \mathcal{R}^r$, $\boldsymbol{v}[k] \in \mathcal{R}^r$, $\{\boldsymbol{w}[k]\}$ and $\{\boldsymbol{v}[k]\}$ are white zero mean Gaussian random vectors with joint covariance matrix:

$$E\left[\begin{pmatrix} \boldsymbol{w}[k] \\ \boldsymbol{v}[k] \end{pmatrix} (\boldsymbol{w}^{\boldsymbol{T}}[k] \quad \boldsymbol{v}^{\boldsymbol{T}}[k])\right] = \begin{bmatrix} \boldsymbol{Q} & 0 \\ 0 & \boldsymbol{R} \end{bmatrix} \tag{4.3}$$

and they represent the process and measurement noise respectively.

Let $\hat{\boldsymbol{x}}[k|k-1]$ denotes a priori state estimate at time k given the knowledge of the system prior to time k, and $\hat{\boldsymbol{x}}[k|k]$ denotes a posteriori state estimate at time k. The a priori and a posteriori estimate errors are respectively defined as:

$$\boldsymbol{e}[k|k-1] = \boldsymbol{x}[k] - \hat{\boldsymbol{x}}[k|k-1] \tag{4.4}$$

$$\boldsymbol{e}[k|k] = \boldsymbol{x}[k] - \hat{\boldsymbol{x}}[k|k] \tag{4.5}$$

The a priori estimate error covariance is defined by:

$$\boldsymbol{P}[k|k-1] = E\left[\boldsymbol{e}[k|k-1]\boldsymbol{e}^{\boldsymbol{T}}[k|k-1]\right] \tag{4.6}$$

And the a posteriori estimate error covariance is:

$$\boldsymbol{P}[k|k] = E\left[\boldsymbol{e}[k|k]\boldsymbol{e}^{\boldsymbol{T}}[k|k]\right] \tag{4.7}$$

In Kalman filter algorithm, the a posteriori state estimate is essentially a corrected state estimate based on the a priori state estimate and noisy measurement $\boldsymbol{z}[k]$ at time *k*, given by:

$$\hat{\boldsymbol{x}}[k|k] = \hat{\boldsymbol{x}}[k|k-1] + \boldsymbol{L}[k](z[k] - \mathbf{C}\hat{\boldsymbol{x}}[k|k-1]) \tag{4.8}$$

The time-variant matrix, $\boldsymbol{L}[k]$, is called the Kalman gain matrix and the optimal solution that minimizes the minimum error covariance in (4.7), as elaborated in [121], [123], is given by:

$$\boldsymbol{L}[k] = \boldsymbol{P}[k|k-1]\mathbf{C}^{\boldsymbol{T}}(\mathbf{C}\boldsymbol{P}[k|k-1]\mathbf{C} + \boldsymbol{R})^{-\mathbf{1}} \tag{4.9}$$

Kalman filtering process itself is essentially a recursive algorithm that involves two stages: prediction and correction stages. In the prediction stage, the a priori estimate and error covariance matrix are obtained by updating the values from the previous cycle:

$$\hat{\boldsymbol{x}}[k|k-1] = \mathbf{A}\hat{\boldsymbol{x}}[k-1|k-1] + \mathbf{B}\boldsymbol{u}[k] \tag{4.10}$$

$$\boldsymbol{P}[k|k-1] = \boldsymbol{A}\boldsymbol{P}[k-1|k-1]\boldsymbol{A}^{\boldsymbol{T}} + \mathbf{G}\mathbf{Q}\mathbf{G}^{\mathbf{T}} \tag{4.11}$$

In the correction stage, the Kalman gain matrix is computed using (4.9) and then the measurement $\boldsymbol{z}[k]$ is obtained. These parameters are then used in the computation of the a posteriori estimate and the corresponding error covariance matrix as follows:

$$\hat{\boldsymbol{x}}[k|k] = \hat{\boldsymbol{x}}[k|k-1] + \boldsymbol{L}[k](z[k] - \mathbf{C}\hat{\boldsymbol{x}}[k|k-1]) \tag{4.12}$$

$$\boldsymbol{P}[k|k] = \boldsymbol{P}[k|k-1] - \boldsymbol{G}(\boldsymbol{C}\boldsymbol{P}[k|k-1]) \tag{4.13}$$

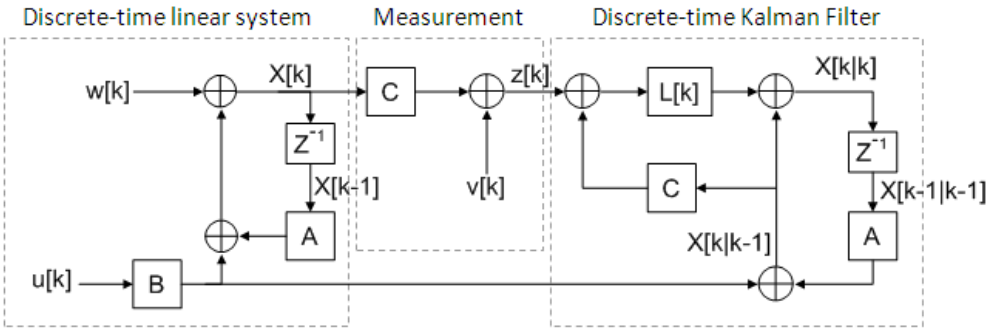

Figure 4.1 Block diagram of linear system, measurement model, and Kalman filter

These two stages are counted as one cycle in the recursive Kalman filter algorithm. This repetitive nature is one of the appealing features of Kalman filter, as the current estimates are conditioned on all of the past measurements summarized in the estimate from the previous cycle [124]. The relation of the filter to the system itself is depicted in a block diagram of Figure 4.1 [125].

Due to the robust nature and relative simplicity of the filter, it is used in many practical areas, such as image processing [126], [127], tracking [128], and navigation [129]-[131]. Particularly in wireless communication systems, Kalman filter has been used in channel estimation and equalization of Rayleigh fading channel based on autoregressive model [24], [25], [132]-[136].

In this dissertation, Kalman filter is used to handle the stochastic parameter that is present in the system due to the imperfect channel prediction, as will be discussed in the next section.

4.3 Adaptive Modulation based on Imperfect CSI

In Chapter 3, a novel rate adaptation is proposed assuming that the channel is perfectly known at the transmission to be used in the computation of the modulation parameter. The system dynamics equations are described by the state-space representation:

$$x_1[k+1] = x_1[k] + x_2[k] \tag{4.14}$$

$$x_2[k+1] = \frac{-1.6\Gamma S_n[k]p_c[k]}{M[k]-1} - x_1[k] - x_2[k] - ln(5BER_{tg}) \tag{4.15}$$

However, in practice, the true channel power gain is not available at the transmission due to the time-varying nature of the wireless channel. It is in fact modeled as a stochastic variable with some statistical characteristics, as discussed in the Chapter 2.

An unbiased power predictor is proposed in [137] based on MMSE-optimal linear prediction of the channel with known statistics:

$$\widetilde{p_c}[k] = \boldsymbol{\theta^H \varphi}[k]\boldsymbol{\varphi}^H[k]\boldsymbol{\theta} + \sigma_h^2 - \boldsymbol{\theta^H R_\varphi \theta} \tag{4.16}$$

where $\boldsymbol{\varphi}[k]$ is the vector of the past observations of which the correlation matrix is denoted by $\boldsymbol{R_\varphi}$, σ_h^2 is the average channel power gain, and $\boldsymbol{\theta}$ is the optimal complex coefficients that minimized the mean square error. The power prediction error of the unbiased predictor has zero mean and the variance is given by:

$$\sigma_{\varepsilon_p}^2 = (\sigma_h^2)^2 - \left|\boldsymbol{r}_{h\varphi}^H \boldsymbol{R}_\varphi^{-1} \boldsymbol{r}_{h\varphi}\right|^2 \tag{4.17}$$

Assuming noiseless channel estimation at the receiver, the correlation matrix $\boldsymbol{R_\varphi}$ and $\boldsymbol{r}_{h\varphi}$ for Rayleigh fading channel can be computed for a given Doppler frequency.

For a constant power rate adaptation as proposed in Chapter 3, the constellation size is therefore adjusted based on the predicted channel power gain instead:

$$M[\mathrm{k}] = \frac{-1.6\Gamma S_n \widetilde{p_c}[k]}{u[k] + ln(5BER_{tg})} + 1, \tag{4.18}$$

where $u[k] = -\mathbf{K}\boldsymbol{x}[k] \neq ln\left(5BER_{tg}\right)$. Substituting the constellation size (4.18) into the system dynamics (4.15), results in the closed-loop system dynamic equations:

$$\boldsymbol{x}[k+1] = \begin{bmatrix} 1 & 1 \\ -1 & -1 \end{bmatrix} \boldsymbol{x}[k] + \begin{bmatrix} 0 \\ \dfrac{p_c[k]}{\widetilde{p_c}[k]} \end{bmatrix} u[k] + \begin{bmatrix} 0 \\ \left(\dfrac{p_c[k]}{\widetilde{p_c}[k]} - 1\right) ln(5BER_{tg}) \end{bmatrix} \tag{4.19}$$

The unknown channel power gain can be expressed as the sum of the predicted channel power gain (4.16) and its prediction error, $p_c[k] = \widetilde{p_c}[k] + \varepsilon_p[k]$. Therefore, the closed loop system can further be expressed as the function of prediction channel power and the prediction error:

$$\boldsymbol{x}[k+1] = \begin{bmatrix} 1 & 1 \\ -1 & -1 \end{bmatrix} \boldsymbol{x}[k] + \begin{bmatrix} 0 \\ 1 + \dfrac{\varepsilon_p[k]}{\widetilde{p_c}[k]} \end{bmatrix} (-\mathbf{K}\boldsymbol{x}[k]) + \begin{bmatrix} 0 \\ \dfrac{\varepsilon_p[k]}{\widetilde{p_c}[k]} ln(5BER_{tg}) \end{bmatrix}$$

$$= \mathbf{G}\boldsymbol{x}[k] + \mathbf{H}(\boldsymbol{x}[k])\varepsilon_p[k],$$

$$\mathbf{G} = \begin{bmatrix} 1 & 1 \\ -1 - k_1 & -1 - k_2 \end{bmatrix}, \quad \mathbf{H}(\boldsymbol{x}[k]) = \begin{bmatrix} 0 \\ \dfrac{-\boldsymbol{K}\boldsymbol{x}[k] + ln(5BER_{tg})}{\widetilde{p_c}[k]} \end{bmatrix} \tag{4.20}$$

The resulted system is a linear deterministic/stochastic system in the presence of power prediction error that can be treated as the process noise with a known variance, denoted by $\sigma_{\epsilon p}^2$. By using Kalman filter, the channel states can be optimally estimated given that some statistical properties of the noise present in the system and the measurement vector, $z[k] = \boldsymbol{C}\boldsymbol{x}[k] + v[k]$, where $v[k]$ is the measurement error assumed to be zero-mean Gaussian with a known variance σ_v^2. Due to transmission and feedback delay, only state $x_1[k]$ can be computed at the transmitter from the delayed channel gain fed back from the receiver:

$$x_1[k] = ln(5BER[k-1]) - ln(5BER_{tg})$$

$$= -\frac{-1.6\Gamma S_n p_c[k-2]}{M[k-2]-1} - ln\left(5BER_{tg}\right) \tag{4.21}$$

and the measurement gain is given by $\mathbf{C} = [1 \quad 0]$.

The algorithm for the states update based on Kalman filter can be summarized as following, assuming that the initial a priori estimate and error covariance matrix are known:

$$\hat{\boldsymbol{x}}[k|k-1] = \mathbf{G}\hat{\boldsymbol{x}}[k-1|k-1] \tag{4.22}$$

$$\boldsymbol{P}[k|k-1] = \mathbf{G}\boldsymbol{P}[k-1|k-1]\mathbf{G}^T + \boldsymbol{H}[k]\sigma_{\epsilon p}^2\boldsymbol{H}[k]^T \tag{4.23}$$

$$\boldsymbol{L}[k] = \boldsymbol{P}[k|k-1]\mathbf{C}^{\boldsymbol{T}}(\mathbf{C}\boldsymbol{P}[k|k-1]\mathbf{C} + \sigma_v^2)^{-1} \tag{4.24}$$

$$\hat{\boldsymbol{x}}[k|k] = \hat{\boldsymbol{x}}[k|k-1] + \boldsymbol{L}[k](z[k] - \mathbf{C}\hat{\boldsymbol{x}}[k|k-1]) \tag{4.25}$$

$$\boldsymbol{P}[k|k] = \boldsymbol{P}[k|k-1] - \boldsymbol{L}[k](\mathbf{C}\boldsymbol{P}[k|k-1]) \tag{4.26}$$

where matrix $\boldsymbol{H}[k]$ is updated in every iteration based on the a priori estimate:

$$\boldsymbol{H}[k] = \begin{bmatrix} 0 \\ \dfrac{-\boldsymbol{K}\hat{\boldsymbol{x}}[k|k] + ln(5BER_{tg})}{\widetilde{p_c}[k]} \end{bmatrix} \tag{4.27}$$

Having estimated the states through Kalman filtering, the continuous rate adaptation can be performed by adjusting the constellation size based on predicted channel power gain and the a posteriori estimate:

$$M[k] = \frac{-1.6\Gamma S_n \widetilde{p_c}[k]}{-\mathbf{K}\hat{\boldsymbol{x}}[k|k] + ln(5BER_{tg})} + 1 \tag{4.28}$$

The computed transmission rate is further quantized to the nearest lower rate available to transmit data in general adaptive modulation system with a set of *N* discrete constellations. Note that in stochastic systems, Kalman filtering helps to compensate some noise to a certain extent and the resulted estimated state would have some fluctuation around the actual state due to the randomness of the process noise. Hence, the BER resulting from the rate adaptation will also experience some fluctuation around the expected value. However, rounding down the computed constellation size would result in a lower or equal BER of the expected value, and this would compensate the undesirable BER fluctuation resulting from the process noise.

The block diagram of the adaptation system with Kalman filter at the transmitter side is shown in Figure 4.2, where M(.) represents the feedback controller that determines the modulation size in (4.28), and this value is rounded to the appropriate discrete *M* used in QAM to encode the information bits into analog signal $x_T[k]$. Note that the channel gain $h[k-2]$ is fed back from the receiver and the channel power gain is computed and predicted based on this feedback and known statistical properties of the channel.

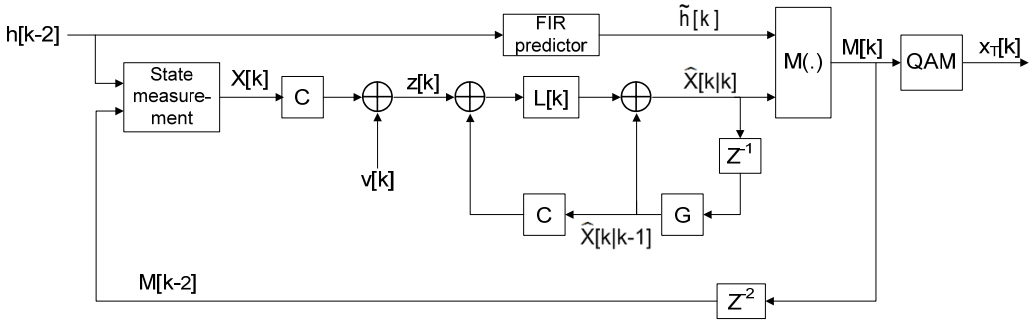

Figure 4.2 Block diagram of the adaptation system with Kalman filter

In environments where the channel is varying slowly enough to achieve accurate estimation, Kalman filter should be an optimal estimator to mitigate the noise such that the estimated state variables are close to the actual values, and the BER fluctuation should not be as severe. In this case, the transmit power might also be adjusted along with the number of bits per symbol to achieve a higher throughput. Hence, after obtaining the decimal constellation size, the transmit power can be increased to a certain limit to choose the next higher modulation size within the available sets for transmission. If the transmit power required to achieve the same BER with a higher constellation is above the upper bound, S_{max}, a lower constellation is chosen instead. The instantaneous transmit power adaptation is mathematically written as:

$$S_q[k] = \frac{M_q[k]-1}{M[k]-1}\overline{S_n}, \qquad S_q[k] \le S_{max} \tag{4.29}$$

where $\overline{S_n}$ is the initial constant transmit power, $M[k]$ is the continuous constellation size computed from feedback control input, $M_q[k]$ is the quantized constellation size, and $S_q[k]$ is the corresponding transmit power subject to S_{max}.

In the next section, the performance of an adaptive M-QAM system with the proposed methods is analyzed through simulations in MATLAB.

4.4 Simulation Results and Discussion

Simulations are performed in MATLAB to evaluate the performance of the proposed adaptation method based on the noisy prediction of the channel state. The proposed adaptation method with Kalman filter is compared with an existing adaptation method based on optimal SNR region boundaries as presented in the literature [115]. First of all, a random flat Rayleigh fading channel object based on Jake's model is generated with a sampling frequency of 20 kHz and the additive white Gaussian noise with SNR of 25 dB is used. The maximum Doppler frequency is adjusted accordingly such that unbiased power prediction in (4.16) generates a specific channel power prediction error variance. A feedback control gain vector of $\mathbf{K} = [-0.4 \;\; -0.5]$ is used in the system. The variance of measurement error is set to $\sigma_v^2 = 0.01$ to accommodate possible error in computation of the state $x_1[k]$, which might rise from some reasonably small noise in the feedback channel. Finally the discrete rate adaptation is performed based on a set of six constellations $\boldsymbol{M} = \{2, 4, 16, 64, 256, 1024\}$ available at the transmitter. Simulations are performed for $\sigma_{\epsilon p}^2 = 0.01$ and $\sigma_{\epsilon p}^2 = 0.1$ to illustrate the performance of adaptation methods in coping with different scales of prediction errors.

The rate adaptation and resulted BER over time are presented in Figure 4.3 and Figure 4.4 for BER constraints of 10^{-3} over Rayleigh channel with maximum Doppler frequency where prediction error covariance, $\sigma_{\epsilon p}^2$, is equal to 0.01.

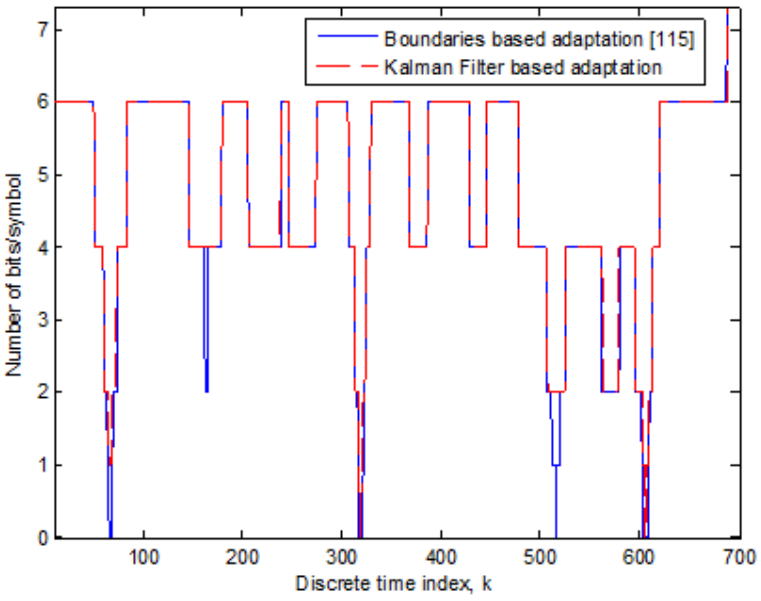

Figure 4.3 Rate variations for adaptive modulation with $\sigma_{\epsilon p}^2 = 0.01$

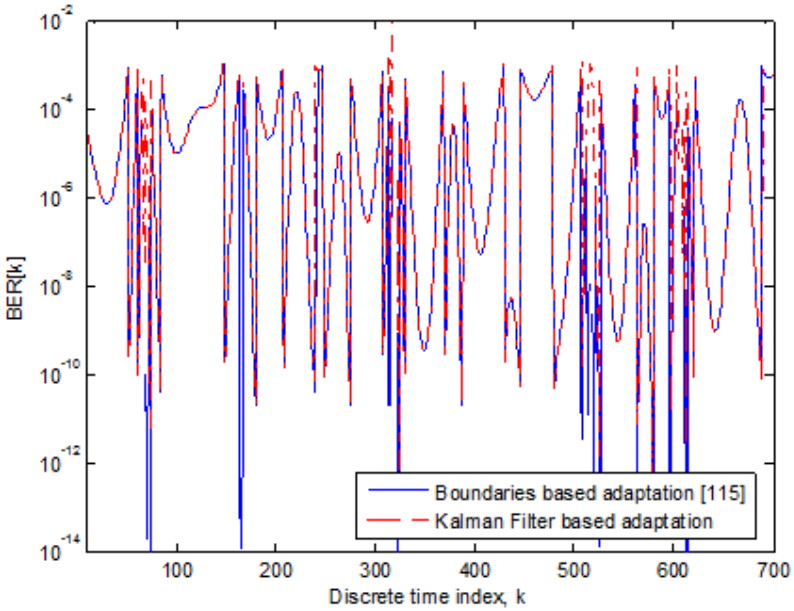

Figure 4.4 Resulted BER for adaptive modulation with $\sigma_{\epsilon p}^2 = 0.01$

Figure 4.3 shows that over a relatively small prediction error, both discrete rate adaptation methods behave in a similar manner. The variations of resulted BER over time presented in Figure 4.4 are reasonably lower than the required value. However, when the prediction error increases with the increase of channel variation, rate adaptation with Kalman filtering results in a slightly higher rate over time compared with the existing adaptation method, as showed in Figure 4.5.

The resulted BER over time is showed in Figure 4.6 and it can be seen that a higher rate in the proposed adaptation method results in higher BER. However, these values are reasonably within the BER requirement, with occasional slight rises above the upper bound. The occasionally higher resulted BER occurs mainly due to the limitation of Kalman filter in compensating the process noise as discussed earlier. However, it is not completely unreasonable as this value is within an order of magnitude of the BER requirement.

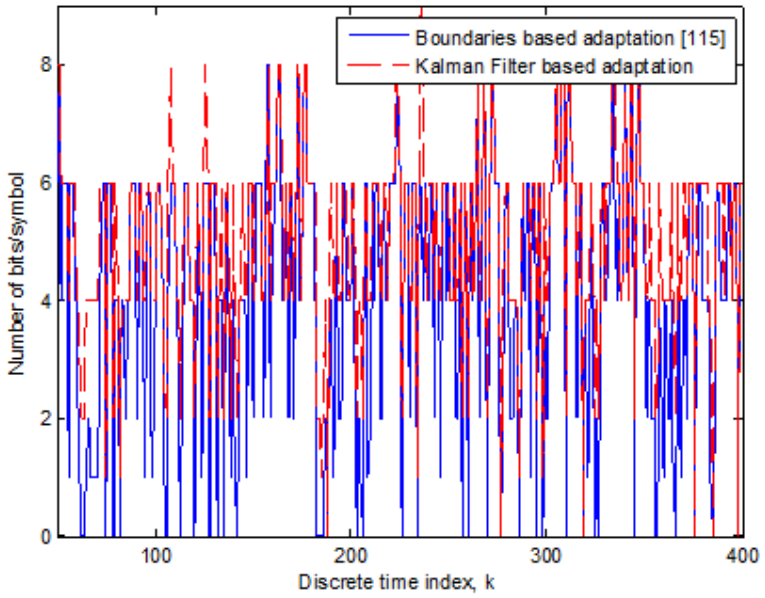

Figure 4.5 Rate variations for adaptive modulation with $\sigma_{\epsilon p}^2 = 0.1$

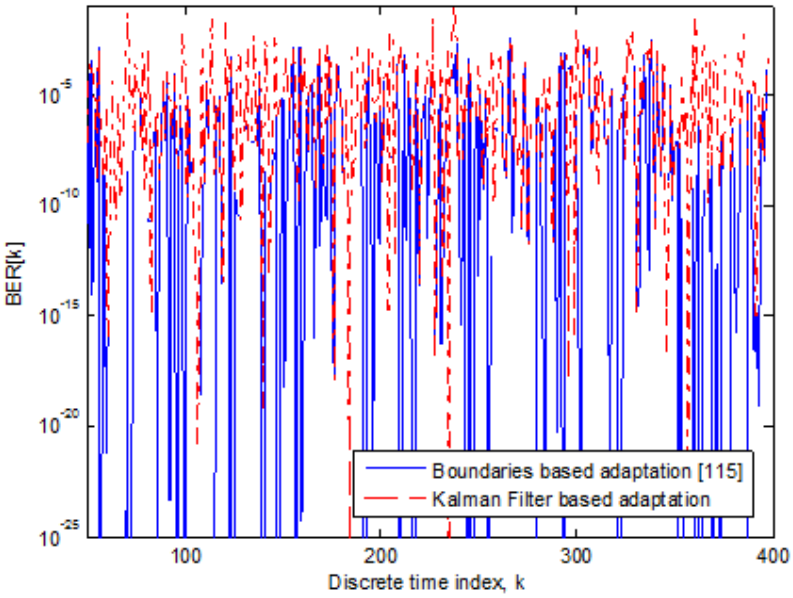

Figure 4.6 Resulted BER for adaptive modulation with $\sigma_{\epsilon p}^2 = 0.1$

The same simulations are performed for a lower BER constraint of 10^{-5} and the results are shown in Figure 4.7 to Figure 4.10.

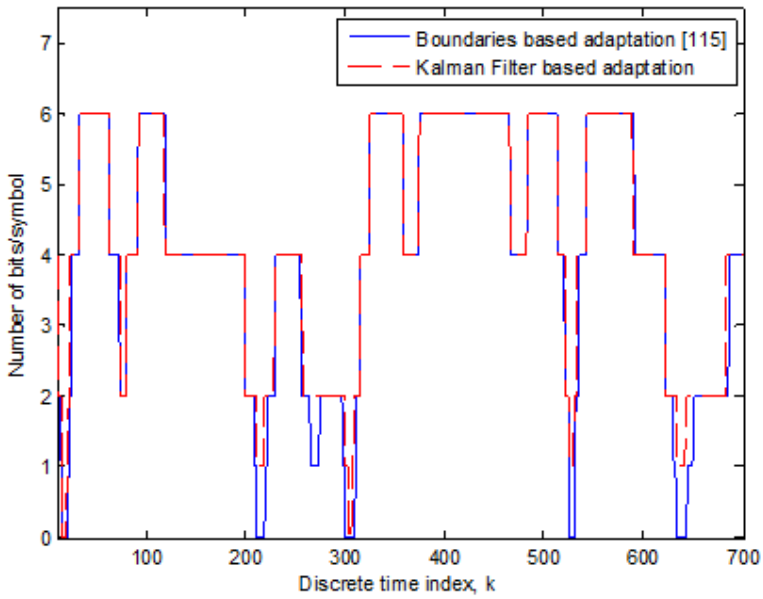

Figure 4.7 Rate variations for adaptive modulation with $\sigma_{\epsilon p}^2 = 0.01$

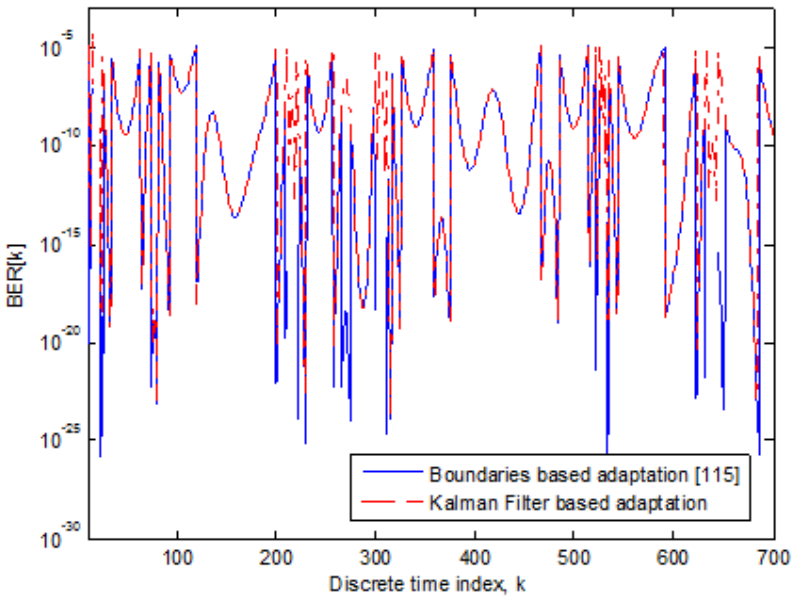

Figure 4.8 Resulted BER for adaptive modulation with $\sigma_{\epsilon p}^2 = 0.01$

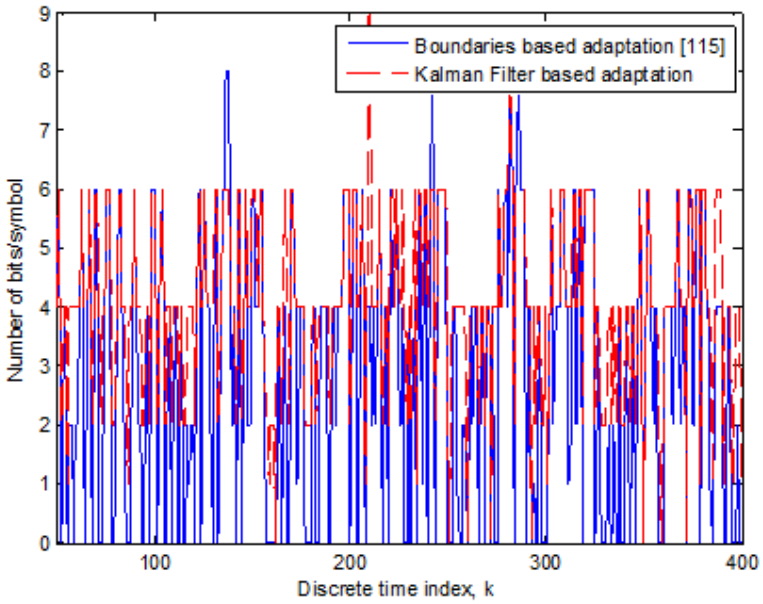

Figure 4.9 Rate variations for adaptive modulation with $\sigma_{\epsilon p}^2 = 0.1$

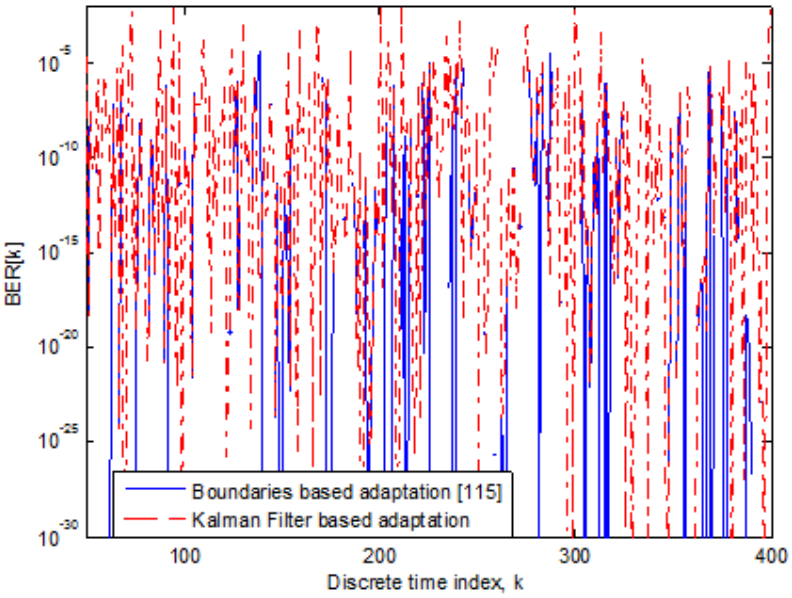

Figure 4.10 Resulted BER for adaptive modulation with $\sigma_{\epsilon p}^2 = 0.1$

These results show that when the prediction error variance is higher, the variation of resulted BER is also greater and the BER is occasionally higher than the targeted value, just as the case for BER_{tg} of 10^{-3}. These results are expected as Kalman filter is used to compensate the noise to a certain extent whereas in the conventional rate adaptation, the optimal SNR boundaries for choosing the constellation size are obtained from a strictly constrained optimization method to anticipate the worst prediction error.

Having verified that the adaptation method does account for the BER requirement in adapting the rate with respect to the channel variation, the question shifts to how well the proposed method performs in terms of efficiency. Recall that in adaptive modulation with constant symbol rate, the spectral efficiency is defined as the average number of bits per symbol as the symbol, the numerical value of this parameter is calculated over 2 million channel samples in the simulation. For both the proposed and existing adaptive modulation methods based on prediction channel power with error variance 0.01 and 0.1, the spectral efficiencies of the system are

evaluated for different values of average SNR. The results for the case of BER constraint equal to 10^{-3} are shown in Figure 4.11, where the graph for Kalman filter based adaptation method is plotted in dotted line and the graph for the optimal SNR region boundaries based adaptation method is plotted in diamond-marked line. The red and blue lines correspond to $\sigma_{\epsilon p}^2 = 0.01$ and $\sigma_{\epsilon p}^2 = 0.1$ respectively.

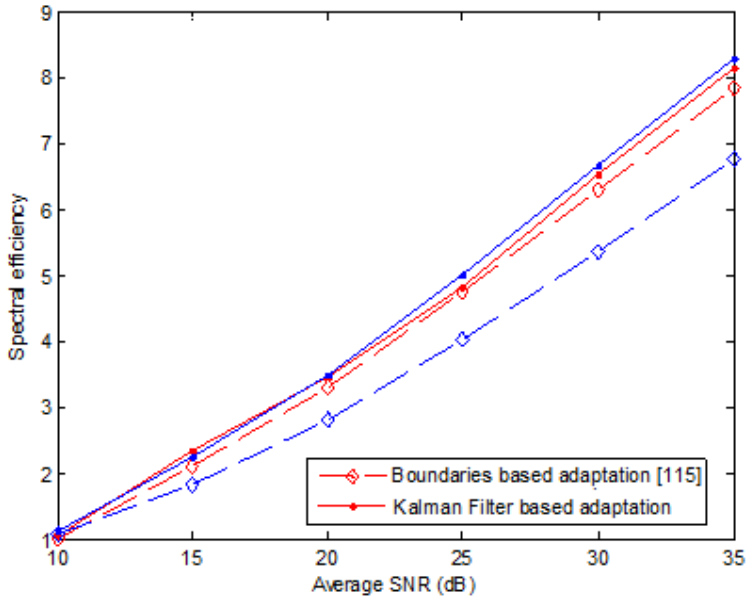

Figure 4.11 Spectral efficiency vs. SNR of for $BER_{tg} = 10^{-3}$

Indeed, it is shown that with Kalman filter, the resulting spectral efficiency is similar for different prediction error variance, which implies the robustness of the scheme against the quality of channel power gain prediction.

The performance of discrete rate adaptation with variable power for low error variance of channel power prediction is also investigated through simulation in MATLAB for BER_{tg} of 10^{-3} and 10^{-5}. The fading channel is sampled at 20 kHz with average SNR of 25 dB and channel power prediction is performed with error variance of 0.02. The same set of six constellations $\boldsymbol{M} = \{2, 4, 16, 64, 256, 1024\}$ is used in the simulation. The discrete rate and continuous power adaptations over time are presented in Figure 4.12 and Figure 4.13 for BER constraints of 10^{-3}.

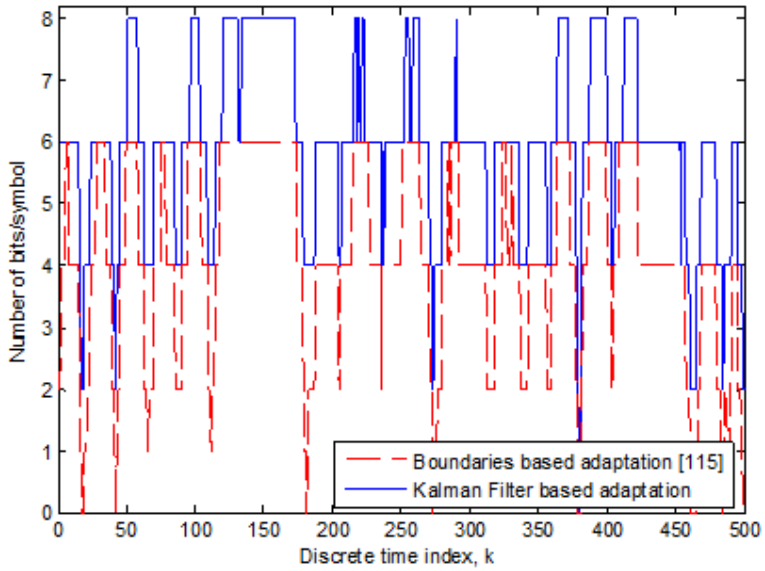

Figure 4.12 Rate variations for adaptive modulation with $\sigma_{\epsilon p}^2 = 0.02$

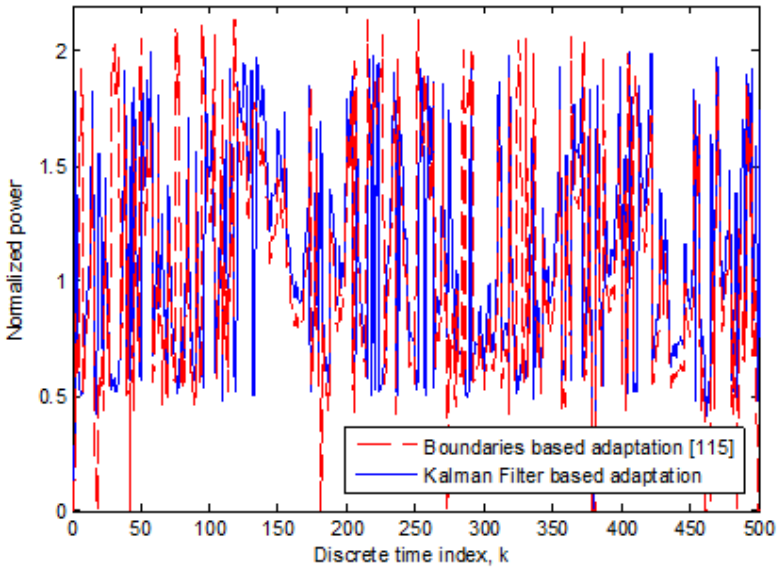

Figure 4.13 Transmit power variations for adaptive modulation with $\sigma_{\epsilon p}^2 = 0.02$

Figure 4.12 shows that in comparison with optimal region boundaries adaptation method, the proposed adaptation method applies higher number of bits per symbol most of the time. As discussed before, it is possible to do this without violating the BER requirement by applying higher transmit power within an acceptable level, which results in the variation of transmit power as shown in Figure 4.13. It is seen from the graph that the transmit power of the proposed adaptation method fluctuates within the same range with the counterpart method. The instantaneous BERs are plotted in Figure 4.14. It is shown that these values fall within an order of magnitude to the prescribed upper bound of BER, with occasional rises that occurs when the predicted channel power gain do not account for the actual value as expected. These high values of BER happen more frequently in the proposed method due to the limitation of Kalman filter in compensating the process noise which has been discussed previously.

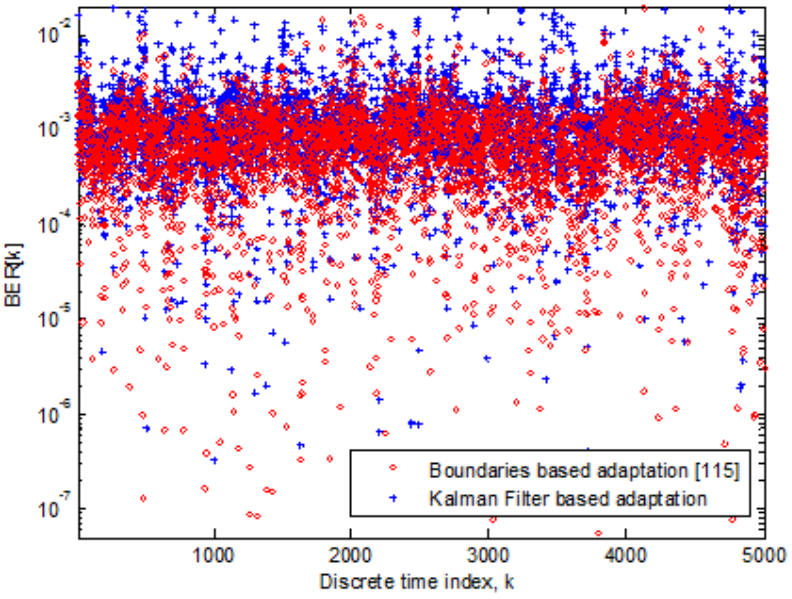

Figure 4.14 Resulted BER for adaptive modulation with $\sigma_{\epsilon p}^2 = 0.02$

For both the proposed and the existing discrete rate and continuous power adaptive modulation methods, the spectral efficiencies of the system are evaluated for different values of average SNR, based on prediction channel power with error variance of 0.02. The results for the case of BER constraint equal to 10^{-3} are shown in Figure 4.15.

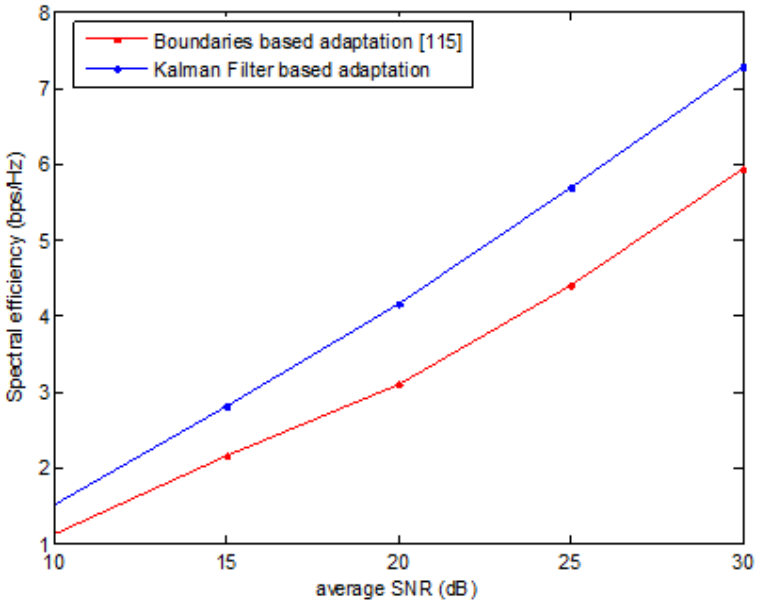

Figure 4.15 Spectral efficiency vs. SNR for $BER_{tg} = 10^{-3}$ and $\sigma_{\epsilon p}^2 = 0.02$

This graph clearly shows that the discrete rate and continuous power adaptation based on Kalman filter feedback analysis results in higher spectral efficiency in comparison with the conventional discrete rate and continuous power adaptation based on optimal region boundaries. However, the increase in spectral efficiency comes with a cost of a slightly higher BER as discussed previously.

The average transmit power and average BER are also evaluated for different channel noise levels, and the results are plotted in Figure 4.16.

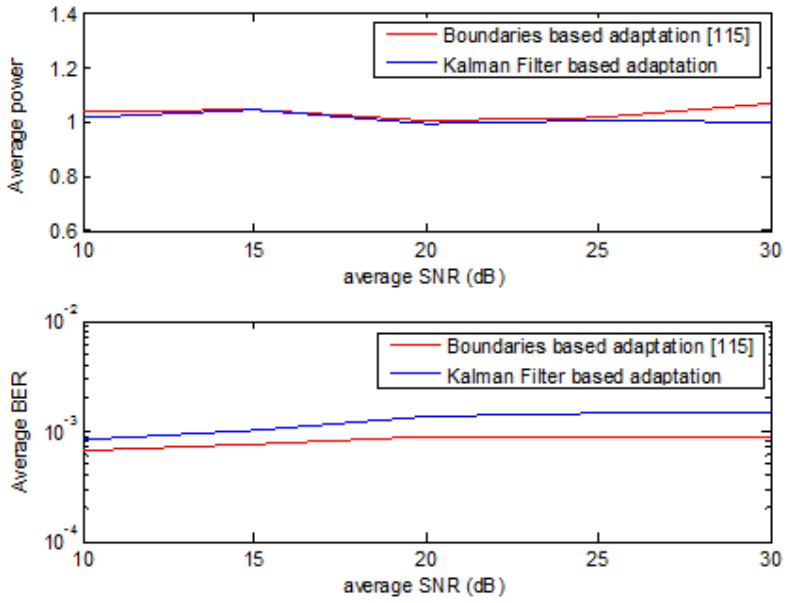

Figure 4.16 Average transmit power and average BER vs. SNR of for $BER_{tg} = 10^{-3}$ and $\sigma_{\epsilon p}^2 = 0.02$

It is shown that the normalized transmit power for both discrete rate and continuous power adaptation methods is indeed averaged to one in fulfillment of the average power constraint. It is also shown that the average BER for the proposed discrete rate and continuous power adaptation method is slightly higher than the prescribed BER. Again, this is not surprising as Kalman filter is used to approximate the systems states to the vicinity of the actual state without a strict upper limit on the states itself. Using Kalman filter as an optimal state estimator for linear stochastic systems might sometimes result in less optimal performance of the proposed adaptation system due to the input-to-state linearization process of the system model. When the actual system is non-linear, some errors will be expected as the non-linear behavior of the system is not taken into account. This issue will be addressed in the next chapter. The author will present an alternative way of modeling the dynamics of the non-linear system where the BER at different moments are considered as the state variables to describe the dynamics of the system. Similar approach of system dynamic analysis is used to design a non-linear controller to adjust the constellation size and additional power adjustment to optimize the performance of the system.

4.5 Conclusion

In this chapter, imperfection of channel gain prediction is taken into account by including the prediction error in the dynamics equations. The resulted system dynamics therefore are described by stochastic difference equations and the concept of Kalman filtering is adopted as a well-known recursive algorithm for performing statistically optimal estimation of unknown states of a system based on a series of noisy measurement. Having estimated the system states through Kalman filtering, the constellation size is chosen based on the predicted channel power gain and the optimal state estimates. Moreover, power adjustment can be performed to increase the spectral efficiency of the overall system.

The performance of the proposed scheme is then compared with the conventional scheme through simulations in MATLAB. For discrete rate adaptation method with constant power, the behavior of rate adaptation is presented for two cases of imperfect channel power prediction to observe the responses of the proposed adaptation method to different quality of prediction. The results show that the discrete rate adaptation method based on feedback analysis with Kalman filtering is more robust to the different qualities of channel prediction in comparison with the existing method. In addition, discrete rate and continuous power adaptation method is developed for slowly varying channel with accurate prediction and it results in higher spectral efficiency for the given average transmit power while the average BER is observed within an order of a magnitude of the targeted value.

Chapter 5

Non-linear Controller for Adaptation Method with Channel Mean Feedback

5.1 Introduction

In this chapter, a novel non-linear feedback control scheme is established to adjust the constellation size relative to the channel condition. First of all, an alternative state-space representation is introduced assuming perfect channel gain at the transmitter. Then, a non-linear controller that results in a stable system in the vicinity of the equilibrium point is developed. The feedback control is then modified to incorporate partial CSI based on mean feedback, where the channel information resides in the mean value of the distribution and degree of the channel estimation error is represented by the white variance

For a Rayleigh channel model, the channel fading gain is distributed according to a complex Gaussian distribution $h \sim CN(\bar{h}, {\sigma_\xi}^2)$ where $\bar{h}$ is the mean value conditioned on the feedback information from the receiver and ${\sigma_\xi}^2$ is the variance of the noise to account for the possible variation that happens within the time frame after it is estimated at the receiver.

The expected values of the system state variables based on the statistical properties of the channel, namely the conditional mean and white noise variance, are used to estimate the actual state and the estimated state is fed to the feedback controller to compute the constellation size for the next transmission. Simulations in MATLAB are performed to support the analysis.

5.2 Non-linear Adaptation System

This section presents the mathematical analysis of the dynamical system in designing the appropriate non-linear feedback controller for rate adaptation.

5.2.1 State-space Representation

Similar to Chapter 3, the state variables need to be defined to describe the mathematical state of the dynamic system. Depending on the choice of these state variables the behavior of the system may be represented in different forms of state-space equations. In chapter 3, a form of state-space equation has been established where the state variables are chosen as log functions of the BER at different time instant so that the non-linear system dynamic can be described by linear dynamic equations after performing input-to-state feedback linearization. However, with the presence of noise, this nonlinearity cannot be fully cancelled and hence causes performance degradation of the controller feedback. In this chapter, the BER at different instant are directly chosen as the state variables,

$$x_1[k] = BER[k-1]$$

$$x_2[k] = BER[k] \tag{5.1}$$

and delayed BER is defined as the output of the system because it is available at the transmitter via feedback communication:

$$y[k] = x_1[k] \tag{5.2}$$

Recall that the BER can be approximated as a function of transmission parameters and channel gain as presented in (3.5). Hence state variables can be expressed by the following equations for the case of transmission:

$$x_1[k+1] = x_2[k]$$

$$x_2[k+1] = 0.2exp\left(\frac{-1.6\Gamma S_n|h[k]|^2}{M[k]-1}\right) \tag{5.3}$$

Rate adaptation is then performed by designing a feedback controller to adjust $M[k]$ such that the system output converges to a desired value. Hence, the constellation size is assigned based on the knowledge of the output $y[k]$ and the channel gain $h[k]$, starting with the assumption that is perfectly known at the transmitter. Consequently, a non-linear feedback based adaptation of constellation size is proposed as following:

$$M[k] = 1 - \frac{1.6\Gamma\, S_n|h[k]|^2 g(y[k])}{ln(5BERtg)} \tag{5.4}$$

where $g(y[k])$ is a feedback controller that is chosen to drive the system to the equilibrium.

The closed-loop system dynamics for this adaptation method is given by a couple of difference equations, substituting the output of the system (5.3):

$$x_1[k+1] = x_2[k]$$

$$x_2[k+1] = 0.2\ exp\left(\frac{ln\left(5BER_{tg}\right)}{g(x_1[k])}\right) \tag{5.5}$$

5.2.2 Stability Analysis

Having derived the dynamics of the system, it is imperative that stability analysis is done to prove that the system converges to a stable operating point at steady state. Hence, the feedback controller $g(x_1[k])$ should be chosen such that for a stable closed-loop system, the system states will converge to the equilibrium point.

A state $\boldsymbol{x}^{\infty}$ is an equilibrium state of the system if once $\boldsymbol{x}[k]$ is equal to $\boldsymbol{x}^{\infty}$, it remains at that state for all future time. In this case, the equilibrium point for the second order system can be found as follows:

$$\lim_{k\to\infty} x_1[k+1] = \lim_{k\to\infty} x_2[k]$$

$$\lim_{k\to\infty} x_2[k+1] = \lim_{k\to\infty} 0.2\ exp\left(\frac{ln\left(5BER_{tg}\right)}{g(x_1[k])}\right) \tag{5.6}$$

The equations above shows that the equilibrium point is highly dependent on BER_{tg} and the feedback controller $g(x_1[k])$applied to the system. Linearization about the equilibrium point is performed on non-linear system (5.2) and the Jacobian matrix [138] is constructed for the linearized system below:

$$\Delta\boldsymbol{x}[k+1] = \boldsymbol{A}\Delta\boldsymbol{x}[k] \tag{5.7}$$

where $\boldsymbol{A}$ is Jacobian matrix of the system (5.5) evaluated at the equilibrium point:

$$\boldsymbol{A} = \begin{bmatrix} \frac{\partial f_1}{\partial x_1} & \frac{\partial f_1}{\partial x_2} \\ \frac{\partial f_2}{\partial x_1} & \frac{\partial f_2}{\partial x_2} \end{bmatrix} | \ \boldsymbol{x}[k] = \boldsymbol{x}^{\infty} \tag{5.8}$$

Functions f_1 and f_2 are dictated by the system dynamics equations as given:

$$f_1(\boldsymbol{x}) = x_2$$

$$f_2(\boldsymbol{x}) = 0.2\ exp\left(\frac{ln\left(5BER_{tg}\right)}{g(x_1)}\right) \tag{5.9}$$

Taking partial derivatives of the functions resulting in the Jacobian matrix:

$$\boldsymbol{A} = \begin{bmatrix} 0 & 1 \\ \Lambda & 0 \end{bmatrix},$$

$$\Lambda = \frac{-g'(x_1[k])}{g^2(x_1[k])}\ ln\left(5BER_{tg}\right)\ 0.2exp\left(\frac{ln\left(5BER_{tg}\right)}{g(x_1[k])}\right) | \ \boldsymbol{x}^{\infty} \tag{5.10}$$

It has long been known that in control theory, a linear system in the form (5.7) is stable if the eigenvalues of matrix $\boldsymbol{A}$ are inside the unit circle. For the given matrix $\boldsymbol{A}$ in (5.10), the characteristic equation is given by:

$$\lambda^2 - \Lambda = 0 \tag{5.11}$$

and the eigenvalues are inside the unit circle when $|\Lambda| < 1$. It is clear from (5.10) that this parameter is highly dependent on the choice of feedback controller.

Given that the closed loop system is stable by an appropriate design of feedback controller, the state variables will converge to an equilibrium point as defined in (5.6):

$$\boldsymbol{x}^{\infty} = \lim_{k \to \infty} \boldsymbol{x}[k] = (x^*,\ x^*) \tag{5.12}$$

where $x^*$is related to BER_{tg} by the following equation:

$$x^* = 0.2exp\left(\frac{ln\left(5BER_{tg}\right)}{g(x^*)}\right) \tag{5.13}$$

Substituting (5.12) and (5.13) into (5.10) results in:

$$\begin{aligned} \Lambda &= \frac{-g'(x^*)}{g(x^*)} \frac{ln\left(5BER_{tg}\right)}{g(x^*)} x^* \\ &= \frac{-g'(x^*) ln(5x^*) x^*}{g(x^*)} \end{aligned} \tag{5.14}$$

The feedback controller is chosen as:

$$g(x_1[k]) = \frac{ln(x_1[k])}{ln(K\ BER_{tg})} \tag{5.15}$$

such that

$$g'(x_1[k]) = \frac{1}{x_1[k] ln(K\ BER_{tg})} \tag{5.16}$$

Substituting the feedback controller (5.15) and its derivation (5.16) at equilibrium point results in:

$$\begin{aligned} \Lambda &= \frac{-1}{x^* ln(K\ BER_{tg})} \frac{ln(K\ BER_{tg})}{ln(x^*)} x^* \\ &= \frac{ln(5x^*)}{ln(x^*)} \end{aligned} \tag{5.17}$$

As logarithmic function is monotonically increasing, $ln(x^*) < ln(5x^*)$. Furthermore, for $5x^* < 1$, the logarithmic function is negative, $ln(x^*) < ln(5x^*) < 0$. Accordingly,

$$|ln(x^*)| > |ln(5x^*)|, \quad x^* < 0.2 \tag{5.18}$$

Therefore,

$$\left|\frac{ln(5x^*)}{ln(x^*)}\right| < 1, \quad x^* < 0.2 \tag{5.19}$$

Following the analysis, the linearized system is stable as condition $|\Lambda| < 1$ is fulfilled and the overall system states will converge to the equilibrium point. The equilibrium point itself is dependent on the value of K. Substituting the chosen function $g(x_1[\mathrm{k}])$ to (5.6) results in:

$$ln(5x^*)\, ln(x^*) = ln\big(5BER_{tg}\big)\, ln\big(K\, BER_{tg}\big) \tag{5.20}$$

Setting $K = 1$ results in $x^* = BER_{tg}$ and because the linearized system is stable, at steady state the system operates around this point. For $K > 1$, the equilibrium point will be greater than BER_{tg}. Hence, the control parameter is bounded by $K \in (0,1]$ such that the equilibrium point is bounded by:

$$K\, BER_{tg} < x^* \leq BER_{tg} \tag{5.21}$$

The system response for different values of *K* is plotted in Figure 5.1. It can be seen that choosing a lower value of *K* results in a lower BER at equilibrium.

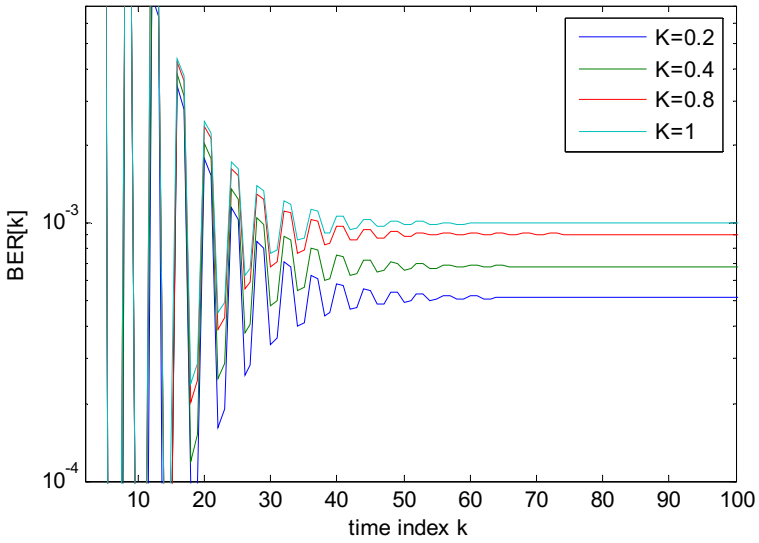

Figure 5.1 System response for different values of control gain

Through the system stability analysis, it is established that for the proposed rate adaptation scheme, there exists a feedback controller with control parameter $K \in (0,1]$ such that the closed-loop system is asymptotically stable under the condition:

$$x^* \leq BER_{tg} < 0.2 \tag{5.22}$$

In the next section, the assumption of perfect CSI at the transmitter is relaxed to perform more practical modulation scheme for situations where only the partial knowledge of the channel gain is available based on the delayed information from the receiver.

5.2.3 Rate Adaptation Based on Partial CSI

In this section, the assumption of perfect CSI at transmitter is relaxed to the partial CSI available at the transmitter. As explained in literature [139], [140], for a flat Rayleigh fading channel modeled by a circularly symmetric complex Gaussian variable, there are two main methods in providing information-theoretic insight into formulation of adaptive transmission based on partial CSI, namely mean feedback

and covariance feedback. In this study, the concept of channel mean feedback is adopted. Given the channel feedback from the receiver, the transmitter knows that the channel is distributed according to a complex Gaussian distribution $h \sim CN\left(\bar{h}, {\sigma_\xi}^2\right)$ where $\bar{h}$ is the mean value conditioned on the feedback information from the receiver and ${\sigma_\xi}^2$ is the variance of the noise to account for the possible variation that happens within the time frame after it is estimated at the receiver.

In the literature, the conditional mean is directly related to the instantaneous feedback by the autocorrelation coefficient of the particular channel [141], [140] such that $\bar{h}[k] = \rho h[k-1]$ where the autocorrelation coefficient characterizes the variation of the channel over time. The autocorrelation coefficient also represents the effect of Doppler effect on the rapid variation of the channel. In this study, the conditional mean of the channel is modified to consider the last *M* feedback for more accurate model. In this case, the conditional mean is given by the predicted channel based on the past observations:

$$\bar{h}[k] = \mathbf{a}\boldsymbol{h}[k] \tag{5.23}$$

where $\mathbf{a}$ is a vector that represents the linear weight of the past feedback and $\boldsymbol{h}[k] = [\, h[k-1], \dots, h[k-(M-1)]\,]$ is the column vector of past channel estimated perfectly at the receiver. Note that the optimal weighing vector is equivalent to the optimal linear prediction coefficient (2.8) discussed in Chapter 2, if the prediction is performed to account for the estimation error at the receiver. Therefore, the optimal linear FIR predictor (2.6) can be used instead, and the variance of noise ${\sigma_\xi}^2$ can be obtained as the variance of the channel prediction error:

$${\sigma_\xi}^2 = \sigma_h^2 - \boldsymbol{r}_{h\varphi}^H \boldsymbol{R}_\varphi^{-1} \boldsymbol{r}_{h\varphi} \tag{5.24}$$

where $\boldsymbol{R}_\varphi$ is the covariance matrix of the estimated channel gains and $\boldsymbol{r}_{h\varphi}$ is the cross-covariance between the channel and the noisy estimation as described in (2.9) - (2.12).

Since the perfect channel gain is not available at the transmitter, the system states cannot be computed based on the dynamic equations (5.3). The estimated

values of state variables are used instead, which are based on the statistical knowledge of the system parameters. For wireless channels with time-varying channel gain modeled as a Gaussian random variable with known second order statistics described by $h \sim CN\left(\bar{h}, {\sigma_\xi}^2\right)$, the expectation of BER is given by [142]:

$$\overline{BER}[k] = \frac{0.2}{1 + \Omega\sigma_\xi^2} exp\left(-\frac{\Omega\left|\bar{h}\right|^2}{1 + \Omega\sigma_\xi^2}\right) \tag{5.25}$$

where

$$\Omega = \frac{-1.6\Gamma S_n}{M - 1} \tag{5.26}$$

Given the expected value of BER, the system dynamics equations (5.3) are approximated by the expected values, given as:

$$\begin{aligned} \overline{x_1}[k+1] &= \overline{x_2}[k] \\ \overline{x_2}[k+1] &= \frac{0.2}{1 + \Sigma[k]} exp\left(-\frac{\Theta[k]^2}{1 + \Sigma[k]}\right) \end{aligned} \tag{5.27}$$

where

$$\Theta[k] = \frac{-1.6\Gamma S_n\left|\bar{h}[k]\right|^2}{M[k] - 1} \tag{5.28}$$

$$\Sigma[k] = \frac{-1.6\Gamma S_n}{M[k] - 1}\sigma_\xi^2 \tag{5.29}$$

The control parameter is therefore adjusted based on these expected values to account for the random variation of the channel gain. Hence, the constellation size can be written as:

$$M[k] = 1 - \frac{1.6\,\Gamma S_n\left|\bar{h}[k]\right|^2 g(\overline{x_1}[k])}{ln(5BERtg)} \tag{5.30}$$

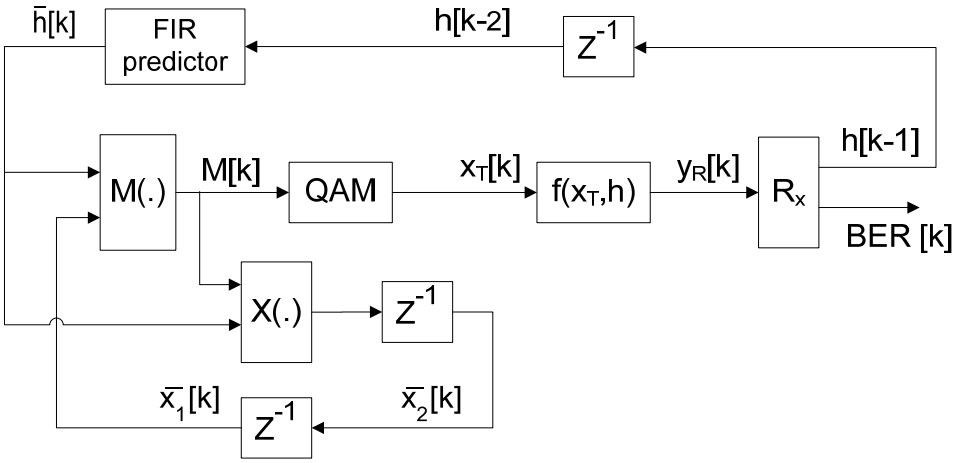

Figure 5.2 Block diagram of the transmission system

As mentioned in the earlier sections, the computed constellation size needs to be rounded to the appropriate value in the restricted set of *N* square QAMs and this can be done with or without adjusting the transmit power. For discrete rate adaptation method with constant power, modulation is performed by appying the nearest lower value available such that the instantaneous BER is lower than or equal to the expected value.

The expected values of the system states at transmitter however remain unchanged as they are computed based on the decimal value of constellation size. The resulted system is depicted in Figure 5.2, where X(.) represents the estimated state transition in (5.27) and M(.) represents the feedback controller that determines the modulation size in (5.30). By introducing the expected values of the BER and the system states estimation at the transmitter, the closed loop adaptation system can be realized at the transmitter with only partial CSI feedback from the receiver.

In the case of discrete rate adaptation with power adjustment, unless the resulted transmit power exceeds the limit, the constellation size can be rounded to the nearest higher value available, following the rule in (4.29). This results in variable rate and power adaptation which further improves the spectral efficiency of the system. The performances of the proposed rate adaptation methods are presented in the next section, based on simulations performed in MATLAB.

5.3 Performance Analysis

The proposed adaptation scheme is simulated in MATLAB to verify the accuracy of the system dynamic model and investigate the performance of the proposed adaptation method. The proposed discrete rate adaptation scheme without power adaptation is simulated over a flat Rayleigh fading channel generated in MATLAB with sampling frequency of 20 kHz and maximum Doppler shift of 680 Hz, which corresponds to correlation coefficient of 0.95. The additive white Gaussian noise with SNR of 25 dB is considered, resulting in channel prediction error variance given by $\sigma_{\xi}{}^{2} = 0.01$. The proposed adaptation method based on non-linear feedback control and the conventional adaptation method based on optimal region boundaries are both simulated under the same environment with the same set of constellations, $\boldsymbol{M} = \{2, 4, 16, 64, 256, 1024\}$ and the same normalized power, S_n, for a fair comparison. The behavior of the discrete rate adaptation and the result BER for both adaptation methods are shown in Figure 5.3 to Figure 5.8 for $BER_{tg} = 10^{-3}$, $BER_{tg} = 10^{5}$, and $BER_{tg} = 10^{-7}$ respectively.

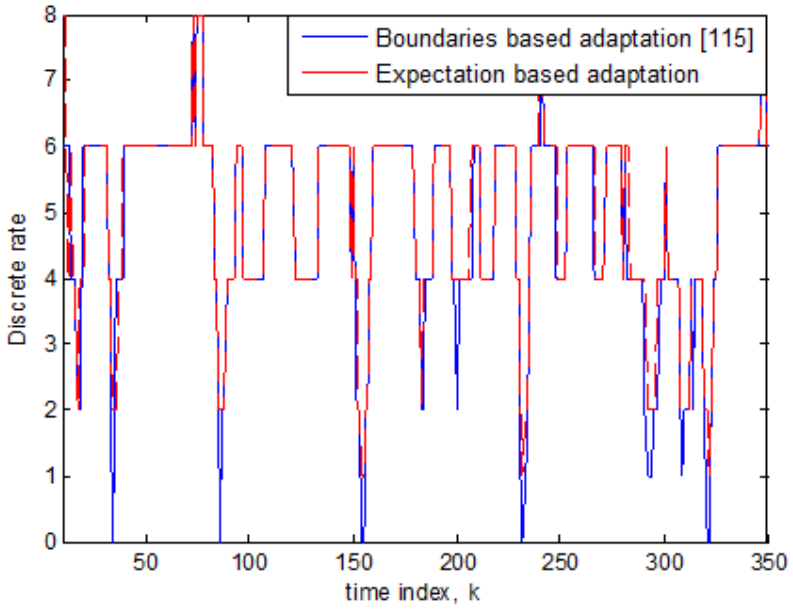

Figure 5.3 Discrete rate adaptation based on partial CSI for $BER_{tg} = 10^{-3}$

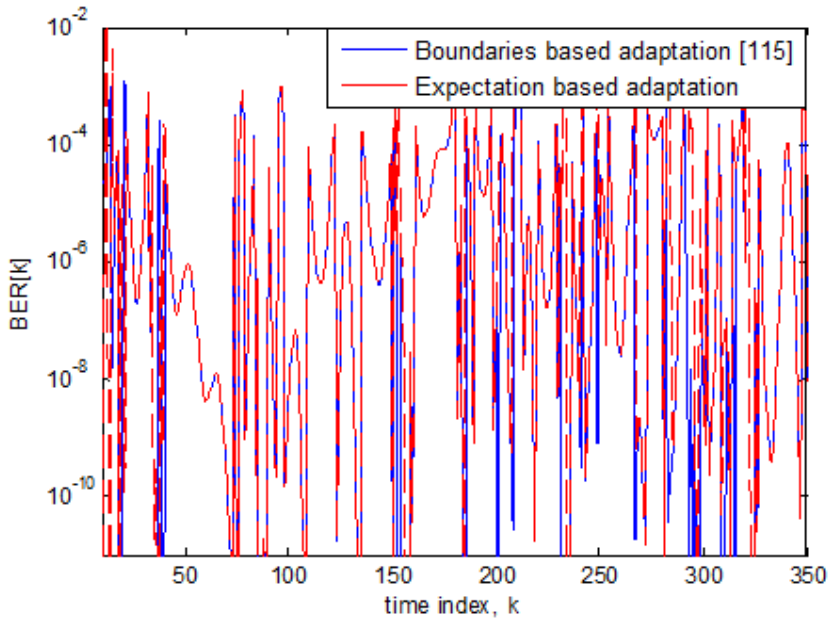

Figure 5.4 Instantaneous BER for $BER_{tg} = 10^{-3}$

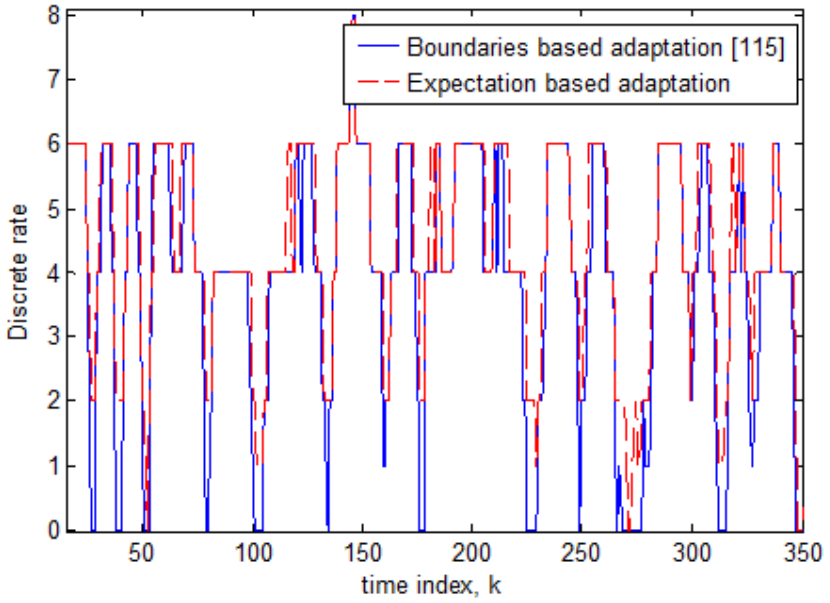

Figure 5.5 Discrete rate adaptation based on partial CSI for $BER_{tg} = 10^{-5}$

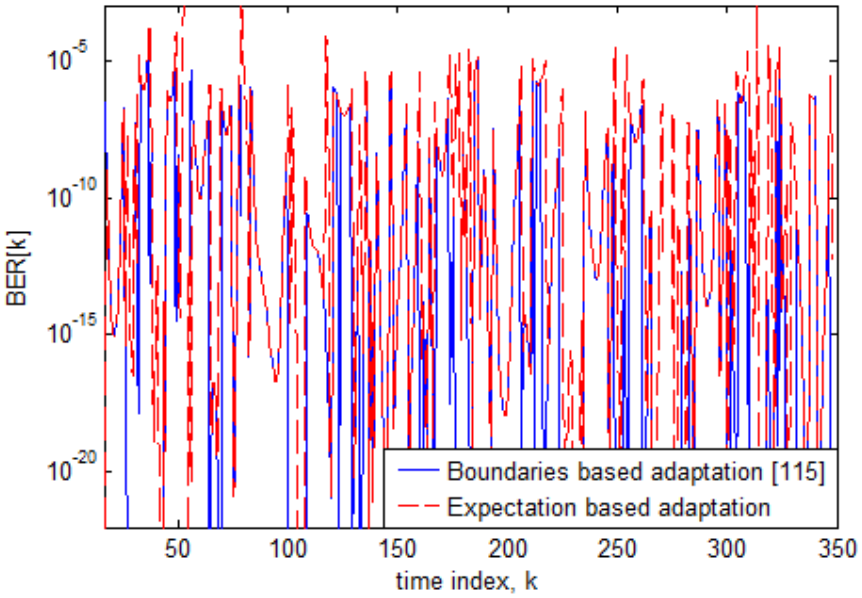

Figure 5.6 Instantaneous BER for $BER_{tg} = 10^{-5}$

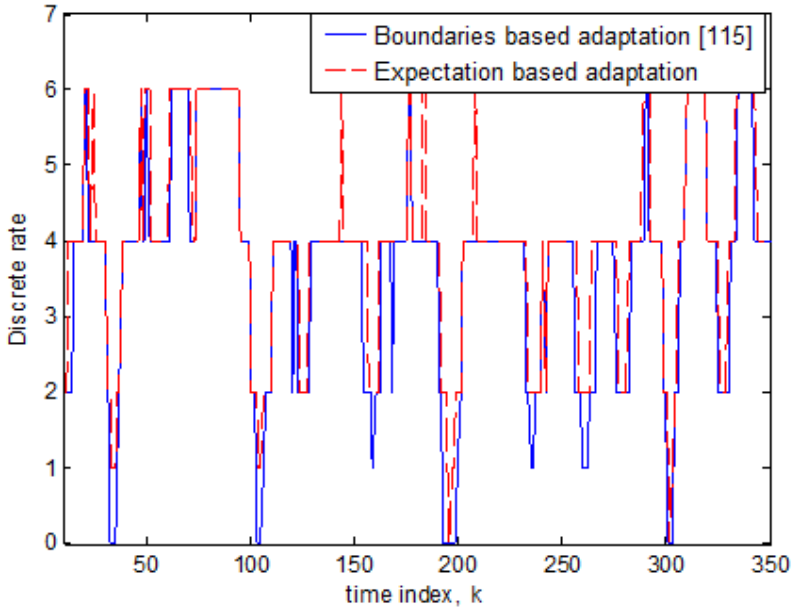

Figure 5.7 Discrete rate adaptation based on partial CSI for $BER_{tg} = 10^{-7}$

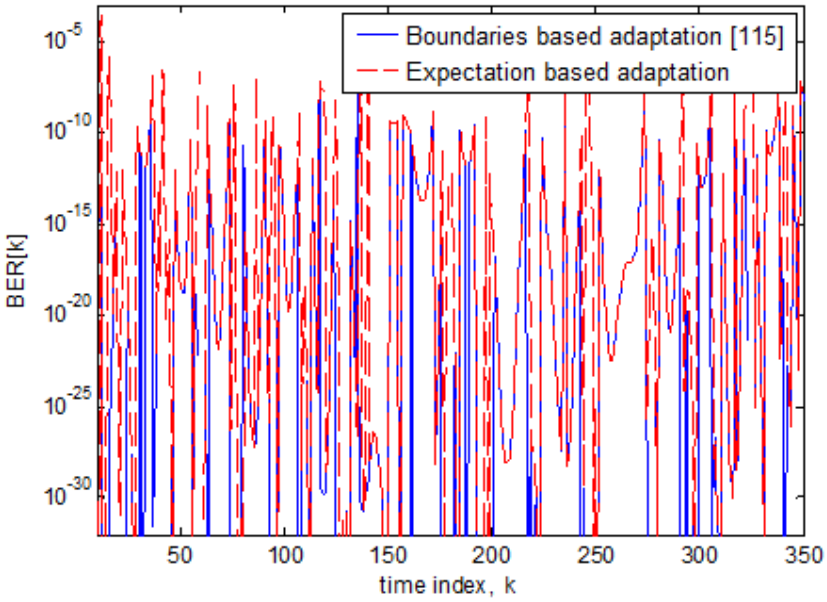

Figure 5.8 Instantaneous BER for $BER_{tg} = 10^{-7}$

These results show that the proposed non-linear feedback control adjust the constellation size in the same manner as the conventional adaptation method based on optimal region boundaries for various BER_{tg} with slight difference at some instants. Hence, the system dynamic equations established in this chapter is verified.

Another set of simulations is performed to evaluate the performance of the M-QAM adaptive system in terms of the spectral efficiency and average received BER under different Doppler effect as indicated by the correlation coefficient of the channel. Both the expectation based rate adaptation method and the boundary-based rate adaptation method are performed for the same set of modulations $\boldsymbol{M} = \{2, 4, 16, 64, 256, 1024\}$, and under the same fading environment and BER requirement of 10^{-3}. Assuming ideal Nyquist data pulses with bandwidth $B = 1/T_s$, and a fixed symbol rate for all modulation modes, the spectral efficiency of adaptive QAM systems can be computed as the average number of bits per symbol sent. The results are plotted over a range of average SNR values, Γ, for various correlation coefficient of 0.3, 0.6 , and 0.9.

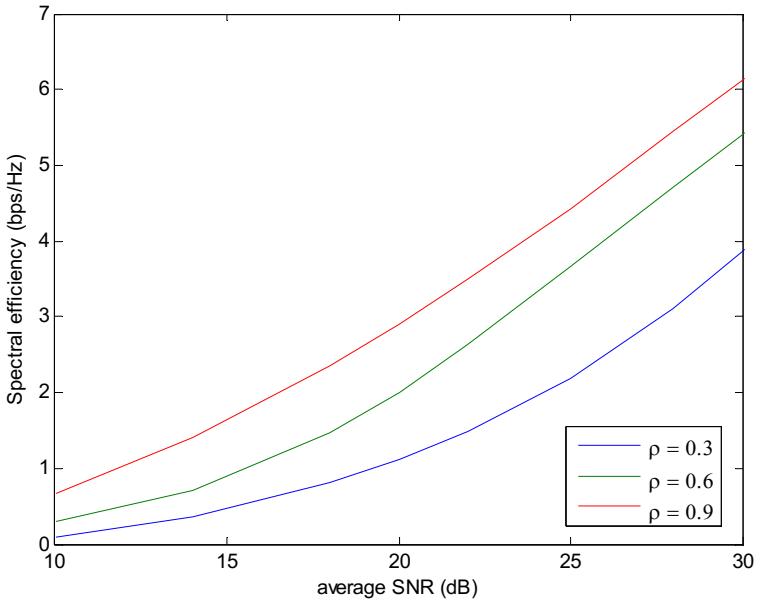

Figure 5.9 Spectral efficiency vs. SNR for discrete rate adaptation based on optimal boundaries solution

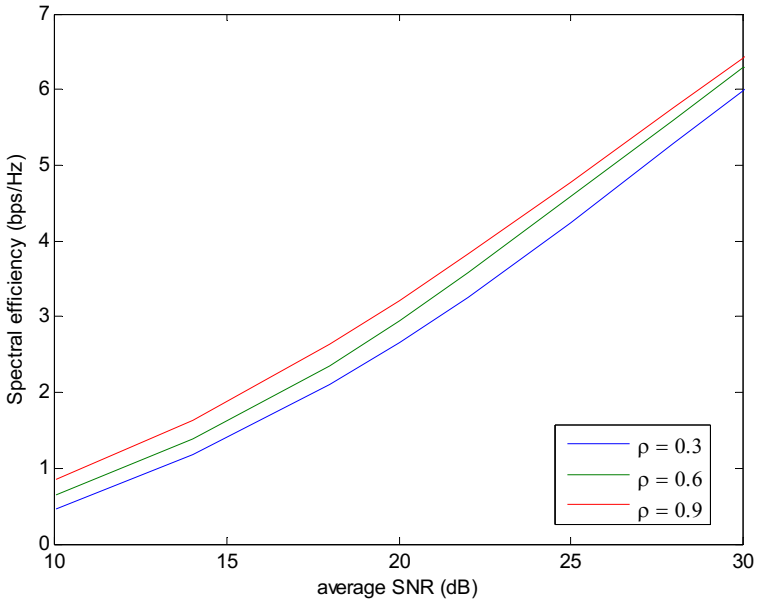

Figure 5.10 Spectral efficiency vs. SNR for discrete rate adaptation based on non-linear feedback controller

Comparing Figure 5.9 to Figure 5.10, it can be seen that the series of resulted spectral efficiency for the proposed system are closer together in comparison with that of the conventional adaptive QAM system. This implies that the proposed non-linear feedback adaptation method is more robust against the variation of Doppler effect on the wireless channels.

The performance of discrete rate adaptation with variable power is also investigated through simulation in MATLAB. The fading channel is sampled at 20 kHz with average SNR of 25 dB, and the same set of six constellations $\boldsymbol{M} = \{2, 4, 16, 64, 256, 1024\}$ is used in the simulation. The results of adaptive modulation based on two different qualities of channel prediction, repesented by the prediction error variance of $\sigma_{\xi}{}^2 = 0.02$ and $\sigma_{\xi}{}^2 = 0.05$, are presented under two different BER constraints, $BER_{tg} = 10^{-3}$ and $BER_{tg} = 10^{-7}$. The results of adaptation method based on Kalman filter feedback and adaptation method based on optimal SNR region boundaries under the same environment are also presented for comparison.

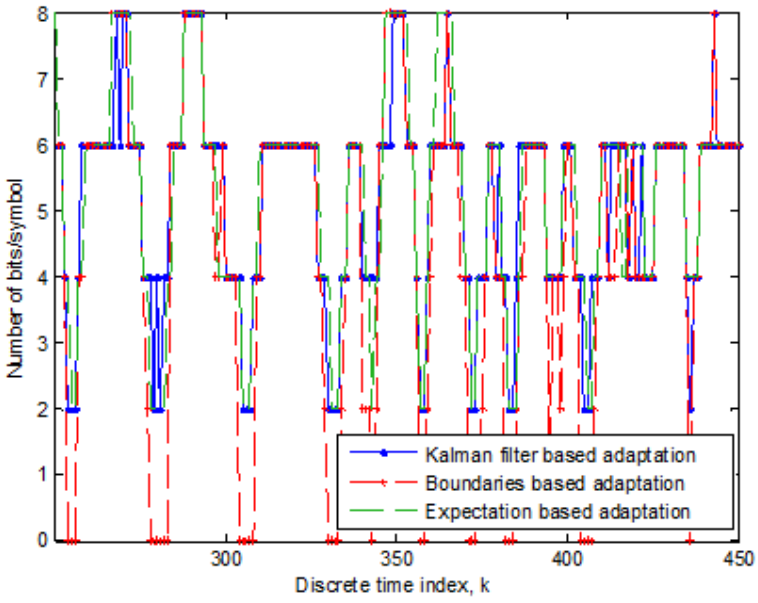

Figure 5.11 Rate adaptations with $\sigma_{\xi}{}^2 = 0.02$ for $BER_{tg} = 10^{-3}$

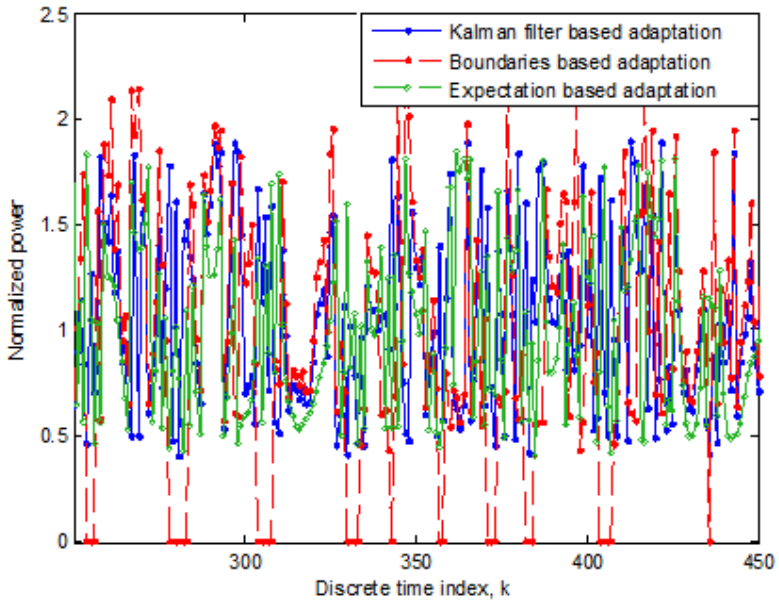

Figure 5.12 Power adaptations with $\sigma_{\xi}^{2} = 0.02$ for $BER_{tg} = 10^{-3}$

Figure 5.11 and Figure 5.12 show the behavior of the rate and power adaptation respectively, based on channel prediction with error variance of 0.02 under BER requirement of 10^{-3}. It is clearly shown in Figure 5.11 that all three adaptation methods respond in a similar manner to the variation of channel with respect to time. However, the proposed adaptation methods based on the system dynamic analysis result in transmission with low bits per symbol whereas the conventional adaptation method resolves not to transmit at some occasions. Unless these transmissions are backed up with sufficiently high transmit power, they might result in undesirable BER. The corresponding power allocation is presented in Figure 5.12 and it can be seen that the variation of transmit power is within a similar range for all three adaptation methods.

The resulted instantaneous BERs of the adaptation schemes are shown in Figure 5.13 over 5,000 sampling points. In the previous chapter, we have resolved that discrete rate and power adaptation method based on Kalman filter feedback is only suitable for high quality channel prediction with in mitigating the process noise.

It is shown in this chapter that discrete rate and power adaptation method based on non-linear feeback results in a much better BER performance compared to Kalman filtering method.

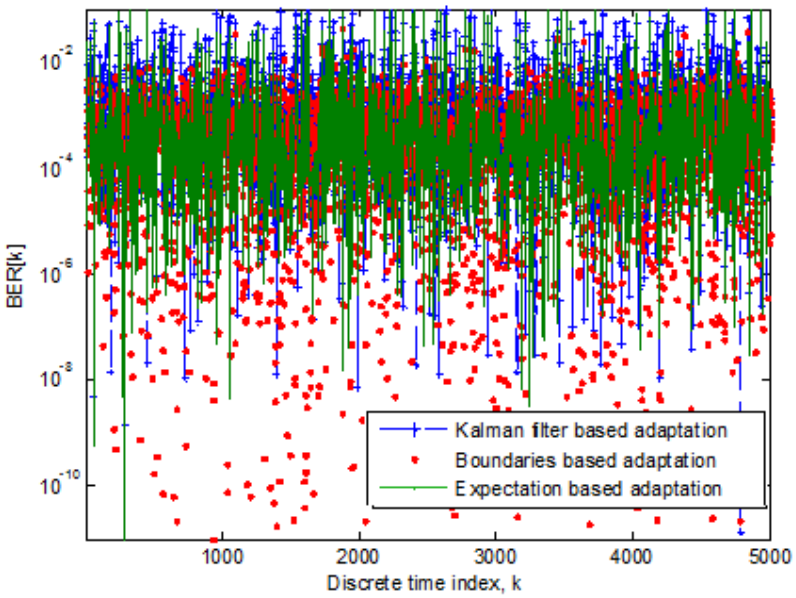

Figure 5.13 Instantaneous BER of adaptive QAM with $\sigma_{\xi}{}^2 = 0.02$ for $BER_{tg} = 10^{-3}$

Figure 5.13 shows that in general, BERs fall within an order of magnitude of the required value, with slightly more frequent raise compared to the overall BERs of the optimal region boundaries based adaptation method. It is worth noting that with the proposed non-linear feedback adaptation method, the resulted BERs do not fall below the prescribed limit either, in comparison with the conventional adaptation method. A lower range of BER fluctuation is expected for adaptation method based on feedback controller, as the feedback control input is designed to drive the system states to the optimal operating point. The noisy prediction of channel is accounted for in calculating the expectation of BER, which results in a small fluctuation around the prescribed value, BER_{tg}.

The behavior of rate adaptation and the behavior of power adaptation based on channel prediction with error variance of 0.05 under BER requirement of 10^{-3} are presented in Figure 5.14 and Figure 5.15 respectively. The results of adaptation method based on linear Kalman filter feedback controller is also included to show the

decrease in the fluctuation of BER due to the prediction error by applying non-linear feedback controller.

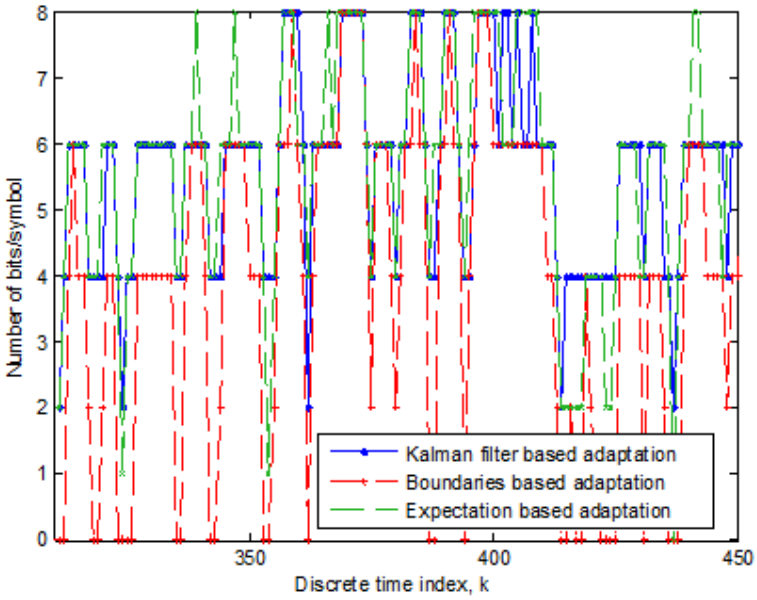

Figure 5.14 Rate adaptations with $\sigma_{\xi}{}^2 = 0.05$ for $BER_{tg} = 10^{-3}$

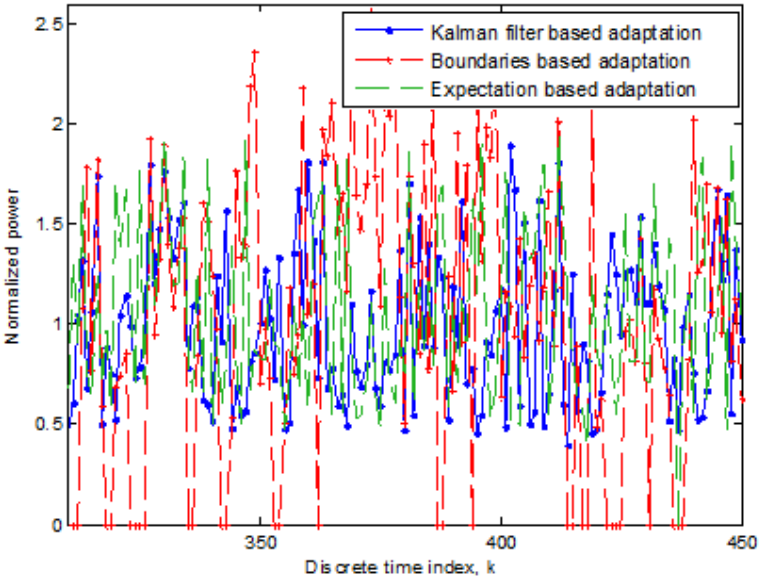

Figure 5.15 Power adaptations with $\sigma_{\xi}{}^2 = 0.05$ for $BER_{tg} = 10^{-3}$

It is shown in Figure 5.14 that in most of the time, the optimal region boundaries based adaptation method adapts the modulation to apply lower bits per symbol than both dynamical rate adaptations based on feedback controller proposed in this dissertation. Comparing Figure 5.14 to Figure 5.11, it can be seen that optimal region boundaries based adaptation method resolves to lower discrete rate in general for the worse quality of channel prediction. The variation of transmit power in Figure 5.15 is within a similar range with that in Figure 5.12 regardless of the different quality of channel prediction.

The corresponding BERs of the discrete rate and power adaptation methods are shown in Figure 5.16. As expected, the BER performance of Kalman filter based adaptation method has degraded due to the high channel gain prediction error. However, the overall BERs of the non-linear feedback adaptation method still fall within the range of 10^{-6} to 10^{-2} while as the BERs of the optimal region boundaries based adaptation method are scattered within a range of 10^{-8} to 10^{-2}.

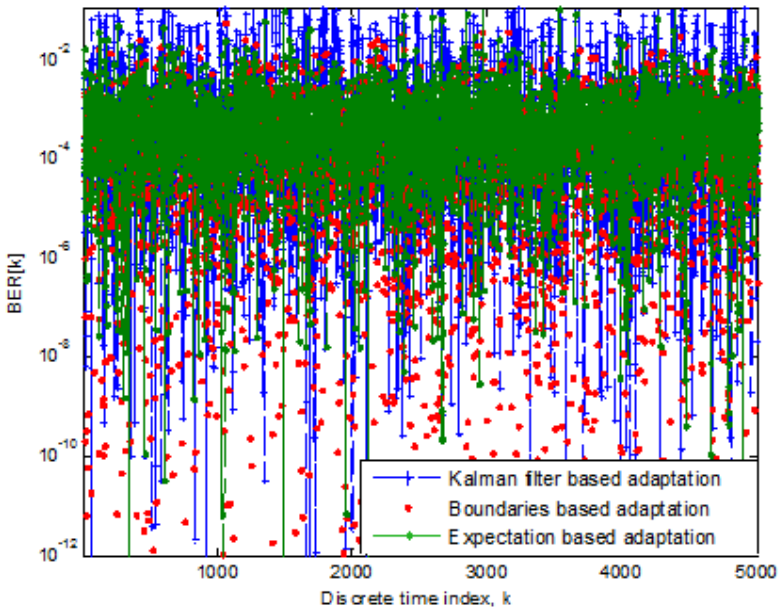

Figure 5.16 Instantaneous BER of adaptive QAM with $\sigma_{\xi}{}^{2} = 0.05$ for $BER_{tg} = 10^{-3}$

Similar sets of simulation are performed in MATLAB for $BER_{tg} = 10^{-7}$ to observe the behavior of adaptation which might differ under lower BER constraint. It is expected that lower modulation modes like BPSK and QPSK will be more frequently used to reduce the probability of symbol error and hence resulting in lower BER. The behavior of the rate and power adaptation based on channel prediction with error variance of 0.02 are presented in Figure 5.17 and Figure 5.18 respectively.

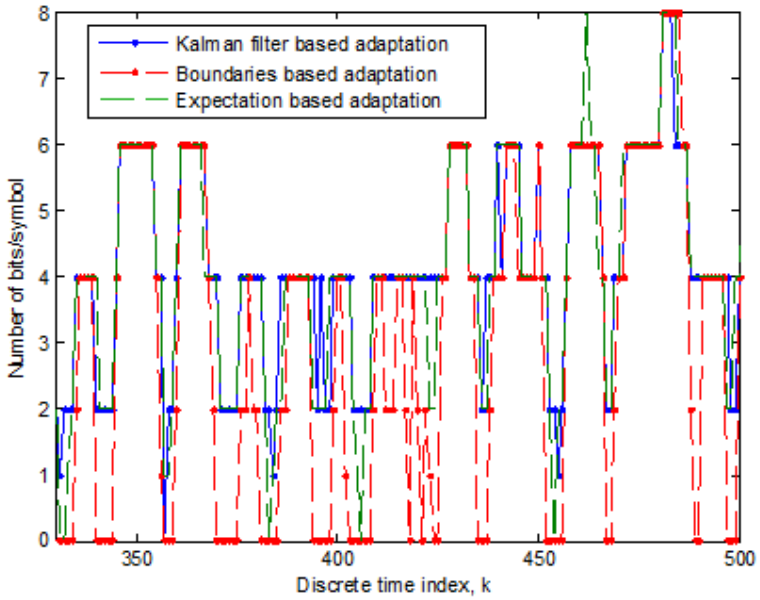

Figure 5.17 Rate adaptations with $\sigma_{\xi}{}^{2} = 0.02$ for $BER_{tg} = 10^{-7}$

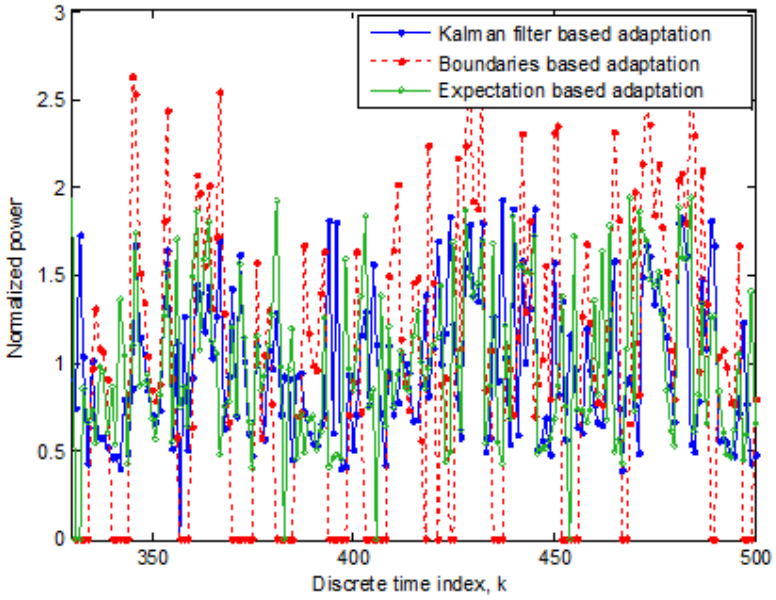

Figure 5.18 Power adaptations with $\sigma_{\xi}{}^{2} = 0.02$ for $BER_{tg} = 10^{-7}$

In Figure 5.17, the overall numbers or bits per symbols are indeed lower compared to Figure 5.11 for $BER_{tg} = 10^{-3}$. Both dynamical rate adaptations based on linear Kalman filter and expectation based adaptation method with non-linear feedback controller agree with the rate adaptation based on optimal region boundaries in adjusting the constellation size relative to the channel variation over the time. The variations of transmit power in Figure 5.15 and the variance of transmit power for optimal region boundaries adaptation method is slightly higher than those of Kalman filter method and expectation based adaptation method with non-linear feedback controller.

The resulted BER rate and power adaptation based on channel prediction with error variance of 0.02 is plotted in Figure 5.19 and it is seen that the expectation based adaptation method with non-linear feedback controller results in a smaller range of BER fluctuation in comparison to the conventional optimal region boundaries based adaptation method.

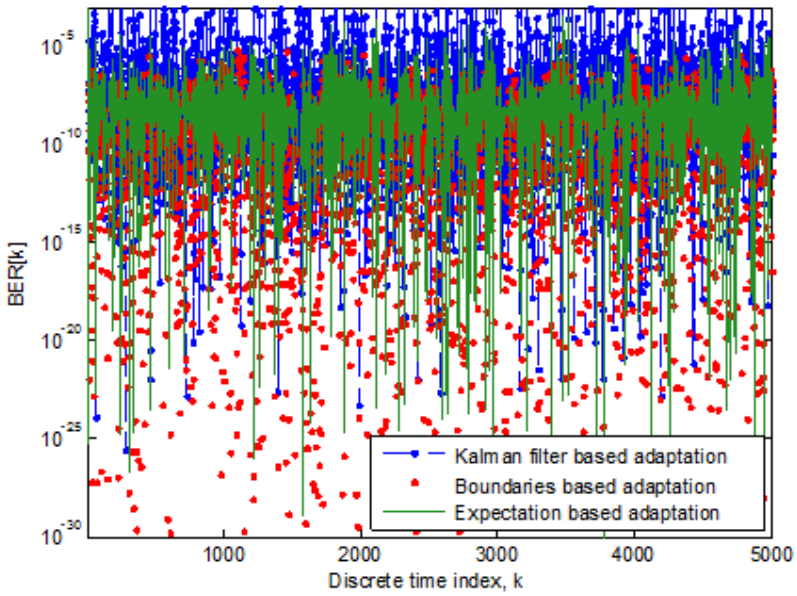

Figure 5.19 Instantaneous BER of adaptive QAM with $\sigma_{\xi}^{2} = 0.02$ for $BER_{tg} = 10^{-7}$

The same adaptation methods are simulated with the channel prediction error variance increased from 0.02 to 0.05. Figure 5.20 and Figure 5.21 show the resulting rate and power adaptations respectively.

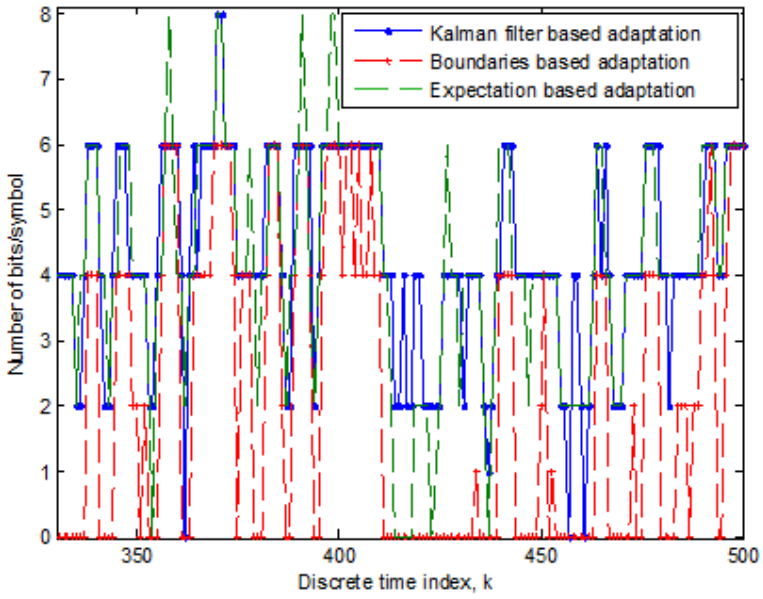

Figure 5.20 Rate adaptations with $\sigma_{\xi}^{2} = 0.05$ for $BER_{tg} = 10^{-7}$

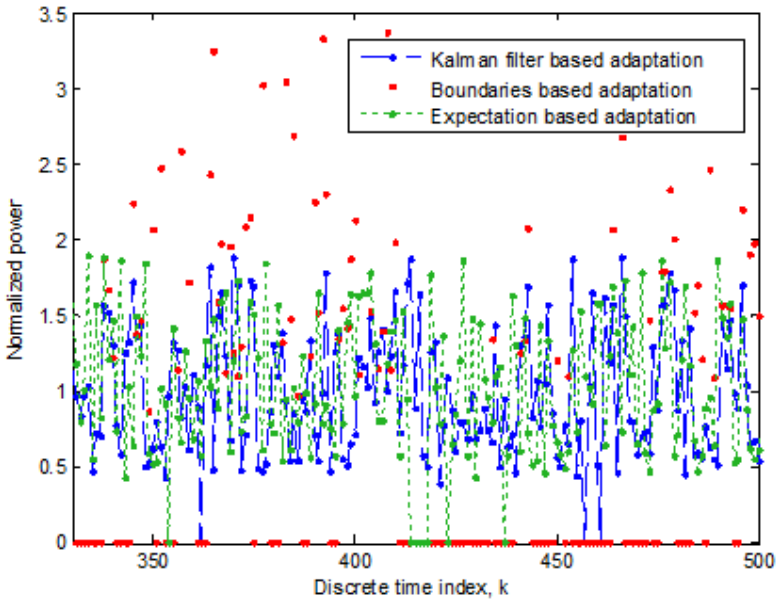

Figure 5.21 Power adaptations with $\sigma_{\xi}{}^{2} = 0.05$ for $BER_{tg} = 10^{-7}$

As observed in Figure 5.21, the range of transmit power for optimal region boundaries based adaptation method has increased significantly compared to the same adaptation method with a better quality of channel prediction, which is shown in Figure 5.18.

The corresponding BERs of the discrete rate and power adaptation methods are shown in Figure 5.22. It is clear that the proposed adaptation method based on non-linear feedback results in a smaller range of BER variation compared to adaptation method based on linear Kalman filter and the adaptation method based on optimal region boundaries even though the fluctuation has also become more severe as the channel prediction degrades. These results suggest that the proposed adaptation methods based on partial CSI are more suitable for adaptive modulation with average BER constraint.

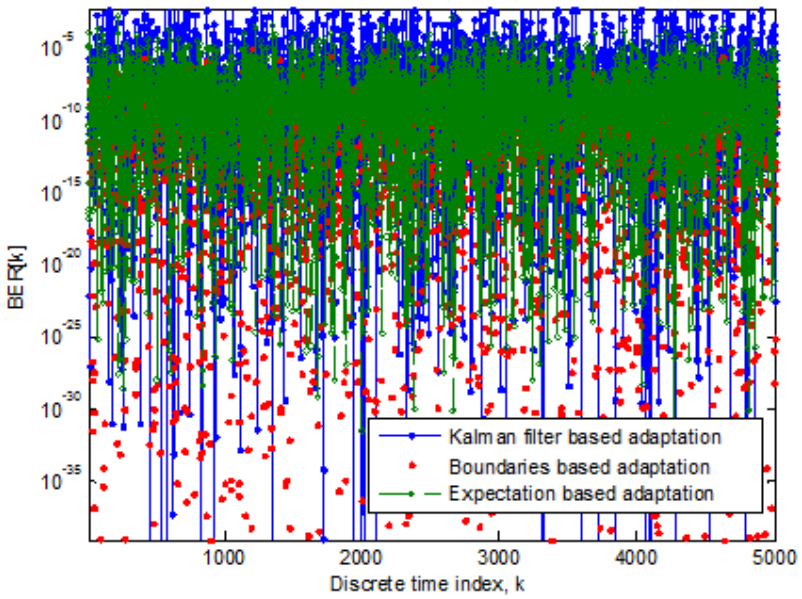

Figure 5.22 Instantaneous BER of adaptive QAM with $\sigma_{\xi}{}^2 = 0.05$ for $BER_{tg} = 10^{-7}$

Finally, the spectral efficiency of the system is evaluated for both expectation based adaptation method with non-linear feedback controller and optimal boundaries based adaptation method. In order to obtain sufficient data for accurate computation of average value, both adaptation methods are simulated repeatedly for each of the two different qualities of channel information, represented by the prediction error variance of 0.02 and 0.05, under BER of 10^{-3}. The results are presented in Figure 5.23, where dotted lines and diamond marked lines correspond to $\sigma_{\xi}{}^2 = 0.02$ and $\sigma_{\xi}{}^2 = 0.05$ respectively.

Figure 5.23 shows that the spectral efficiencies of adaptive system with rate and power adaptation based on non-linear feedback are higher than the spectral efficiencies of adaptive system with rate and power adaptation based on optimal SNR region boundaries solution. Moreover, the graphs for $\sigma_{\xi}{}^2 = 0.02$ and $\sigma_{\xi}{}^2 = 0.05$ are very close together, which suggests that the spectral efficiency resulted from the proposed rate and power adaptation method is very much robust against different quality of channel prediction.

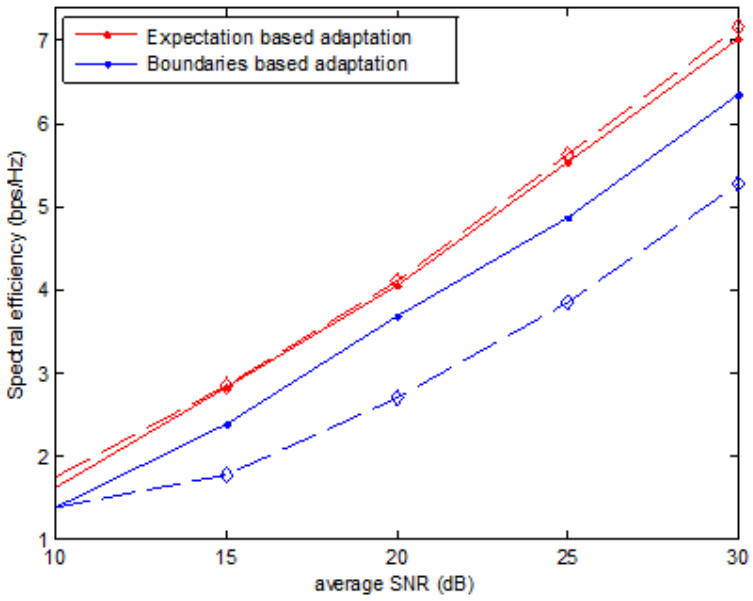

Figure 5.23 Spectral efficiencies vs. average SNR for $BER_{tg} = 10^{-3}$

The impact of Doppler effect on the performance of the rate and power adaptation method is also investigated. This is accomplished by repeating the same set of simulation over Rayleigh channel with various correlation coefficients that are directly related to the maximum Doppler frequency in accordance with (2.3), where the channel is sampled at a fixed sampling rate of 20 kHz. The results are presented in Figure 5.24 for discrete rate and continuous power adaptation method based on optimal SNR region boundaries and Figure 5.25 for discrete rate and continuous power adaptation method based on non-linear feedback controller.

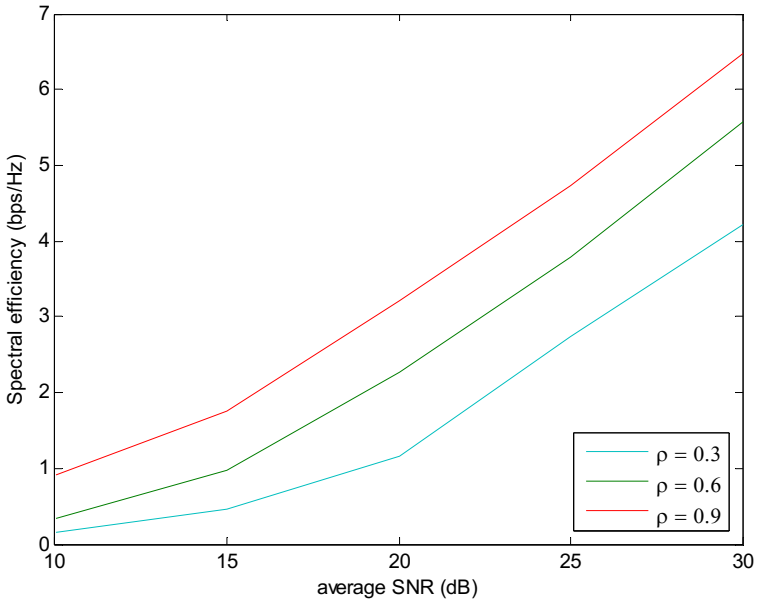

Figure 5.24 Spectral efficiency vs. SNR for discrete rate and continuous power adaptation based on optimal region boundaries solution

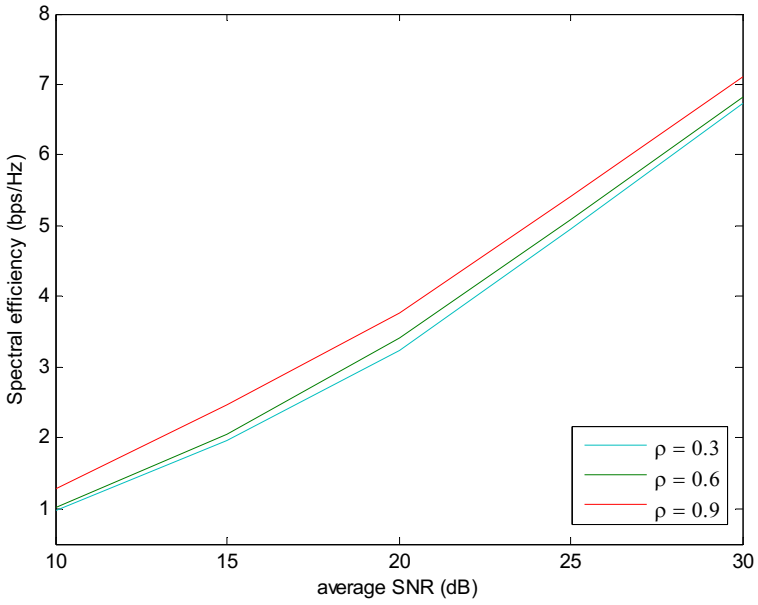

Figure 5.25 Spectral efficiency vs. SNR for discrete rate and continuous power adaptation based on non-linear feedback controller

Figure 5.24 shows that for adaptation method based on optimal SNR region boundaries, a decrease in the correlation coefficient results in a significant loss of spectral efficiency. On the other hand, Figure 5.25 shows that that the series of resulted spectral efficiency for the proposed adaptation method are very close together. This demonstrates that the proposed non-linear feedback adaptation method is more robust to the variation of Doppler effects on the wireless channels.

Note that the lower correlation coefficient implies a more severe Doppler effect. This also means that the channel gain changes more rapidly over time. Hence, the proposed adaptation method is also robust against the different variations of channel gain over time.

5.4 Conclusion

In this chapter, an alternative state-space representation is established with BER at different time instant as the state variables. Assuming perfect channel gain at the transmitter, an appropriate choice of non-linear controller is designed to obtain a stable system that is linearized about the equilibrium point. In the absence of perfectly known channel gain, the expectation of the systems states at the transmitter are computed to estimate the states and the non-linear controller is then modified to adopt these estimations along with the partial CSI in the form of conditional mean of the channel and white variance. In this case, the actual channel is modeled as a Gaussian random variable with distribution $h \sim CN\left(\bar{h}, {\sigma_\xi}^2\right)$. It is shown that the conditional mean of the channel, $\bar{h}$, can be computed from the noisy prediction based on the past observations fed back from the receiver and the channel prediction error variance therefore defines the variance of the random channel, ${\sigma_\xi}^2$.

The performance of the rate adaptation method based on partial CSI is investigated through simulations in MATLAB. The behavior of rate adaptation with constant power is presented for various BER constraints. The results show that the expectation based adaptation method with non-linear feedback controller established

in this chapter responds to the channel variation in a similar manner to the conventional adaptation method based on optimal region boundaries. Transmit power is further adjusted for the appropriate choice of discrete constellation size to achieve maximum spectral efficiency while maintaining the BER within the requirement. Simulation results show that the spectral efficiencies of adaptive system with rate and power adaptation based on non-linear feedback are higher than the spectral efficiencies of adaptive system with rate and power adaptation based on optimal SNR region boundaries solution while the BER constraint is observed within an order of magnitude. These results also suggest that the proposed adaptation methods based on partial CSI are more suitable for adaptive modulation with average BER constraints as the resulted BER fluctuates around the prescribed value.

In addition, the performances of the adaptation methods are also evaluated for different correlation coefficients of the Rayleigh fading channel. The results reveal that the proposed expectation based adaptation method with non-linear feedback controller is more robust to the variation of Doppler shifts on the wireless channels compared to the existing optimal boundaries based adaptation method.

Chapter 6

Conclusions and Future Work

This chapter recapitulates the contributions of this thesis and presents some possible future research directions based on the study.

6.1 Summary of Contributions

This thesis has investigated the dynamic analysis of adaptive modulation in wireless communications. The focus of this research is adaptive modulation technique for QAM transmission over flat Rayleigh fading channels. Different from conventional adaptive modulation schemes, the proposed adaptation scheme is approached from system dynamic analysis. Using dynamic analysis approach has not only solved the adaptation problem without involving complex optimization technique, but also has resulted in robustness against various qualities of channel prediction at the transmitter and also against different time variations of the channel due to Doppler shift. The key contributions of this thesis are summarized as follows.

In chapter 3, an analytical model of the rate adaptive QAM system is proposed for flat Rayleigh fading channels. The system dynamic equations are established in the form of state-space representation. The adaptation of constellation size is then approached by applying a state feedback controller that results in a stable

closed-loop system. It is shown that under assumption of perfect CSI, the system states converge to the equilibrium for a range of feedback controller gain vector. The analytical model built in this chapter is verified through simulation in MATLAB. Simulation results affirm that, in the presence of perfect CSI, the proposed adaptation method behaves similarly to the conventional adaptation method discussed in literature.

The imperfection of CSI at transmitter is still the major challenge in performing optimal adaptive modulation over wireless channels. Chapter 4 specifically addresses this problem and state estimation by Kalman filter is implemented to mitigate the process noise due to the inaccurate prediction of channel power gain. The performance of the proposed adaptation scheme with Kalman filter is evaluated through simulations in MATLAB and it is compared with the conventional adaptation schemes based on predicted channel. Simulation results reveal that the spectral efficiency of an QAM system with the proposed rate and power adaptation method is less sensitive to different qualities of channel prediction in comparison with the existing rate and power adaptation method. It is seen that the instantaneous BER performance of the proposed adaptation method is degraded by the low quality of the channel power gain prediction. To the best of author's knowledge, this problem occurs because the nonlinearity of the system is not accounted in the input/state linearized system and Kalman filtering algorithm therefore produces less optimal solution. However, the discrete rate adaptation with constant power based on the feedback controller with Kalman filter results in higher spectral efficiency compared with the conventional discrete rate adaptation with constant power based on optimal region boundaries while the resulted instantaneous BER is still observed within an order of a magnitude of the targeted value.

In Chapter 5, the non-linear dynamical system is modeled using alternative state-space equations without cancelation of the system's nonlinearity. A non-linear controller that results in a stable system in the vicinity of the equilibrium point is established under assumption of perfect CSI. The feedback control is then modified to incorporate partial CSI based on mean feedback, where the channel information

resides in the mean value of the distribution, with white variance to take into account of the estimation error. The effect of channel uncertainty on the system state is taken into account by estimating the system states using the expected value of BER conditioned on the channel mean feedback. The constellation size is then adjusted based on the predicted channel power gain and the estimated state feedback. Simulations results have verified the accuracy of the dynamic model. The BER performance of the adaptive system in the simulation suggests that the proposed adaptation methods based on partial are more suitable for adaptive modulation with average BER constraints. Furthermore, is is shown that the proposed system is more robust against different time variations of the channel due to Doppler shift represented by the correlation coefficent.

Finally, modeling the dynamic of adaptive modulation system as proposed in this thesis has provided flexibility in designing an appropriate feedback controller to adjust a transmission parameter such as transmission rate based on the channel condition. It is hoped that the work of this thesis will stimulate further investigations in this field and some idea of possible future work are given below.

6.2 Future Research

The work in this thesis can be extended in some possible directions as follows:

1. Implementation of H_∞ filter as a robust state estimator

In this thesis, the estimation of system state is performed by using a simple linear Kalman filter in Chapter 4 and using the expected value based on the statistics of the noise in Chapter 5. Through simulations in MATLAB, it is shown that appropriate designs of feedback controller in adjusting the constellation size based on the estimated state variables in the presence of prediction noise have given reasonably good performance in terms of spectral efficiency and average BER performance. The fluctuation of the resulted BER may be further reduced by implementing more accurate estimation method to cope with the random noise.

Recently, the H_∞ filtering algorithms have received considerable attention as they are more robust to modeling error and noise uncertainty than the Kalman filter [143]-[145]. Different from Kalman filter which requires the process and measurement noises to have zero mean and specific covariance matrix, H_∞ filter does not make any assumption about these noises, and the filter is designed to minimize the worse case estimation error [146], [147]. It is thus less sensitive to the knowledge of the noise statistics. Because of the robust characteristic of H_∞ filter, it is worth investigating its potential as an optimal state estimator for optimal control of constellation size to maintain the instantaneous BER lower or equal to the criterion for various qualities of channel prediction error.

2. Adaptive modulation for MIMO wireless systems

In this dissertation, the proposed adaptation scheme is considered based on wireless transmission between single antenna transmitter and receiver as documented in literature. However, in the last decade, the idea of multiple input multiple output (MIMO) antennas at transmitter and receiver has been developed as a solution to reliable and more spectrally efficient communication systems. The increase in reliability and efficiency can be achieved by arranging the antennas in a way that achieves a high diversity gain to overcome the fading effect [148]-[150].

Recent studies have demonstrated that MIMO transceivers indeed result in the capacity of the wireless without the need of additional power or spectrum, especially in rich scattering environments [151]-[153]. This finding has motivated the industries to develop the future wireless systems that incorporate the concept of multiple antennas at transmitter and receiver with high diversity gain. Based on the work done in this dissertation, an important question to answer is how the state-space representation of system dynamics developed in this thesis can be extended for the case of adaptive modulation in MIMO transmission systems with diversity antennas.

List of Publications

A. C. Tjiam, Z. Man and Z. Cao, "A novel rate adaptive modulation method in wireless communication based on system dynamics analysis," in *Proceedings of the International Conference on Electronics, Communications and Control (ICECC)*, Zhou Shan, China, October 2012.

A. C. Tjiam, Z. Man, M. T. Do and Z. Cao, "Non-linear feedback rate-adaptive modulation scheme in wireless communications over Rayleigh channels," in *Proceedings of the 8th IEEE Conference on Industrial Electronics and Applications (ICIEA)*, Melbourne, Australia, June 2013.

A. C. Tjiam, Z. Man, J. Jin and Z. Cao, "System dynamics analysis of adaptive modulation problem for Rayleigh flat-fading channel," *IEEE Wireless Communications Letters,* 2013, submitted for publication.

Bibliography

[1] J. Hayes, "Adaptive feedback communications," *IEEE Transactions on Communication Technology,* vol. 16, no. 1, pp. 29-34, 1968.

[2] S. Lundqvist, Physics: 1901-1921, 1998: World Scientific, Singapore.

[3] J. De Vriendt, P. Laine, C. Lerouge and X. Xu, "Mobile network evolution: a revolution on the move," *IEEE Communications Magazine,* vol. 40, no. 4, pp. 104-111, 2002.

[4] E. Dahlman, 3G Evolution HSPA and LTE for Mobile Broadband, Amsterdam; Oxford: Elsevier Academic Press, 2007.

[5] A. Goldsmith, Wireless Communications, New York: Cambridge University Press, 2005.

[6] M. Jamil, S. Shaikh, M. Shahzad and Q. Awais, "4G: The future mobile technology," *2008 IEEE Region 10 Conference,* pp. 1-6, 2008.

[7] A. Khan, M. Qadeer, J. Ansari and S. Waheed, "4G as a next generation wireless network," *International Conference on Future Computer and Communication 2009,* pp. 334-338, 2009.

[8] K. R. Santhi and G. Kumaran, "Migration to 4G: Mobile IP based solutions," *International Conference on Internet and Web Applications and Services,* pp. 76-81, 2006.

[9] A. Akan and C. Edemen, "Path to 4G wireless networks," *IEEE 21st International Symposium on Personal, Indoor and Mobile Radio Communications Workshops ,* pp. 405-407, 2010.

[10] A. Vaish, "Plenary talk: Ericcson's initiatives on 4G technologies," *International Conference on Recent Trends in Information Technology,* p. 3, 2011.

[11] Z. Han and K. J. R. Liu, Resource Allocation for Wireless Networks: Basics, Techniques, and Applications, New York: Cambridge University Press, 2008.

[12] W.C.Jakes, Microwave Mobile Communications, New York: John Wiley & Sons, 1974.

[13] F. Davarian, "Channel simulation to facilitate mobile-satellite communications research," *IEEE Transactions on Communications,* vol. 35, no. 1, pp. 47-56, 1987.

[14] T. Aulin, "Characteristics of a digital mobile radio channel," *IEEE Transactions on Vehicular Technology,* vol. 30, no. 2, pp. 45-53, 1981.

[15] D. Giancristofaro, "Correlation model for shadow fading in mobile radio channels," *Electronics Letters,* vol. 32, no. 11, pp. 958-959, 1996.

[16] T. Eyceoz, A. Duel-Hallen and H. Hallen, "Deterministic channel modeling and long range prediction of fast fading mobile radio channels," *IEEE Communications Letters,* vol. 2, no. 9, pp. 254-256, 1998.

[17] F. Graziosi and F. Santucci, "A general correlation model for shadow fading in mobile radio systems," *IEEE Communications Letters,* vol. 6, no. 3, pp. 102-104, 2002.

[18] S. Semmelrodt and R. Kattenbach, "Investigation of different fading forecast schemes for flat fading radio channels," *2003 IEEE 58th Vehicular Technology Conference,* vol. 1, pp. 149-153, 2003.

[19] K. E. Baddour and N. C. Beaulieu, "Autoregressive modeling for fading channel simulation," *IEEE Transactions on Wireless Communications,* vol. 4, no. 4, pp. 1650-1662, 2005.

[20] D. Baum, J. Hansen and J. Salo, "An interim channel model for beyond-3G systems: extending the 3GPP spatial channel model (SCM)," *2005 IEEE 61st Vehicular Technology Conference,* vol. 5, pp. 3132-3236, 2005.

[21] T. S. Rappaport, Wireless Communications: Principles and Practice, 2 ed., Upper Saddle River, NJ: Prentice Hall PTR, 2002.

[22] Y. S. Cho, J. Kim, W. Y. Yang and C. G. Kang, MIMO-OFDM wireless communications with MATLAB, Singapore: John Wiley & Sons, 2010.

[23] A. R. S. Bahai, B. R. Saltzberg and M. Ergen, Multi-Carrier Digital Communications: Theory and Applications of OFDM, Springer Verlag, 2004.

[24] M. Tsatsanis, G. Giannakis and G. Zhou, "Estimation and equalization of fading channels with random coefficients," *Proceedings of the IEEE International Conference on Acoustics, Speech, and Signal Processing,* vol. 2,

pp. 1093-1096, 1996.

[25] C. Komninakis, C. Fragouli, A. Sayed and R. Wesel, "Channel estimation and equalization in fading," *Conference Record of the Thirty-Third Asilomar Conference on Signals, Systems, and Computers,,* vol. 2, pp. 1159-1163, 1999.

[26] A. D'Andrea, A. Diglio and U. Mengali, "Symbol-aided channel estimation with non-selective Rayleigh fading channels," *IEEE Transaction on Vehicular Technology,* vol. 44, no. 1, pp. 41-49, 1995.

[27] J. Hagenauer, F. Dolainsky, E. Lutz, W. Papke and R. Schweikert, "The maritime satellite communication channel - channel model, performance of modulation and coding," *IEEE Journal on Selected Areas in Communications,* vol. 5, no. 4, pp. 701-713, 1987.

[28] J. Hagenauer and W. Papke, "Data transmission for maritime and land mobiles using stored channel simulation," *The 32nd IEEE Vehicular Technology Conference,* vol. 32, pp. 379-383, 1982.

[29] X. Liu, "Probability of strictly positive secrecy capacity of the Rician-Rician fading channel," *IEEE Wireless Communications Letters,* vol. 2, no. 1, pp. 50-53, 2013.

[30] G. Hess, "Land-mobile satellite excess path loss measurement," *IEEE Transactions on Vehicular Technology,* vol. 29, no. 2, pp. 290-297, 1980.

[31] J. An, "Empirical analyses on maritime radio propagation," *IEEE 59th Vehicular Technology Conference,* vol. 1, pp. 176-180, 2004.

[32] Z. B. Krusevac and P. Rapajic, "Adaptive AR channel model identification of time-varying communication systems," *IEEE 10th International Symposium on Spread Spectrum Techniques and Applications,* pp. 618-622, 2008.

[33] H.-S. Wang and N. Moayeri, "Finite-state Markov channel-a useful model for radio communication channels," *IEEE Transactions on Vehicular Technology,* vol. 44, no. 1, pp. 163-171, 1995.

[34] C. Tan and N. Beaulieu, "On first-order Markov modeling for the Rayleigh fading channel," *IEEE Transactions on Communications,* vol. 48, no. 12, pp. 2032-2040, 2000.

[35] P. Sadeghi, R. Kennedy, P. Rapajic and R. Shams, "Finite-state Markov modeling of fading channels - a survey of principles and applications," *IEEE Signal Processing Magazine,* vol. 25, no. 5, pp. 57-80, 2008.

[36] J. K. Cavers, "An analysis of pilot symbol assisted modulation for Rayleigh fading channels," *IEEE Transactions on Vehicular Technology,* vol. 40, no. 4, pp. 686-693, 1991.

[37] S. Sampei and T. Sunaga, "Rayleigh fading compensation for QAM in land mobile radio communications," *IEEE Transactions on Vehicular Technology,* vol. 42, no. 2, pp. 137-147, 1993.

[38] J. Torrance and L. Hanzo, "Comparative study of pilot symbol assisted modem schemes," *Proceedings of the Sixth International Conference on Radio Receivers and Associated Systems,* pp. 36-41, 1995.

[39] E. Okamoto, H.-B. Li and T. Ikegami, "Rayleigh fading compensation for QAM by using FFT," *Seventh IEEE International Symposium on Personal, Indoor and Mobile Radio Communications,* vol. 3, pp. 1079-1082, 1996.

[40] P. Hoeher, S. Kaiser and P. Roberton, "Two-dimensional pilot-symbol-aided channel estimation by Wiener filtering," *Proceedings of the 1997 IEEE International Conference on Acoustics, Speech, and Signal Processing,* vol. 3,

pp. 1845-1848, 1997.

[41] M. Valenti and B. Woerner, "Iterative channel estimation and decoding of pilot symbol assisted turbo codes over flat-fading channels," *IEEE Journal on Selected Areas in Communications,* vol. 19, no. 9, pp. 1697 - 1705, 2001.

[42] S. Takaoka and F. Adachi, "Pilot-assisted adaptive interpolation channel estimation for OFDM signal reception," *IEEE 59th Vehicular Technology Conference,* vol. 3, pp. 1777-1781, 2004.

[43] M. Dong, L. Tong and B. Sadler, "Optimal insertion of pilot symbols for transmissions over time-varying channels," *IEEE Transactions on Signal Processing,* vol. 42, no. 5, pp. 1403-1418, 2004.

[44] K. Baddour and N. Beaulieu, "Improved pilot-assisted prediction of unknown time-selective Rayleigh channels," *Proceedings of the IEEE International Conference on Communications, 2006,* vol. 11, pp. 5192-5199, 2006.

[45] A. Soysal, S. Ulukus and C. Clancy, "Channel estimation and adaptive M-QAM in cognitive radio links," *IEEE International Conference on Communications,* pp. 4043 - 4047, 2008.

[46] A. Omar and A. Ali, "Adaptive channel characterization for wireless communication," *2008 IEEE Radio and Wireless Symposium,* pp. 543-546, 2008.

[47] G. Xu, H. Liu, L. Tong and T. Kailath, "A least-squares approach to blind channel identification," *IEEE Transactions on Signal Processing,* vol. 43, no. 12, pp. 2982-2993, 1995.

[48] J.-J. van de Beek, O. Edfors, M. Sandell, S. Wilson and P. Ola Borjesson, "On channel estimation in OFDM systems," *IEEE 45th Vehicular Technology*

Conference, vol. 2, pp. 815-819, 1995.

[49] T. Ekman, "Prediction of Mobile Radio Channels, Modeling and Design," Ph.D. dissertation, Uppsala University, 2002.

[50] M. Biguesh and A. Gershman, "Training-based MIMO channel estimation: a study of estimator tradeoffs and optimal training signals," *IEEE Transactions on Signal Processing,* vol. 54, no. 3, pp. 884-893, 2006.

[51] X. Cai and G. Giannakis, "Adaptive PSAM accounting for channel estimation and prediction errors," *IEEE Transactions on Wireless Communications,* vol. 4, no. 1, pp. 246-256, 2005.

[52] J. Sun and D. Yuan, "A new up bound of spacing between pilot symbols over fading channels in PSAM systems," *Wireless Communications and Networking Conference,* pp. 2296-2299, 2007.

[53] K. Yadav, N. Singh and M. C. Srivastava, "Analysis of adaptive pilot symbol assisted modulation with optimized pilot symbol spacing for Rayleigh fading channel," *International Conference on Signal Processing, Communications and Networking,* pp. 405-410, 2008.

[54] M. Karami and N. Beaulieu, "Channel adaptive power allocation and pilot optimization for OFDM systems," *IEEE Global Communications Conference,* pp. 4893-4898, 2012.

[55] Y. Kamio, S. Sampei, H. Sasaoka and N. Morinaga, "Performance of modulation-level-controlled adaptive-modulation under limited transmission delay time for land mobile communications," *The IEEE 45th Vehicular Technology Conference,* vol. 1, pp. 221-225, 1995.

[56] A. Goldsmith and S.-G. Chua, "Variable-rate variable-power M-QAM for

fading channels," *IEEE Transaction on Communications,* vol. 45, no. 10, pp. 1218-1230, 1997.

[57] A. Goldsmith and S.-G. Chua, "Adaptive coded modulation for fading channels," *IEEE Transactions on Communications,* vol. 46, no. 5, pp. 595-602, 1998.

[58] J. Hossain, P. Vitthaladevuni, M.-S. Alouini, V. Bhargava and A. Goldsmith, "Adaptive hierarchical modulation for simultaneous voice and multiclass data transmission over fading channels," *IEEE Transactions on Vehicular Technology,* vol. 55, no. 4, pp. 1181-1194, 2006.

[59] A. Duel-Hallen, S. Hu and H. Hallen, "Long-range prediction of fading signals," *IEEE Signal Processing Magazine,* vol. 17, pp. 62-75, 2000.

[60] M. Sternad, T. Ekman and A. Ahlen, "Power prediction on broadband channels," *Proceedings of the IEEE Vehicular Technology Conference,* vol. 4, pp. 2328-2332, 2001.

[61] S. Haykin, Adaptive Filter Theory, Upper Saddle River, New Jersey: Prentice Hall, 2002.

[62] T. Ekman, M. Sternad and A. Ahlen, "Unbiased power prediction of Rayleigh fading channels," *Proceedings of the IEEE 56th Vehicular Technology Conference,* vol. 1, pp. 280-284, 2002.

[63] W. Shin, S. J. Lee and D.-S. Kwon, "LMMSE channel estimation with soft statistics for turbo-MIMO receivers," *IEEE Communications letters,* vol. 13, no. 8, pp. 585-587, 2009.

[64] K.-C. Hung and D. Lin, "Pilot-based LMMSE channel estimation for OFDM systems with power–delay profile approximation," *IEEE Transactions on*

Vehicular Technology, vol. 59, no. 1, pp. 150-159, 2010.

[65] C. Huang, R. Liu and H. Wang, "A new MMSE estimator based on signal correlation property," *The 6th International Conference on Wireless Communications Networking and Mobile Computing,* pp. 1-3, 2010.

[66] J. Proakis, Digital communications, New York: McGraw-Hill, 1989.

[67] M. Rice, Digital Communications: A Discrete-time Approach, Upper Saddle River, NJ: Prentice Hall, 2009.

[68] W. Webb, "QAM: the modulation scheme for future mobile radio communications?," *Electronics & Communication Engineering Journal ,* vol. 4, no. 4, pp. 167-176, 1992.

[69] D. Yoon, K. Cho and J. Lee, "Bit error probability of M-ary quadrature amplitude modulation," *IEEE 52nd Vehicular Technology Conference,* vol. 5, pp. 2422-2427, 2000.

[70] L.-L. Yang and L. Hanzo, "A recursive algorithm for the error probability evaluation of M-QAM," *IEEE Communications Letters,* vol. 4, no. 10, pp. 304-306, 2000.

[71] K. Cho and D. Yoon, "On the general BER expression of one- and two-dimensional amplitude modulations," *IEEE Transactions on Communications,* vol. 50, no. 7, pp. 1074-1080, 2002.

[72] W. Lopes, F. Madeiro and M. Alencar, "Closed-form expression for the bit error probability of rectangular QAM subject to Rayleigh fading," *IEEE 66th Vehicular Technology Conference,* pp. 915-919, 2007.

[73] J. Lu, K. Letaief, J. C.-I. Chuang and M.-L. Liou, "M-PSK and M-QAM BER computation using signal-space concepts," *IEEE Transactions on*

Communications, vol. 47, no. 2, pp. 181-184, 1999.

[74] I. A. Glover and P. M. Grant, Digital Communications, Prentice Hall, 1998.

[75] S. Chung and A. Goldsmith, "Degrees of freedom in adaptive modulation: a unified view," *IEEE Transactions on Communications,* vol. 49, no. 9, p. 1561–1571, 2001.

[76] J. K. Cavers, "Variable rate transmission for Rayleigh fading channels," *IEEE Transactions on Cornmunications Technology,* Vols. COM-20, pp. 15-22, 1972.

[77] A. Goldsmith and P. Varaiya, "Capacity of fading channels with channel side information," *IEEE Transactions on Information Theory,* vol. 43, no. 6, pp. 1986-1992, 1997.

[78] H. Zhang, S. Wei, G. Ananthaswamy and D. Goeckel, "Adaptive signaling based on statistical characterizations of outdated feedback in wireless communications," *Proceedings of the IEEE,* vol. 95, no. 12, pp. 2337-2353, 2007.

[79] J. Paris, M. Del Carmen Aguayo-Torres and J. Entrambasaguas, "Optimum discrete-power adaptive QAM scheme for Rayleigh fading channels," *IEEE Communications Letters,* vol. 5, no. 7, pp. 281-283, 2001.

[80] L. Yun and D. Messerschmitt, "Variable quality of service in CDMA systems by statistical power control," *Proceedings of the IEEE International Communications Conference,* vol. 2, pp. 713-719, 1995.

[81] W. Webb and R. Steele, "Variable rate QAM for mobile radio," *IEEE Transactions on Communications,* vol. 43, no. 7, pp. 2223-2230, 1995.

[82] S. Otsuki, S. Sampei and N. Morinaga, "Square-QAM adaptive modulation/TDMA/TDD systems using modulation level estimation with Walsh function," *Electronics Letters,* vol. 31, no. 3, pp. 169-171, 1995.

[83] Y. Kamio, S. Sampei, H. Sasaoka and N. Morinaga, "Performance of modulation-level-controlled adaptive-modulation under limited transmission delay time for land mobile communications," *Proceedings of the IEEE 45th Vehicular Technology Conference,1995,* vol. 1, pp. 25-28, 1995.

[84] K. Hamaguchi and E. Moriyama, "Multicarrier/QAM-level-controlled adaptive modulation for land mobile communication systems," *Proceedings of the 8th IEEE International Symposium on Personal, Indoor and Mobile Radio Communications,1997,* vol. 3, pp. 1105-1109, 1997.

[85] R. Cox, J. Hagenauer, N. Seshadri and C. -E. W. Sundberg, "Subband speech coding and matched convolutional channel coding for mobile radio channels," *IEEE Transactions on Signal Processing,* vol. 38, no. 8, pp. 1717-1731 , 1991.

[86] B. Vucetic, "An adaptive coding scheme for time-varying channels," *IEEE Transactions on Communications,* vol. 39, no. 5, pp. 653-663, 1991.

[87] M.-S. Alouini and A. J. Goldsmith, "Capacity of Rayleigh fading channels under different adaptive transmission and diversity-combining techniques," *IEEE Transactions on Vehicular Technology,* vol. 48, no. 4, pp. 1165-1181, 1999.

[88] S. M. Alamouti and S. Kallel, "Adaptive trellis-coded multiple-phasedshift keying for Rayleigh fading channels," *IEEE Transactions on Communications,* vol. 42, no. 6, pp. 2305-2314, 1994.

[89] T. Ue, S. Sampei and N. Morinaga, "Symbol rate and modulation level controlled adaptive modulation/TDMA/TDD for personal communications

systems," *Proceedings of the IEEE 45th Vehicular Technology Conference, 1995,* vol. 1, pp. 306-310, 1995.

[90] A. Furuskar, S. Mazur, F. Muller and H. Olofsson, "EDGE: enhanced data rates for GSM and TDMA/136 evolution," *IEEE Personal Communications,* vol. 6, no. 3, pp. 56-66, 1999.

[91] J. Yang, A. Khandani and N. Tin, "Statistical decision making in adaptive modulation and coding for 3G wireless systems," *IEEE Transactions on Vehicular Technology,* vol. 54, no. 6, pp. 2066-2073, 2005.

[92] S. Ci and M. Guizani, "A dynamic resource scheduling scheme for CDMA2000 systems," *The 3rd International Conference on Computer Systems and Applications,* 2005.

[93] J.-L. Wu, H.-H. Liu and Y.-J. Lung, "An adaptive multirate IEEE 802.11 wireless LAN," *Proceedings of the 15th International Conference on Information Networking,* pp. 411-418, 2001.

[94] R. Grünheid, E. Bolinth, H. Rohling and K. Aretz, "Adaptive modulation for the HIPERLAN/2 air interface," *Proceedings of the 5th International OFDM Workshop,* 2000.

[95] C. Kim, K. Jeong, K. Ko and J. Lee, "SNR-based adaptive modulation for wireless LAN systems," *IEEE International Symposium on Circuits and Systems,* pp. 758-761, 2012.

[96] T. Ue, S. Sampei and N. Morinaga, "Symbol rate and modulation level controlled adaptive modulation/TDMA/TDD for personal communication systems," *IEEE 45th Vehicular Technology Conference,* vol. 1, pp. 306-310, 1995.

[97] S. Gao, L. Qian, D. Vaman and Q. Qu, "Energy efficient adaptive modulation in wireless cognitive radio sensor networks," *Proceedings of the International Conference on Communications,* pp. 3980-3986, 2007.

[98] Y. Yadong, Z. Rong and D. Jingjing, "An energy-efficient physical layer adaptive modulation ccheme for wireless sensor networks," *Proceedings of the 1st International Conference on Information Science and Engineering,* pp. 3963-3966, 2009.

[99] M. Filip and E. Vilar, "Optimum utilization of the channel capacity of a satellite link in the presence of amplitude scintillations and rain attenuation," *IEEE Transactions on Communications,* vol. 38, no. 11, pp. 1958-1965, 1990.

[100] A. Monk and L. Milstein, "Open-loop power control error in a land mobile satellite system," *IEEE Journal on Selected Areas in Communications,* vol. 13, no. 2, pp. 205 - 212 , 1995.

[101] A. Goldsmith and P. Varaiya, "Increasing spectral efficiency through power control," *IEEE International Conference on Communications,* vol. 1, pp. 600-604, 1993.

[102] R. G. Gallager, Information Theory and Reliable Communication, New York: Wiley, 1968.

[103] P. S. Chow, Bandwidth optimized digital transmission techniques for spectrally shaped channels with impulse noise, Ph.D. dissertation, Stanford University, 1993.

[104] W. Yu and J. Cioffi, "Constant-power waterfilling: performance bound and low-complexity implementation," *IEEE Transactions on Communications,* vol. 54, no. 1, pp. 23-28, 2006.

[105] M. K. Simon and M.-S. Alouini, Digital Communication over Fading Channels, New Jersey: John Wiler & Sons, Inc., 2005.

[106] M. Alouini and A. Goldsmith, "Adaptive modulation over Nakagami fading channels," *Wireless Personal Communications,* vol. 13, no. 1-2, pp. 119-143, 2000.

[107] K. Hole, H. Holm and G. Oien, "Adaptive multidimensional coded modulation over flat fading channels," *IEEE Journal on Selected Areas in Communications,* vol. 18, no. 7, pp. 1153-1158, 2000.

[108] T. Quazi and H. Xu, "Performance analysis of adaptive M-QAM over a flat-fading Nakagami-m channel," *South African Journal of Science,* vol. 107, 2011.

[109] Y. Ma and J. Jin, "Effect of channel estimation errors on M -QAM with MRC and EGC in Nakagami fading channels," *IEEE Transaction on Vehicular Technology,* vol. 56, no. 3, pp. 1239-1250, 2007.

[110] F. Digham and M.-S. Alouini, "Variable-rate noncoherent M-FSK modulation for power limited systems over Nakagami-fading channels," *IEEE Transactions on Wireless Communications,* vol. 3, no. 4, pp. 1295-1304, 2004.

[111] A. Svensson, "An introduction to adaptive QAM modulation schemes for known and predicted channels," *Proceedings of IEEE,* vol. 95, no. 12, pp. 2322-2336, 2007.

[112] X. Tang, M.-S. Alouini and A. J. Goldsmith, "Effect of channel estimation error on M-QAM BER performance in Rayleigh fading," *IEEE Transactions on Communications,* vol. 47, no. 12, pp. 1836-1864, 1999.

[113] P. Jain, On the impact of channel and channel quality estimation on adaptive modulation, Master Thesis, Faculty of the Virginia Polytechnic Institute and

State University, 2002.

[114] T. Jiang, N. Sidiropoulos and G. Giannakis, "Kalman filtering for power estimation in mobile communications," *IEEE Transactions on Wireless Communications,* vol. 2, no. 1, pp. 151-161, 2003.

[115] S. Falahati, A. Svensson, T. Ekman and M. Sternad, "Adaptive modulation systems for predicted wireless channels," *IEEE Transaction on Communications,* vol. 52, no. 2, pp. 307-316, 2004.

[116] K. Ogata, Discrete-time Control Systems, 2 ed., Upper Saddle River, New jersey: Prentice Hall, 1995.

[117] R. S. Esfandiari and B. Lu, Modeling and Analysis of Dynamic Systems, Boca Raton, FL: CRC Press, 2010.

[118] Y. Mori, T. Mori and Y. Kuroe, "Classes of discrete linear systems having common quadratic Lyapunov functions," *Proceedings of the American Control Conference,* vol. 5, pp. 3364-3365, 1995.

[119] C. Sun, B. Fang and W. Huang, "Existence of a common quadratic Lyapunov function for discrete switched linear systems with m-stable subsystems," *IET Control Theory Applications,* vol. 5, no. 3, pp. 535-537, 2011.

[120] G. D. Forney Jr, R. G. Gallager, G. R. Lang, F. M. Longstaff and S. Quereshi, "Efficient modulation for band-limited channels," *IEEE Journal on Selected Areas in Communications,* Vols. SAC-2, p. 632–647, 1984.

[121] C. K. Chui and G. Chen, Kalman Filtering with Real-Time Applications, Heidelberg: Springer, 1999.

[122] B. D. Anderson and J. B. Moore, Optimal Filtering, Englewood Cliffs, NJ:

Prentice-Hall, 1979.

[123] M. I. Ribeiro, Kalman and extended kalman filters: Concept, derivation and properties, Institute for Systems and Robotics, Portugal, 2004.

[124] G. Bishop and G. Welch, "An Introduction to the Kalman Filter," in *SIGGRAPH 2001, Course 8*, 2001.

[125] M. S. Grewal and A. P. Andrews, Kalman Filtering Theory and Practice, 3 ed., Engelewood Cliffs, New Jersey: Prentice Hall, 1993.

[126] S. Koch, H. Kaufman and D. Angwin, "Recursive Kalman type filter selection for adaptive image restoration," *Sixth Multidimensional Signal Processing Workshop,* pp. 191-192, 1989.

[127] C. Messom, G. Gupta, S. Demidenko and L. Y. Siong, "Improving predictive control of a mobile robot: Application of image processing and Kalman filtering," *Proceedings of the 20th IEEE Instrumentation and Measurement Technology Conference,* vol. 2, pp. 1492-1496, 2003.

[128] L. Rui, D. Zhijiang, H. Fujun, K. Minxiu and S. Lining, "Tracking a moving object with mobile robot based on vision," *IEEE International Joint Conference on Neural Networks,* pp. 716-720, 2008.

[129] A. Schneider and J. Maida, "A Kalman filter for an integrated Doppler/GPS navigation system," *IEEE Position Location and Navigation Symposium, 1988. Record. Navigation into the 21st Century,* pp. 408-415, 1988.

[130] D.-J. Jwo and S.-H. Wang, "Adaptive Fuzzy Strong Tracking Extended Kalman Filtering for GPS Navigation," *IEEE Sensors Journal,* vol. 7, no. 5, pp. 778-789, 2007.

[131] F. Kong, G. Dai and L. Cai, "The composed correcting Kalman filtering method for integrated SINS / GPS navigation system," *2010 IEEE International Conference on Intelligent Computing and Intelligent Systems,* vol. 2, pp. 408-412, 2010.

[132] S. McLaughlin, B. Mulgrew and C. Cowan, "A novel adaptive equaliser for nonstationary communication channels," *International Conference on Acoustics, Speech, and Signal Processing,* vol. 2, pp. 944-947, 1989.

[133] S. Ghandour-Haidar, L. Ros and J. Brossier, "On the use of first-order autoregressive modeling for Rayleigh flat fading channel estimation with kalman filter," *ELSEVIER Signal Processing,* vol. 92, no. 2, pp. 601-606, 2012.

[134] L. Ros and E. P. Simon, "Second-order modeling for Rayleigh flat fading channel estimation with Kalman Filter," *Proceedings of the 17th International Conference on Digital Signal Processing,* pp. 1-6, 2011.

[135] M. McGuire and M. Sima, "Low-order kalman filters for channel estimation," *Proceedings of the IEEE Pacific Rim Conference on Communications, Computers and Signal Processing,* pp. 352-355, 2005.

[136] B. Balakrishnan, T. K. Geethu, N. Govindankutty, P. Pradeep, V. Karnani and S. Kirthiga, "Discrete state space channel modeling and channel estimation using Kalman filter for OFDMA systems," *Proceedings of the 12th International Conference on Networking, VLSI and Signal Processing,* pp. 283-287, 2010.

[137] T.Ekman, "Prediction of MobileRadio Channels, Modeling and Design," Ph.D. dissertation, Uppsala University, 2002.

[138] S. T. Hingham, Modern control systems, Massachussetts: Infinity Science

Press, 2008.

[139] E. Visotsky and U. Madhow, "Space–time transmit precodingwith imperfect feedback," *IEEE Transactions on Information Theory,* vol. 47, no. 6, pp. 2632-2639, 2001.

[140] S. Zhou and G. Giannakis, "Adaptive modulation for multi-antenna transmissions with channel meanfeedback," *IEEE Transaction on Wireless Commununications,* vol. 3, no. 5, p. 1626–1636, 2004.

[141] D. L. Goeckel, "Adaptive coding for time-varying channels using outdated fading estimates," *IEEE Transactions on Communications,* vol. 47, no. 6, p. 844, 1999.

[142] D. Huang, Z. Shen, C.Miao and C. Leung, "Resource allocation in MU-OFDM cognitive radio systems with partial channel state information," *EURASIP Journal on Wireless Communications and Networking,* vol. 2010, no. 12, 2010.

[143] L. Xie, L. Lu, D. Zhang and H. Zhang, "Robust filtering for uncertain discrete-time systems: an improved LMI approach," *Proceedings of the 42nd IEEE Conference on Decision and Control,* vol. 1, pp. 906-911, 2003.

[144] X. Wang, H. Zhang, X. Jiang and Y. Yang, " Target tracking based on the extended H-infinity filter in wireless sensor networks," *Journal of Control Theory and Applications,* vol. 9, no. 4, pp. 479-486, 2011.

[145] X. Chang and G. Yang, "Robust H-infinity filtering for uncertain discrete-time systems using parameter-dependent Lyapunov functions," *Journal of Control Theory and Applications ,* vol. 11, no. 1, pp. 122-127, 2013.

[146] X. Shen and L. Deng, "Game theory approach to discrete H∞ filter design," *IEEE Transactions on Signal Processing,* vol. 45, no. 4, pp. 1092-1095, 1997.

[147] D. J. Simon, " From here to infinity," *Embedded Systems Programming,* vol. 14, no. 11, pp. 20-32, 2001.

[148] R. Vaughan and J. Andersen, "Antenna diversity in mobile communications," *IEEE Transactions on Vehicular Technology,* vol. 36, no. 4, pp. 149-172, 1987.

[149] H. Zhang, Z. Wang, J. Yu and J. Huang, "A compact MIMO antenna for wireless communication," *IEEE Antennas and Propagation Magazine,* vol. 50, no. 6, pp. 104-107, 2008.

[150] J. Mietzner, R. Schober, L. Lampe, W. Gerstacker and P. Hoeher, "Multiple-antenna techniques for wireless communications - a comprehensive literature survey," *IEEE Communications Surveys and Tutorials,* vol. 11, no. 2, pp. 87-105, 2009.

[151] E. Telatar, "Capacity of multiple antenna Gaussian channels," *European Transactions on Telecommunications,* vol. 10, no. 6, pp. 585-595, 1999.

[152] C. C. Martin, J. H. Winters and N. R. Sollenberger, "Multiple-input multiple-output (MIMO) radio channel measurements," *IEEE Antennas and Propagation Society International Symposium,* vol. 1, pp. 418-421, 2001.

[153] T. K. Roy, "Capacity and performance analysis of Rayleigh fading MIMO Channels using CSI at the transmitter side," *International Journal of Applied Research in Computer Science and Information Technology,* vol. 1, no. 3, 2012.